STUDIES ON SODIUM ACETATE TRIHYDRATE FOR LATENT HEAT STORAGE

（酢酸ナトリウム三水塩の潜熱蓄熱への応用に関する研究）

1985

Takahiro Wada

PREFACE

The work described in this thesis was carried out under the research and development of Central Research Laboratory of Matsushita Electric Industrial Co. Ltd.

The object of this thesis is to describe the preparative methods and properties of latent heat storage material consisting of sodium acetate trihydrate as a main component. The author hopes that the work described in this thesis would give a suggestion in this field.

Takahiro Wada

CONTENTS

CHAPTER I GENERAL INTRODUCTION

I. 1 General Background of Latent Heat Storage Material

Efficient and economical heat storage is a key to effective and widespread utilizations of low cost energy such as solar energy or deserted heat from the factory for low temperature thermal application [1, 2]. Among various heat storage techniques of interest, a latent heat storage is particularly attractive due to its ability to provide a high energy storage density and its characteristics to store heat at a constant temperature corresponding to the phase transition temperature of the heat storage substance [3-5].

The term "Latent Heat Storage," as we generally understand it today, applies to the storage of heat as the latent heat of fusion in suitable substance that undergoes melting and freezing at a desired temperature. Consequently it is also often called a "Heat-of-Fusion" storage. Typical examples of heat-of-fusion storage substance are ice, paraffin and salt hydrates such as Glauber's salt [6-8].

Salt hydrates form an important class of heat storage substance due to their large latent heat of fusion per unit volume [9, 10]. In fact, their use as a heat storage material has been proposed from the 19th century [11, 12]. Table 1 provides a list of some salt hydrates melting in the temperature range 20—120°C along with their thermophysical properties [10, 13]. Among the salt hydrates shown in the table, $Na_2SO_4 \cdot 10H_2O$ and $CaCl_2 \cdot 6H_2O$ have been exclusively investigated so far for use in solar energy storage [8, 10, 14, 15]. Both $Na_2SO_4 \cdot 10H_2O$ and $CaCl_2 \cdot 6H_2O$ have high heat of fusion and their melting points are about 30°C, which is optimum temperature for solar energy storage. $Na_2SO_4 \cdot 10H_2O$ is one of least expensive material. It is produced in very large quantities as a by product and obtained from natural resources in salt lake and other deposits [3]. $CaCl_2 \cdot 6H_2O$ is low cost material too. However, $CH_3CO_2Na \cdot 3H_2O$ has been scarcely investigated yet.

Table 1. A list of some salt hydrates melting in the temperature range 20–120°C along with their thermophysical properties

Salt hydrate	Melting point	Property of melting	Heat of fusion
$CaCl_2 \cdot 6H_2O$	29°C	P	180 J/g
$Na_2CO_3 \cdot 10H_2O$	32	P	250
$Na_2SO_4 \cdot 10H_2O$	32	P	251
$Na_2HPO_4 \cdot 12H_2O$	36	P	280
$Ca(NO_3)_2 \cdot 4H_2O$	43	C	142
$Na_2S_2O_3 \cdot 5H_2O$	48	P	200
$CH_3CO_2Na \cdot 3H_2O$	58	P	264
$Ba(OH)_2 \cdot 8H_2O$	78	P	293
$Sr(OH)_2 \cdot 8H_2O$	88	P	352
$Mg(NO_3)_2 \cdot 6H_2O$	89	C	160
$KAl(SO_4)_2 \cdot 12H_2O$	91	C	232
$NH_4Al(SO_4)_2 \cdot 12H_2O$	94	C	251
$MgCl_2 \cdot 6H_2O$	117	P	172

1) P: peritectic point

2) C: congruent melting point

I. 2 Characteristics of Sodium Acetate Trihydrate

A phase diagram of binary system CH_3CO_2Na-H_2O, based on data from Seidell's compilation [16], is shown in Fig. 1. The dotted line is liquidus line for metastable CH_3CO_2Na. The figure shows that $CH_3CO_2Na \cdot 3H_2O$ melts incongruently to a 58 wt% CH_3CO_2Na aqueous solution in equilibrium with the residual solid, anhydrous CH_3CO_2Na.

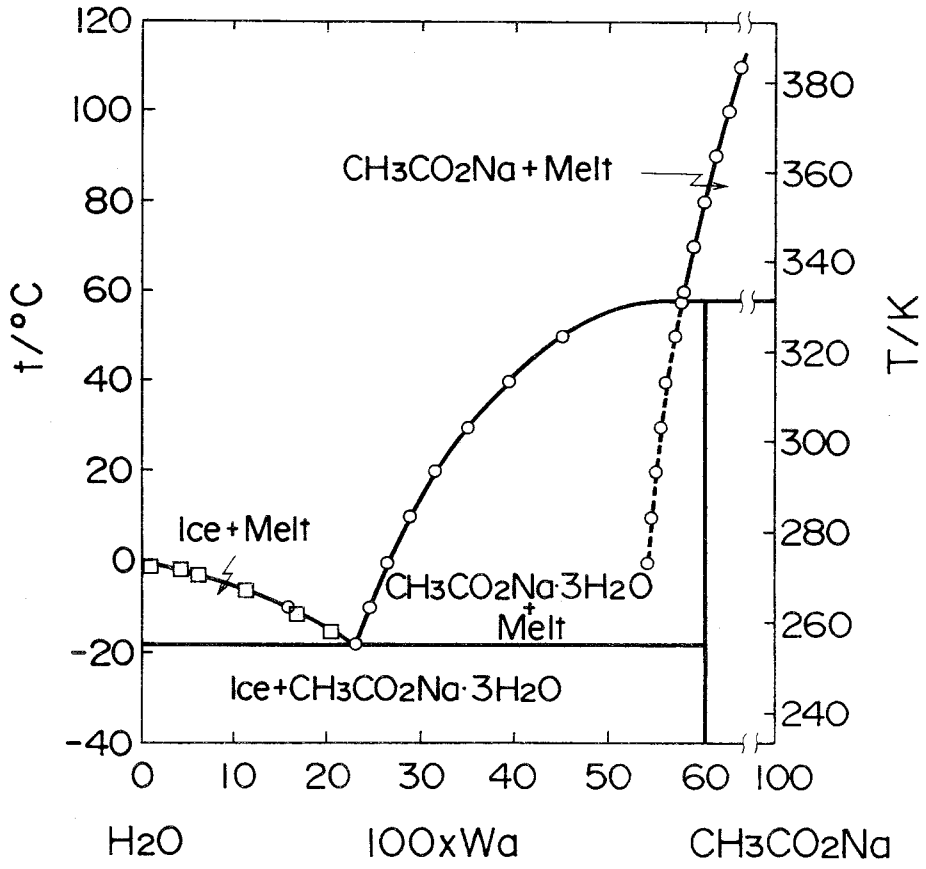

Fig. 1. **Phase diagram of the binary system CH_3CO_2Na-H_2O. ○: The data obtained by Green [18], □: the data obtained by Sidgwick and Gentle [19].**

As shown in Fig. 1 and Table 1, $CH_3CO_2Na \cdot 3H_2O$ has high heat of fusion (264 J/g) and its melting point is 58.4°C, which is an optimum temperature for space heating. $CH_3CO_2Na \cdot 3H_2O$ has the following advantages as a latent heat storage material.

a) It has high heat of fusion (264 J/g).

b) Its melting point (58.4°C) is an optimum temperature for heating.

c) It has high specific gravity (1.45 g/cm^3) [19].

Therefore, it has more heat storage capacity per unit volume.

d) Its corrosion is low. The stainless steel hardly rusts in $CH_3CO_2Na \cdot 3H_2O$ melt.

e) Its crystal growth velocity is high [10, 20].

f) It is not hygroscopic [21].

g) Its toxicity is low. It is used as a food additive [22].

h) It is regarded as a waste in many industries which use acetate anhydride in organic synthesis. Thus, it is expected to be relatively cheap [23].

I. 3 The Problems in Using $CH_3CO_2Na \cdot 3H_2O$ as a Latent Heat Storage Material

a. *Supercooling* The major problem in using $CH_3CO_2Na \cdot 3H_2O$ as a latent heat storage material is its poor nucleating properties resulting in supercooling of $CH_3CO_2Na \cdot 3H_2O$ melt prior to freezing [13, 24]. The same problem is observed on the other salt hydrates shown in Table 1. The prevention of the supercooling is very important, especially when the material is permanently sealed into its container [25]. Reversible melting and recrystallization must be attained around the melting point without opening the container [8, 9]. In addition, external influences can not be adapted, such as stirring, shaking, or applying other mechanical or physical means, except the delivery or withdrawal of thermal energy.

The following methods have been proposed to attain nucleation of salt hydrates including $CH_3CO_2Na \cdot 3H_2O$, when the heat storage materials are sealed into containers and cooled slightly below their melting points.

a) Seed crystal of the original salt hydrate is introduced to the melt [26]. It is called secondary nucleation.

b) Nucleation catalyst for the salt hydrate is added to the melt [8, 27]. The catalyst is a different material from the original substance. It is called heterogeneous nucleation [28]. These nucleation catalysts should not appreciably influence the melting point or the heat of fusion of the original salt hydrate.

c) Use of nucleating device also promote the nucleation. The device has tubular form and it is kept cooler than the melt. It retains seed crystals for subsequent nucleation [13]. This nucleating device is called "cold finger" [29].

The use of methods a) and c) are restricted to large scale heat storage application. The method b), the use of nucleation catalyst, is desirable. Because, according to the method b), the melt is prevented from supercooling without any restriction of heat storage system [10]. Some nucleation catalysts for $CH_3CO_2Na \cdot 3H_2O$ have been proposed [30-34]. However, a practical nucleation catalyst has not been found yet [13].

b. *Decomposition* Another important problem on $CH_3CO_2Na \cdot 3H_2O$ is the phase separation. As shown in Fig. 1, $CH_3CO_2Na \cdot 3H_2O$ melts incongruently and separates to a saturated solution and anhydrous solid phase [10]. When the partly incongruently melting $CH_3CO_2Na \cdot 3H_2O$ is subsequently cooled, recrystallization easily occurs with the stirring of the mixture. When it is cooled in closed container without stirring or mixing, a solid residue at the bottom of container is frozen, being surrounded by solid salt hydrate. Some of the residue, therefore, cannot recombine with its water of crystallization and some saturated solution remains, after the mixture has cooled below the melting point. In such cases, the crystallization processes are not completely reversible. Only a part of the heat required to melt the $CH_3CO_2Na \cdot 3H_2O$ can be recovered when the system is cooled. This phenomenon is called decomposition [5].

The decomposition of Glauber's salt ($Na_2SO_4 \cdot 10H_2O$), whose nucleation catalyst ($Na_2B_4O_7 \cdot 8H_2O$) was found 30 years ago [8], has been investigated by some investigators [35-38]. In these studies, following methods have been proposed to overcome the decomposition of salt hydrates.

a) Using the peritectic composition or its water rich side [35]. The system melts congruently.

b) Providing thickening agents such as attapulgite clay to increase the viscosity of the melt. The solid residue is homogeneously suspended in the melt [36, 37].

c) Using the rolling cylindrical container. The heat storage material is usually stirred in the rotating long cylinder [38].

In the method to use of nearly saturated solution rather than salt hydrate, the heat storage capacity for $Na_2SO_4 \cdot 10H_2O$ is decreased into a half of its actual value [35]. The application of method c) is restricted to a special case. The method b), the use of thickening agents, is considered to be desirable, because the melt is prevented from decomposition without any restriction of heat storage system. However, the study on decomposition of $CH_3CO_2Na \cdot 3H_2O$ has not been made yet.

c. *Lowering the Melting Point* An additional problem in using salt hydrates as a latent heat storage material is that the heat storage temperatures are restricted to their melting points (for example, the melting point of $CH_3CO_2Na \cdot 3H_2O$ is 58°C). A few attempts to lower the melting point of salt hydrates, without reducing the latent heat of fusion, has been made. The melting point of $Na_2SO_4 \cdot 10H_2O$ (mp: 32.4°C) can be depressed to as low as 13°C by the addition of suitable inorganic salts, NaCl and NH_4Cl [39]. This mixture was used as a heat storage material for air cooling in solar house, which was called "Solar One" [40]. The eutectic mixture of $Mg(NO_3)_2 \cdot 6H_2O$ (mp: 89.5°C, ΔH_m = 161 J/g) and $MgCl_2 \cdot 6H_2O$ (mp: 117°C, ΔH_m = 172 J/g) melts at 59.1°C and its heat of fusion is 144 J/g [41]. However, the attempt to lower the melting point of $CH_3CO_2Na \cdot 3H_2O$ has not been made yet. It is ideal that the melting point of salt hydrates can be controlled freely without reducing their heat of fusion.

I. 4 The Scope and Outline of the Present Thesis

$CH_3CO_2Na \cdot 3H_2O$ has many advantages as a latent heat storage material. They are large heat of fusion, high specific gravity and so on. However, there exist two severe problems in using it as a latent heat storage material. One is supercooling and the other is decomposition. Main objectives of the present study are: (1) overcoming the supercooling and decomposition of $CH_3CO_2Na \cdot 3H_2O$ in order to apply it to a latent heat storage material and (2) lowering the melting point of $CH_3CO_2Na \cdot 3H_2O$ without reducing the heat of fusion.

This thesis will describe firstly the crystallization behavior of $CH_3CO_2Na \cdot 3H_2O$ without any additive. Secondly the heterogeneous nucleation of $CH_3CO_2Na \cdot 3H_2O$ from the solution with an addition of a small amount of nucleation catalyst is presented. Thirdly, the change in the heat storage capacity will be mentioned on a few kinds of modified $CH_3CO_2Na \cdot 3H_2O$ during thermal cycling. Finally, the control of the melting point of $CH_3CO_2Na \cdot 3H_2O$ by additing some organic compounds will be described. The thesis consists of 6 chapters and the content of each chapter is as follows.

Chapter 2 presents the crystallization behavior of the binary system, CH_3CO_2Na-H_2O. Crystallization temperature was measured on slow cooling from a melt. Glass transition temperature and crystallization temperature were measured on slow heating from the quenched vitrified solids.

In Chapter 3, a survey of a nucleation catalyst of $CH_3CO_2Na \cdot 3H_2O$ is performed considering the nucleation mechanism. Characteristics of the nucleation catalyst are clarified. Particularly, the effect of thermal history upon the kinetics of heterogeneous nucleation of $CH_3CO_2Na \cdot 3H_2O$ from the solution with an addition of the nucleation catalyst is described in detail. The heterogeneous nucleation mechanism of $CH_3CO_2Na \cdot 3H_2O$ from the solution is discussed on the basis of the experimental results. The new

heterogeneous nucleation model is proposed.

In Chapter 4, the decrease of heat storage capacity of the following three samples during thermal cycling is described. Sample *a*; guaranteed grade $CH_3CO_2Na \cdot 3H_2O$, sample *b*; technical grade $CH_3CO_2Na \cdot 3H_2O$ and sample *c*; technical grade $CH_3CO_2Na \cdot 3H_2O$ thickened by using polyvinyl alcohol.

In Chapter 5, a partial phase diagram of the ternary system, CH_3CO_2Na-H_2O-organic compound [$CO(NH_2)_2$ or $HCONH_2$], is presented to find the posibility to lowering the melting point of $CH_3CO_2Na \cdot 3H_2O$. In the pseudo-binary system, $CH_3CO_2Na \cdot 3H_2O$-$CO(NH_2)_2$, the heat of fusion of the eutectic mixture and the crystallization behavior is reported in detail. In the pseudo-binary system, $CH_3CO_2Na \cdot 3H_2O$-$HCONH_2$, the heat of fusion of the new addition compound, $CH_3CO_2Na \cdot HCONH_2 \cdot 3H_2O$, and the crystallization behavior are described. Summary and conclusion for the present study are presented in Chapter 6.

CHAPTER II CRYSTALLIZATION BEHAVIOR IN THE BINARY SYSTEM CH_3CO_2Na-H_2O

II. 1 Introduction

Sodium acetate trihydrate is known to crystallize hardly from the aqueous solution [24]. If $CH_3CO_2Na \cdot 3H_2O$ is placed in a sealed tube and heated to 58°C, it loses the water of crystallization and partially dissolves in this water. At 80°C all the salt is dissolved. On cooling in the sealed tube, anhydrous CH_3CO_2Na is separated out from the solution. This anhydrous form appears, whether the solution is cooled rapidly or slowly. The crystals remain unaltered as long as the tube is kept sealed. Cooling below 0°C has no effect, but cooling in liquid ammonia or liquid air brings about conversion to the stable trihydrate. In addition, Hook [42] reported that several sealed samples of CH_3CO_2Na aqueous solution, which were saturated at 35°C, had been kept at room temperature without crystallization for 13 years.

Recently Kimura [34, 43] studied the supercooling phenomena of some salt hydrates such as $CH_3CO_2Na \cdot 3H_2O$ from the view point of the chemical potential difference of water molecules in molten and crystalline states.

This chapter reports a quantitative investigation of the crystallization behavior of the binary system, CH_3CO_2Na-H_2O, where crystallization temperature on slow cooling from a melt (t_c), glass transition temperature (T_G), and crystallization temperature on slow heating from a quenched vitrified solid (T_c) were measured by varying the CH_3CO_2Na concentration.

II. 2 Experimental Procedure

Sodium acetate trihydrate was of a guaranteed grade reagent from Wako Pure Chemical Industry. Weighed quantities of $CH_3CO_2Na \cdot 3H_2O$ and distilled water, 30 g in total, were placed in a glass vessel with a stirring bar. The sample temperature was measured by a chromel-alumel thermocouple attached to the inner wall of the glass vessel which was sealed and immersed in a water bath. In order to obtain reproducible data, the sample was heated to a temperature which was about 10°C higher than its liquidus temperature and was stirred to a homogeneous melt [44]. Then, the melt was cooled at the rate of about 5°C/min by consecutive addition of ice to the water bath. When the temperature of the melt reached to 20°C, the vessel was transferred from the water bath to an ethanol bath. Cooling was continued to −70°C at the rate of about 5°C/min by consecutive addition of solid carbon dioxide to the ethanol bath. In such a slow cooling process, crystallization was detected by a sudden rise in temperature of the sample and by visual inspection. The viscosity of melts increased on cooling, which contained CH_3CO_2Na more than $W_a = 0.35$ (W_a is the mass fraction of CH_3CO_2Na), and sometimes the magnetic stirrer failed to operate the stirring bar. The measurement was performed three times for each sample. In this manner, t_c was measured as a function of CH_3CO_2Na concentration. Figure 2 shows crystallization temperatures obtained by the present measurements.

Temperatures, T_G and T_c were measured as a function of the CH_3CO_2Na concentration by the differential scanning calorimetry (DSC). The DSC measurement was performed by using an SSC 560S DSC (Daini Seikosha Co.), which is a heat-flux DSC. One drop of a melt (about 10 mg) was placed in a 15 μl silver crucible. This crucible was sealed and immersed in a water bath, whose temperature was about 10°C higher than a liquidus temperature of the sample. After thirty minutes, the crucible was transferred into liquid nitrogen. The overall cooling rate was about 1000 K/min. DSC measurements were per-

formed at a heating rate of 5°C/min from −130°C to 70°C. This DSC system was calibrated by using ice (mp: 0.0°C), chloroform (mp: −63.5°C), acetone (mp: −94.3°C), and ethanol (mp: −114.2°C) as standards, and the measurements were made two times for each sample.

II. 3 Results and Discussion

II. 3. 1 Crystallization Temperature on Slow Cooling from a Melt (t_c)

The values of obtained t_c are shown in Fig. 2. The numbers on the abscissa, $100 \times W_a$, are the weight percentage of CH_3CO_2Na in the system. The samples of $W_a = 0.35$ and $W_a = 0.40$ did not crystallize in all the runs.

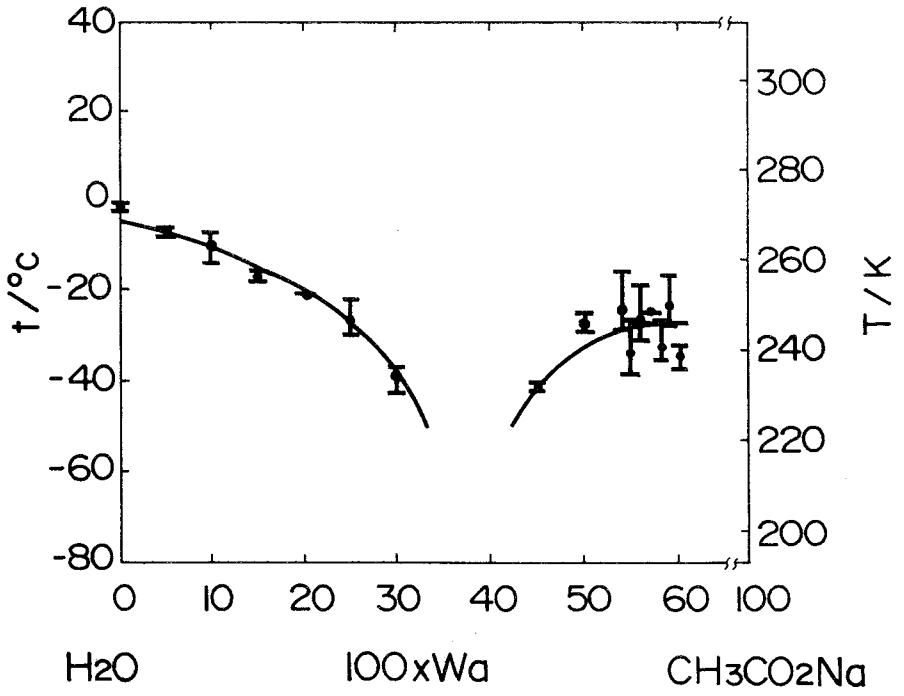

Fig. 2. Crystallization temperature on slow cooling (t_c) in relation to the CH_3CO_2Na concentration.

In the water-rich side of the eutectic composition, ice is crystallized at about 5°C lower temperature than the liquidus line of H_2O. Interestingly, the t_c curve extends beyond the eutectic composition into the CH_3CO_2Na-rich side. Therefore, the crystals that separated out first from the melt in the CH_3CO_2Na rich side of the eutectic composition (W_a= 0.30) is not $CH_3CO_2Na \cdot 3H_2O$, but ice.

From Fig. 2, it is also clear that t_cs of the melts containing CH_3CO_2Na in amount more than W_a= 0.45 are about −30°C, i.e., supercooling of these samples is about 90°C. $CH_3CO_2Na \cdot 3H_2O$ separated out first from both melts of W_a = 0.45 and W_a = 0.50, but from the samples containing CH_3CO_2Na in amount more than W_a = 0.54, anhydrous CH_3CO_2Na crystals separated out at about 10°C lower than their liquidus temperatures, and it was followed by crystallization of $CH_3CO_2Na \cdot 3H_2O$. Anhydrous CH_3CO_2Na crystals were identified by X-ray diffraction. Since the t_c curve varies continuously with the CH_3CO_2Na concentration between W_a = 0.45 and W_a = 0.603 ($CH_3CO_2Na \cdot 3H_2O$), the curve in Fig. 2 also suggests that anhydrous CH_3CO_2Na crystals have little influence on the subsequent crystallization of $CH_3CO_2Na \cdot 3H_2O$.

II. 3. 2 Glass Transition Temperature (T_G)

DSC curves for some quenched samples are illustrated in Fig. 3, where q is a heat flux. T_G and T_c are plotted against the CH_3CO_2Na concentration in Fig. 4. The melt with W_a= 0.25 vitrified by quenching, but the melt with W_a= 0.20 did not, and this result was confirmed by visual observation of these samples in a 3 mm diameter pyrex glass tube put into liquid nitrogen. This observation shows that the glass forming composition is limited to the CH_3CO_2Na-rich side from the eutectic composition (W_a= 0.23). This is due to the difficulty of crystal nucleation of $CH_3CO_2Na \cdot 3H_2O$.

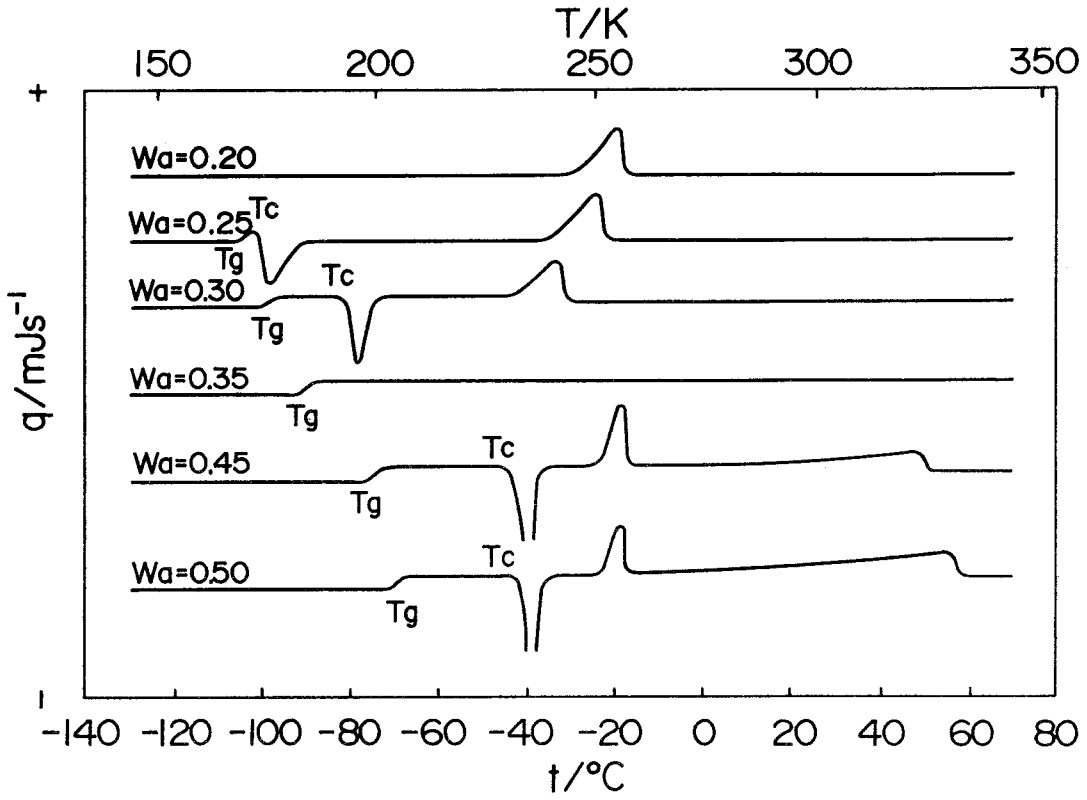

Fig. 3. DSC curves for some quenched samples of the system CH_3CO_2Na-H_2O.

In Fig. 4, T_G varies linearly with the CH_3CO_2Na concentration, and those of the samples containing CH_3CO_2Na in amount more than W_a= 0.55 lie below the T_G line. This deviation results from the decrease of the CH_3CO_2Na concentration caused by separation of CH_3CO_2Na crystals from the quenched samples, which is confirmed by visual observation using thin glass tubes. Williams and Angell, [45] and Kanno et al. [46] have reported that T_G of the sample with W_a= 0.313 ($CH_3CO_2Na \cdot 10H_2O$) is −99 and −102°C, respectively. The T_G estimated from our data is −96°C and it is in good agreement with the reported data. The extrapolation of the obtained T_G to pure water gives −140°C as the T_G of glass water. Angell and Sare [47] also gave a similar value (−138°C) from the studies

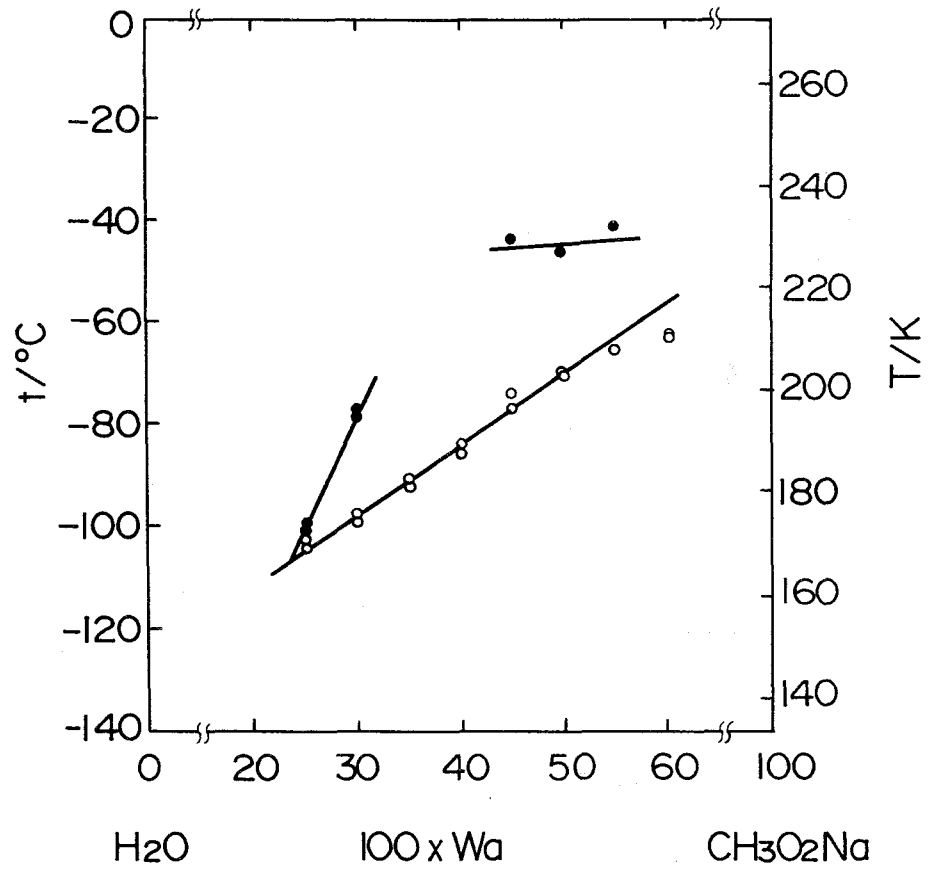

Fig. 4. **Glass transition temperature (T_g) and crystallization temperature on slow heating (T_c) in relation to CH_3CO_2Na concentration.**
○: T_G, ●: T_c.

on a large number of aqueous electrolyte solutions. This value is almost identical with the glass transition temperature (−139°C) obtained for amorphous solid water prepared by the vapor deposition method [48]. The extrapolation to pure $CH_3CO_2Na \cdot 3H_2O$ gives −56°C as the T_G of glassy $CH_3CO_2Na \cdot 3H_2O$.

II. 3. 3 Crystallization Temperature on Slow Heating from a Quenched Sample (T_c)

The quenched samples with W_a= 0.25 and W_a= 0.30 always crystallize on heating after the glass transition. T_c of the sample with W_a= 0.313 ($CH_3CO_2Na \cdot 10H_2O$) has been reported to be −73°C by Kanno et al., [46] which is in good agreement with the T_c estimated from our data, −72°C. The DSC curves show that the melting points of the samples with W_a = 0.25 and W_a = 0.30 are at −22 and −31°C, respectively. These melting points are lower than the eutectic point, −18°C, and lie on the extrapolated liquidus line of H_2O. As shown in Fig. 3, the samples with W_a= 0.25 and W_a= 0.30 do not show the endothermic peak of $CH_3CO_2Na \cdot 3H_2O$ melting. Therefore, ice is the only compound crystallized from the melts with W_a= 0.25 and W_a= 0.30. This result is similar to the crystallization behavior observed on slow cooling of the melt.

The quenched samples with W_a= 0.35 and W_a= 0.40 did not crystallize on heating twice. As mentioned above, these samples did not crystallize on cooling. The quenched samples with W_a= 0.45, W_a= 0.50, and W_a= 0.55 crystallized only once in two runs. In these cases, T_cs are between −40 and −50°C as shown in Fig. 4. $CH_3CO_2Na \cdot 3H_2O$ (W_a= 0.603) did not crystallize on heating in two runs.

II. 3. 4 Relation Between Crystallization Temperature Curves and Phase Diagram

The phase diagram of the binary system CH_3CO_2Na-H_2O (Fig. 1), t_c curves (Fig. 2), and T_G line and T_c curves (Fig. 4) are summarized in Fig. 5. In the temperature region demarcated by t_c and T_c curves, ice or $CH_3CO_2Na \cdot 3H_2O$ is considered to crystallize from the melt in the present experimental condition. The crystallization behavior of the binary system CH_3CO_2Na-H_2O is characterized as follows: (1) the crystallization region of ice extends into the CH_3CO_2Na-rich side from the eutectic composition, (2) a severely super-

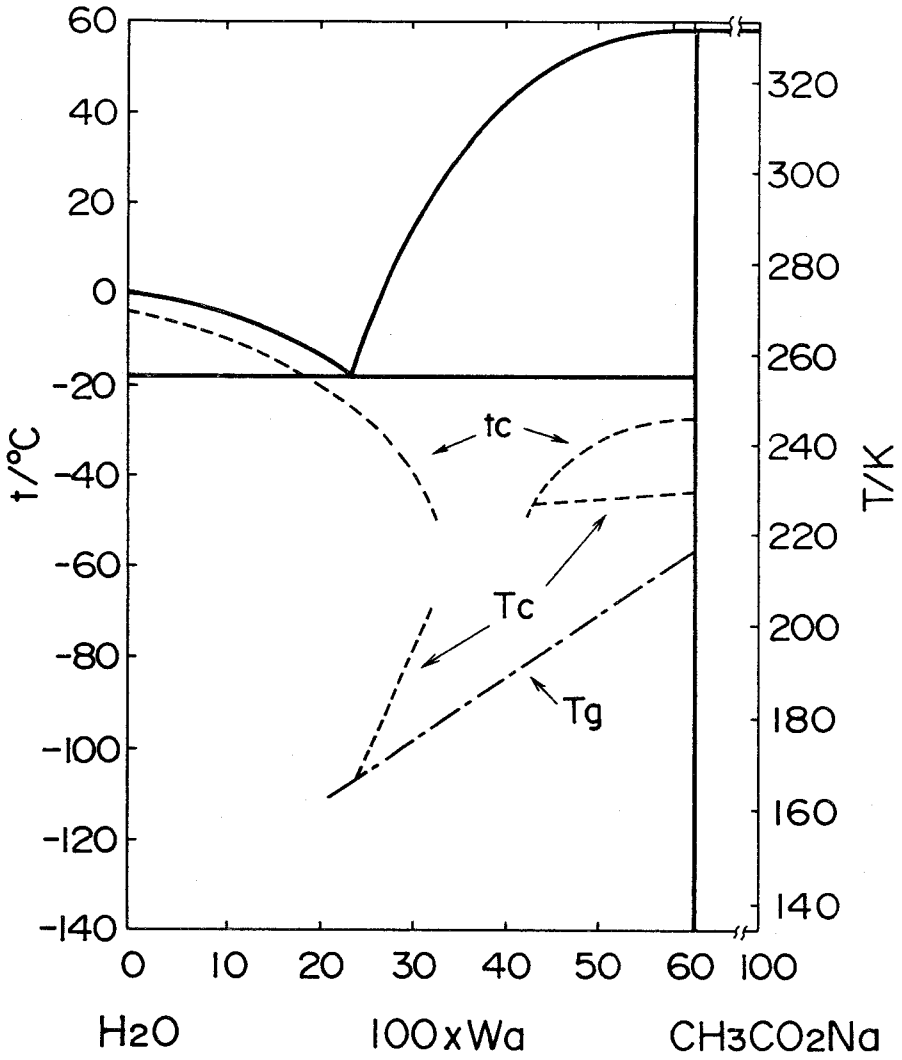

Fig. 5. **Crystallization temperature curves (t_c and T_c curves), and glass transition temperature line shown in the phase diagram of the binary system CH_3CO_2Na-H_2O.**

cooling region exists in the composition between $W_a = 0.35$ and $W_a = 0.40$, (3) the crystallization temperature range of $CH_3CO_2Na \cdot 3H_2O$ is from $-50°C$ to $-30°C$ and very narrow.

The crystallization temperature is generally influenced by the heating and cooling rate, quantity and purity of the sample, stirring method, and so on [49, 50, 51]. In measuring

t_c, if the cooling rate is slower than 5°C/min or the sample quantity is larger than 30 g, t_cs will be higher than the obtained values. In measureing T_c, if the heating rate is slower than 5°C/min or the sample quantity is larger than about 10 mg, T_cs will be lower than the obtained values. Therefore, crystallization temperature breadths of ice and $CH_3CO_2Na \cdot 3H_2O$ are expected to be wider than those shown in Fig. 5.

CHAPTER III HETEROGENEOUS NUCLEATION of $CH_3CO_2Na \cdot 3H_2O$

III. 1 Introduction

As shown in previous chapter, $CH_3CO_2Na \cdot 3H_2O$ melt tends to supercool even if it is cooled considerably below its melting point. Its practical application to latent heat storage has been impaired by this supercooling phenomenon. A desirable approach to this problem is to add a suitable nucleation catalyst to $CH_3CO_2Na \cdot 3H_2O$.

The heterogeneous nucleation of $CH_3CO_2Na \cdot 3H_2O$ has been investigated by several investigators from the 19th entury [27, 32, 52-54]. Gernetz [52] compiled a list of 27 groups within which corresponding crystallization occured, on the basis of observations on the crystallization behavior of over 100 kinds of salt. Boisbaudran [53] indicated that the Mitscherlich type isomorphism was required for corresponding nucleation, although many exceptions were noted. In addition, he pointed out that especially confusing exception was that sodium acetate, which was almost isomorphous with sodium formate or sodium valerate, did not nucleate and grow in these solutions, or vice versa. Many kinds of nucleation catalyst for $CH_3CO_2Na \cdot 3H_2O$, for example, $CaCl_2$ [30], a mixture of Na_2SO_4 and $Na_2SO_4 \cdot 10H_2O$ [32], and $MnCl_2 \cdot 4H_2O$ [33], have already been patented. However, these nucleation catalysts are not practicable, because, in the $CH_3CO_2Na \cdot 3H_2O$ melt with an addition of these nucleation catalysts, $CH_3CO_2Na \cdot 3H_2O$ crystallizes at fairly lower temperature than the melting point of $CH_3CO_2Na \cdot 3H_2O$ [34], or do not crystallize stably at the temperature near the melting point during thermal cycling.

Therefore, in this chapter, it will be firstly tried to apply the theory for heterogeneous nucleation, which has been already established, to the nucleation of $CH_3CO_2Na \cdot 3H_2O$. Search for the practical nucleation catalyst of $CH_3CO_2Na \cdot 3H_2O$ is performed considering the mechanism. Some kinds of practicable nucleation catalyst are found out and their characteristics are shown, such as the effect of thermal history upon kinetics of hetero-

geneous nucleation of $CH_3CO_2Na \cdot 3H_2O$ from the melt with an addition of the nucleation catalyst. Heterogeneous nucleation mechanism is discussed and the modified adsorption model is proposed, taking into account commensurate-incommensurate phase transition of solid adsorbate.

III. 2 Theory and Model of Heterogeneous Nucleation

III. 2. 1 Types of Nucleation

Types of nucleation are summarized in Fig. 6 [55]. Homogeneous nucleation is the process by which nucleation occurs because of configurational fluctuations in a homogeneous melt. The nuclei in this process are small, transient aggregates of atoms or molecules which form spontaneously in the melt. They do not depend on the surfaces, the container, or foreign particles.

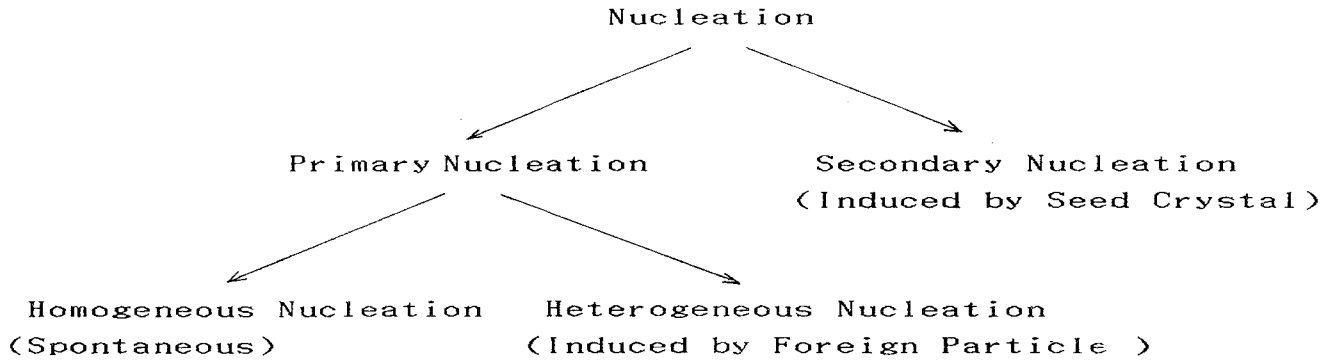

Fig. 6. Types of nucleation.

In heterogeneous nucleation, the nuclei are also formed by configurational fluctuations in the liquid but in this case the fluctuations occur at a surface or on some foreign object in the liquid. The nucleation depends on the existence of foreign matter and is

therefore termed heterogeneous.

Secondary nucleation is defined as the generation of nuclei by the crystals already present in the liquid. This process is important in bulk crystallization (industrial crystallization) [56].

III. 2. 2 Theory of Homogeneous Nucleation

The stability of a nucleus in a supercooled melt depends on two factors. The free energy of liquid decreases when the melt transforms to solid but, for too small particles of solid, the surface energy of such a particle dominates. Small particles can decrease the total free energy of the system by reducing their surface area. Large particles can reduce the free energy of the system by growing the crystal. A balance between these tendencies defines the critical nucleus.

The change in free energy of the system due to a spherical particle of radius r is

$$\Delta G_{homo}(r) = \frac{4\pi r^3}{3v} \Delta\mu + 4\pi r^2 \sigma$$

where $\Delta\mu$ is the difference between the chemical potentials of liquid and solid, v is the volume of a atom or a melecule, and σ is the specific surface energy [57].

The chemical potential difference depends on supercooling and is given by

$$\Delta\mu = \frac{\ell(T_E - T)}{T_E}$$

where ℓ is the latent heat of fusion per one atom or molecule and T_E is the equilibrium temperature between the solid and liquid [58].

The rate of formation of critical size nuclei has been discussed by many investigators [59]. The rate of nucleation is given approximately by

$$J_{homo} = n \nu \exp(-Q_D/kT) \exp(-\Delta G^*_{homo}/kT)$$

$$= J_o \exp(-\Delta G^*_{homo}/kT)$$

where n is the number of moledule in the system; ν is the Debye frequency, kT/h; Q_D is the activation energy for diffusion in the liquid; and ΔG^*_{homo} is the free energy of the cluster of critical size.

III. 2. 3 Basic Theory of Heterogeneous Nucleation

Nucleation which is initiated by foreign nuclei (heterogeneous nucleation) arises from the catalytic effect of their surfaces, as well as from the walls of vessel, grain boundaries, pores and so on. The essential condition is that the surface must be wetted by the growing crystal formed in the presence of liquid.

Volmer [60] has considered the case of a flat surface, S, upon which an embryo of crystal, C, is formed with a contact angle, θ, between the two phases. This condition is shown in Fig. 7 [61]. The interfacial energy equation:

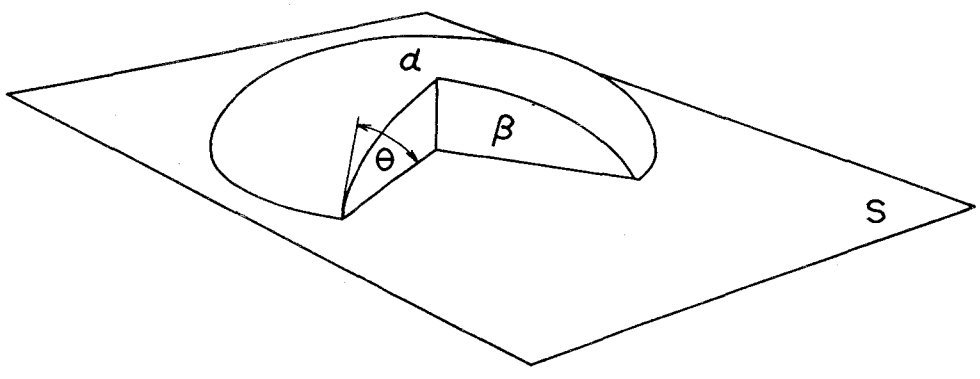

Fig. 7. Heterogeneous nucleation from the α phase on a flat substrate S. The necleus β makes a contact angle θ with the substrate.

$$\sigma_{L,S} = \sigma_{C,S} + \sigma_{L,C} \cos\theta$$

then hold. When this expression is considered, the free energy of formation of a nucleus on the flat surface is:

$$\Delta G_{hetero} = \Delta G_{homo} [(2+\cos\theta)(1-\cos\theta)^2/4]$$

$$= \Delta G_{homo} f(\theta)$$

where ΔG_{homo} is the free energy of homogeneous nucleation, which was explained in previous paragraph (III. 2. 2). As θ decreases to zero, the factor involving $\cos\theta$ also decreases monotonically to limit zero. This means that for an embryo of crystal that spreads perfectly upon the surface of the nucleation catalyst, no activation energy is necessary.

The principal effect of the catalyst is therefore to change the nucleation rate, J_{hetero}:

$$J_{hetero} = J_o \exp(-\Delta G_{hetero}/kT)$$

$$= J_o \exp(-f(\theta) \cdot \Delta G^*_{homo}/kT)$$

$$> J_{homo}$$

III. 2. 4 Epitaxy

Gernetz [52] noted that an isomorphic nuleus was more effective for nucleation than a nonisomorphic nucleus, but required a higher degree of supersaturation than a nucleus of the salt itself. Royer [62] called this phenomenon "epitaxis" and gave serveral examples.

Vonnegut [63] searched for a crystal resembling ice most closely in its crystal structure for the purpose of inducing rainfall. He thought that a crystal resembling ice in its crystal data accelerated the crystallization of supercooled water particles in the cloud. He found that the crystal structure of silver iodide differed from that of ice only in minor

differences. Ice is crystallized at about −5°C in water with an addition of a small amount of silver iodide. The crystallografic data of H_2O and AgI are shown in Table 2 [64].

Table 2. Crystallographic data for ice, silver iodide and lead iodide

	Ice	AgI	PbI_2
Crystal system	Hexagonal	Hexagonal	Hexagonal
Unit-cell parameter			
a/Å	4.52	4.58	4.54
c/Å	7.36	7.49	6.86
Basal misfit [a)]	—	1.4	0.5
Prism misfit [b)]	—	0.5	3.6

a) Difined as $100\times(a-a_o)/a_o$ where suffics o refer to ice

b) Difined as $100\times[(a-a_o)/a_o+(c-c_o)/c_o]/2$ where suffix o refers to ice.

Glauber's salt ($Na_2SO_4\cdot10H_2O$) may not crystallize from an aqueous solution until the solution is supercooled down to 18°C which is 14°C below the equilibrium temperature [50]. Telkes [8] found that the addition of 2–3 % borax ($Na_2B_4O_7\cdot10H_2O$) reduced the supercooling necessary for recrystallization to 1 or 2°C. She pointed out that the effectiveness of borax in nucleating $Na_2SO_4\cdot10H_2O$ was plausible from a crystallographic point of view. The crystallographic data of $Na_2SO_4\cdot10H_2O$ and $Na_2B_4O_7\cdot10H_2O$ are shown in Table 3 [65]. As shown in Table 3, the crystallographic data of $Na_2SO_4\cdot10H_2O$ and that of $Na_2B_4O_7\cdot10H_2O$ are quite similar except for a space group. Moreover, these two compounds have remarkably similar chains which are formed by sharing the two edges of $Na(H_2O)_6$ octahedra. It has been pointed out that the similarity in crystallographic data is the cause of the nucleation catalysis [65].

The basic theory of heterogeneous nucleation was elaborated in great detail, taking into account crystallographic data [66, 67]. It has frequently been assumed that the correspondence in this fit or misfit of lattice distances must be less than a definite limit for nucleation. However, the considerable latitude, which is observed in many systems, suggests that factors other than this distance, for example, electronegativity of the atoms in the system, must be involved [68].

Table 3. Crystallographic data for sodium sulfate decahydrate and sodium tetraborate decahydrate

		$Na_2SO_4 \cdot 10H_2O$	$Na_2B_4O_7 \cdot 10H_2O$
Crystal system		Monoclinic	Monoclinic
Space group		P2/c	C2/c
Unit-cell parameter	a/Å	11.512	11.885
	b/Å	10.370	10.654
	c/Å	12.847	12.206
	β/°	107.79	106.62
	V/Å^3	1460	1481
	Z	4	4

III. 2. 5 Cavity Model

It has been recognized that a melt or solution that has once been crystallized will recrystallize more easily than the initial crystallization. This behavior has been called as the vague term "memory effect" [69].

The effect of thermal history upon the kinetics of many liquid-solid bulk transformations is illustrated shematically in Fig. 8 [70]. $\Delta\theta_h$ is the difference between heating temperature, θ_h, and melting point, θ_m. θ_c is the temperature that a liquid must be

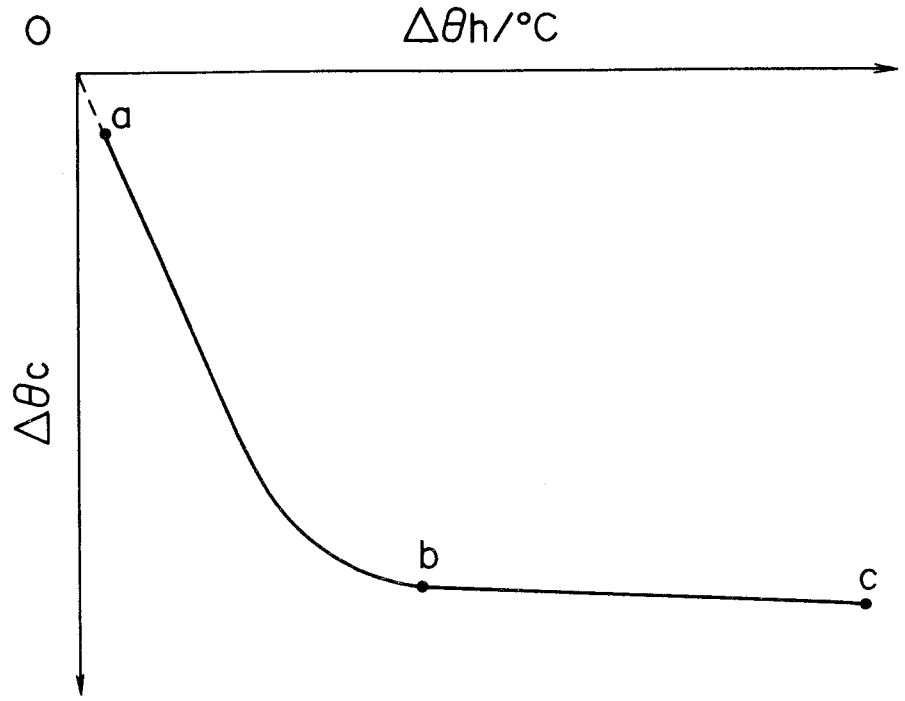

Fig. 8. Effect of thermal history on temperature of rapid nucleation in liquid and solid transformation.

subsequently supercooled in order to get nucleation during some specified holding time at the lower temperature. $\Delta\theta_c$ is the difference between θ_c and θ_m. $\Delta\theta_c$ is strongly dependent upon $\Delta\theta_h$ in the region of the curve *ab* where heating temperature, θ_h, is slightly higher than the melting point. However, it is virtually independent of $\Delta\theta_h$ in the region *bc*.

Turnbull [70] explained theoretically the effect of thermal history upon the kinetics of heterogeneous nucleation which was shown in Fig. 8. He considered that the crystalline embryos could be retained above the bulk melting point in the cavities of suitable extraneous solid present in the melt. This condition is shown in Fig. 9 [71]. Retained crystalline embryos may nucleate the crystals nearly below the melting point. When, in this theory, certain assumptions are given concerning the size of fissures and contact angle of the crystal thereon, estimation of the crystallization temperature can be made [72].

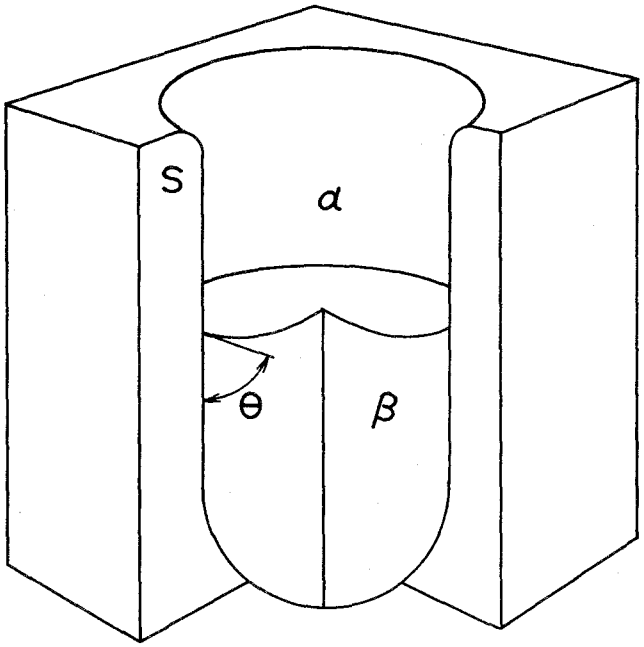

Fig. 9. **Heterogeneous nucleation in a cylindrical cavity, after Turnbull [70]. The nomenclature is the same as for Fig. 7.**

III. 2. 6 Crystalline Adsorption Model

The other explanation to be applied to the effect of thermal history of heterogeneous nucleation is crystalline adsorption model [25, 73, 74]. In the model, the nucleation catalyst is considered to be an active adsorbent and the surface of it is filled with liquid or crystalline adsorbate depending on its previous treatment. The reasonable assumption is made that the entropy change of the transition from free liquid to free crystal, ΔS_m, is not greatly different from that of adsorbed liquid to that of adsorbed crystal, ΔS_m^{ad}. It is further postulated that the heat of adsorption of crystalline adsorbate, ΔH^{ad} (crystalline), is greater than that of liquid adsorbate, ΔH^{ad} (liquid).

$$\Delta H_m^{ad} = \Delta H_m + \Delta H^{ad}(\text{liquid}) - \Delta H^{ad}(\text{cryst.})$$
$$> \Delta H_m$$

where, ΔH_m^{ad} is the heat of transition of crystalline adsorbate and ΔH_m is the heat of fusion of bulk crystal.

$$T_m^{ad} = \frac{\Delta H_m^{ad}}{\Delta S_m^{ad}} \approx \frac{\Delta H_m^{ad}}{\Delta S_m} > \frac{\Delta H_m}{\Delta S_m} = T_m$$

where T_m^{ad} and T_m are the transition temperature of adsorbate and the melting point of bulk crystal, respectively. So, the crystalline $CH_3CO_2Na \cdot 3H_2O$ adsorbed on the adsorbent (nucleation catalyst) is not allowed to fuse at its ordinary melting point. This situation is illustrated in Fig. 10 (A) and (B).

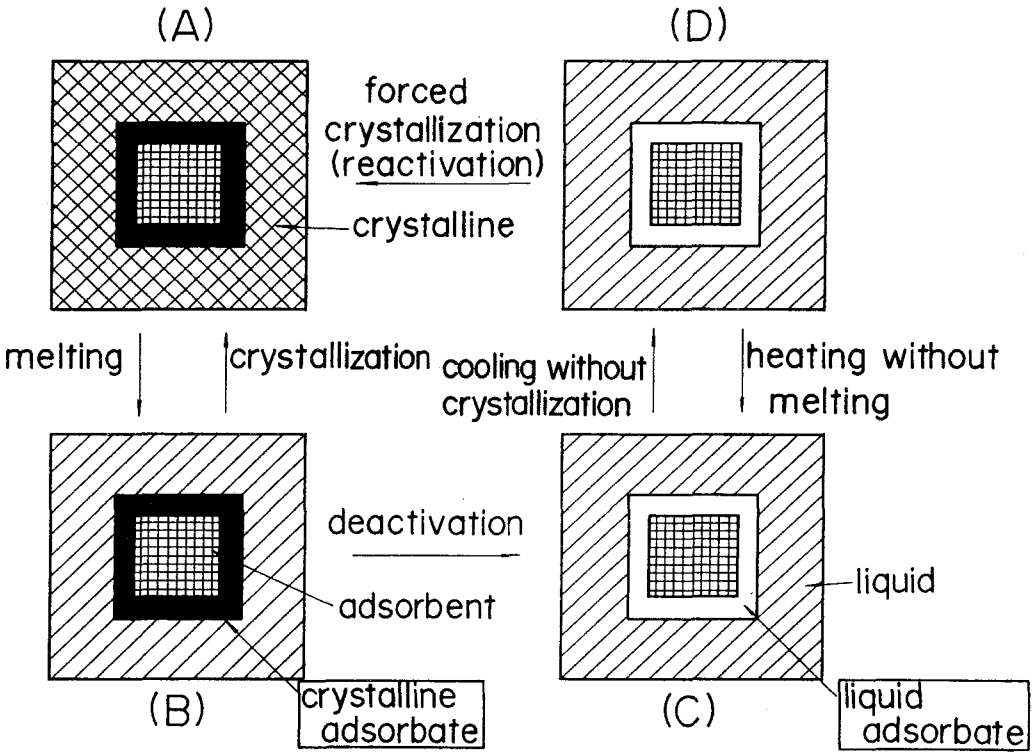

Fig. 10. **The crystalline adsorption model for heterogeneous nucleation.**
(A): crystalline state, (B): melting state with crystalline adsorbate,
(C): melting state with liquid adsorbate, (D): supercooled state.

When crystalline adsorbate has been fused entirely at an elevated temperature, $CH_3CO_2Na \cdot 3H_2O$ hardly crystallizes from the solution. It is shown in Fig. 10 (C) and (D). However, even if the crystalline adsorbate has entirely been fused, it will again be formed during the cooling process because of forced crystallization of $CH_3CO_2Na \cdot 3H_2O$ from the solution containing the nucleation catalyst. This is shown in Fig. 10 (D) and (A).

This model has been received little consideration because thermodynamic properties of adsorbed layer have hitherto been speculative. Evans et al. [75-77] studied the ability of a solid substrate to nucleate ice in supercooled water under high pressure, and explained the results on the basis of an assumption that, on certain substrates, the heterogeneous nucleation of ice was preceded by a change of state (order-disorder transition) of the water monolayer adsorbed on the substrate.

III. 3 Search for the Crystal Nucleation Catalyst of $CH_3CO_2Na \cdot 3H_2O$

The basic theory of heterogeneous nucleation can not give enough explanation about the mechanism of nucleation catalyst. This theory does not directly serve as a tool for search for the nucleation catalyst of $CH_3CO_2Na \cdot 3H_2O$. The crystallographic data of $CH_3CO_2Na \cdot 3H_2O$ is shown in Table 4. In the crystal structure of $CH_3CO_2Na \cdot 3H_2O$, Na^+ ion has distorted octahedral coordination with six oxygen atoms which consist of one acetate oxygen and five water molecules, and adjacent octahedra share an edge and form a continuous chain along the z axis [78, 79]. The substance whose crystal structure resembles to that of $CH_3CO_2Na \cdot 3H_2O$ is difficult to be discovered. The crystal system of $CH_3CO_2Na \cdot 3H_2O$ is monoclinic and coincidence of four parameters, a, b, c, and β is required, and, in addition, its crystal structure is very complex. Further, the substance resembling to $CH_3CO_2Na \cdot 3H_2O$ in crystallographic data does not always work as a practicable nucleation catalyst, even if it is fortunately found out [53].

Table 4. Crystallographic data for sodium acetate trihydrate

		$CH_3CO_2Na \cdot 3H_2O$
Crystal system		Monoclinic
Space group		C2/c
Unit-cell parameter	a/Å	12.353
	b/Å	10.466
	c/Å	10.401
	β/°	111.69
	V/Å^3	1249.5
	Z	8

Neither cavity model nor adsorption model does not also serve as a direct tool for search for the nucleation catalysts but they are very helpful to judge whether the substance is applicable to the nucleation catalyst or not. Therefore, the search for the nucleation catalysts of $CH_3CO_2Na \cdot 3H_2O$ was made, taking into account the effect of thermal history on heterogeneous nucleation kinetics. The procedure of the search for them is shown in Fig. 11. It is different from the preveious procedure that, at the present search, the effect of thermal history or "memory effect" was taking into account. At the present search, it was examined whether the candidate for the catalyst would work effectively on the crystal nucleation after the coagulum containing $CH_3CO_2Na \cdot 3H_2O$ and the candidate for the catalyst had been aged sufficiently.

In this manner, it was firstly found that addition of $Na_4P_2O_7 \cdot 10H_2O$ (later, it is found that $Na_4P_2O_7$ is also effective) was very effective for preventing the supercooling of $CH_3CO_2Na \cdot 3H_2O$ melt. Afterward, Kimura [80] reported that addition of a mixture of Na_2HPO_4 and anhydrous CH_3CO_2Na was also effective. I found that only Na_2HPO_4

served, without anhydrous CH_3CO_2Na, as a nucleation catalyst of $CH_3CO_2Na \cdot 3H_2O$. Recently, we have found out that Na_2WO_4 and LiF are independently effective. The catalytic activity of these compounds is stable in a high temperature region where the former nucleation catalysts, $Na_4P_2O_7 \cdot 10H_2O$ and Na_2HPO_4, do not work.

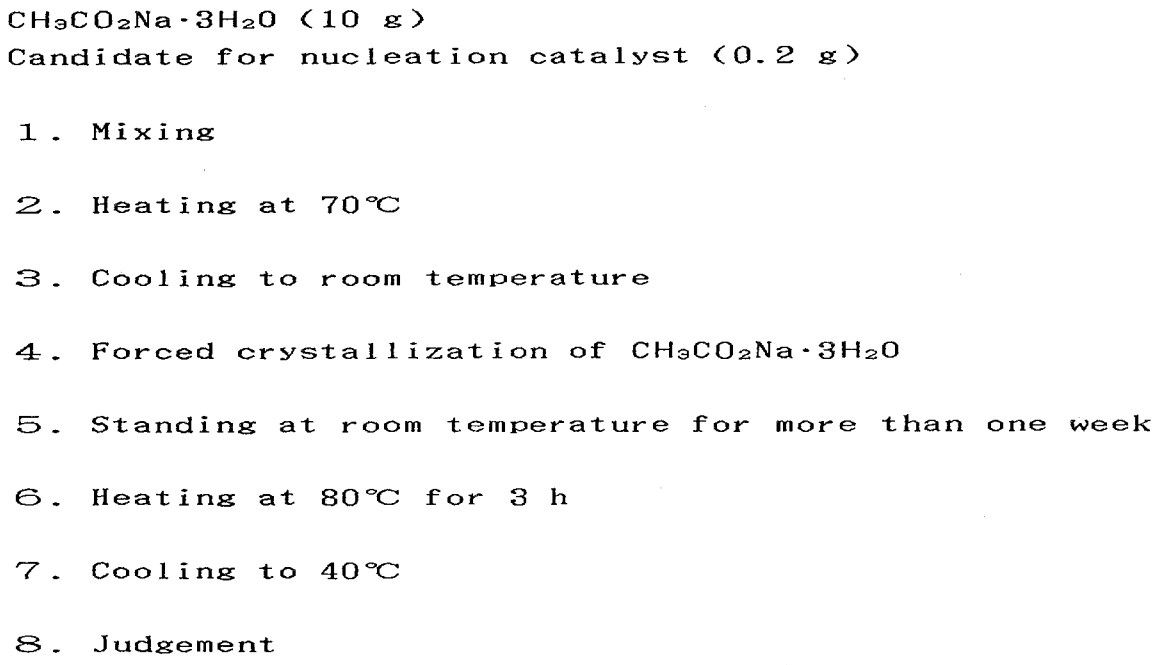

Fig. 11. Search procedure for the nucleation catalyst of $CH_3CO_2Na \cdot 3H_2O$, taking into account the effect of thermal history on heterogeneous nucleation kinetics.

III. 4 Heating and Cooling Cycles of $CH_3CO_2Na \cdot 3H_2O$ Accompanied with a Small Amount of the Nucleation Catalyst

$CH_3CO_2Na \cdot 3H_2O$ accompanied with a small amount of the nucleation catalyst in a sealed glass vessel was heated and cooled consecutively. The sample temperature was recorded as a function of time. The stability of the activity of nucleation catalysts during

these thermal cycling is the most important factor to the latent heat storage material. In this paragraph, the results obtained in the case when $Na_4P_2O_7 \cdot 10H_2O$ was used as a nucleation catalyst are presented.

III. 4. 1 Experimental Procedure

Both reagents of $CH_3CO_2Na \cdot 3H_2O$ and $Na_4P_2O_7 \cdot 10H_2O$, supplied from Wako Pure Chemical Industries Ltd., were of guaranteed grade.

Weighed quantities of $CH_3CO_2Na \cdot 3H_2O$ and $Na_4P_2O_7 \cdot 10H_2O$ were placed in a glass vessel and the sample was covered with liquid paraffin to prevent water evaporation. The temperature of the sample was measured with a thermocouple, whose junction was placed near $Na_4P_2O_7$ precipitates because it was expected that recrystallization of $CH_3CO_2Na \cdot 3H_2O$ would start on the surface of the nucleation catalyst. The sample was heated to 70°C and cooled. $CH_3CO_2Na \cdot 3H_2O$ melt was forcibly crystallized by seeding. After that, the glass vessel was sealed and put into a water bath. The sample was consecutively heated and cooled at a rate of 0.4°C/min between 35 and 70°C, and maintained at 35°C for 30 min and then at 70°C for the same condition. In this manner, the melting point, θ_m, and the temperature at which supercooling was broken, θ_c, were measured. Supercooling, $\Delta\theta_c$ $(=\theta_c - \theta_m)$, was determined in each cycle.

III. 4. 2 Results

The heating and cooling curve for a sample consisting of 30 g of $CH_3CO_2Na \cdot 3H_2O$ and 0.3 g of $Na_4P_2O_7 \cdot 10H_2O$ is shown in Fig. 12. The curve shows that the melting point of this sample is 58.4°C which is the same as that of $CH_3CO_2Na \cdot 3H_2O$ without any additive. The supercooling of the sample is broken at 53.1°C and suddenly the temperature

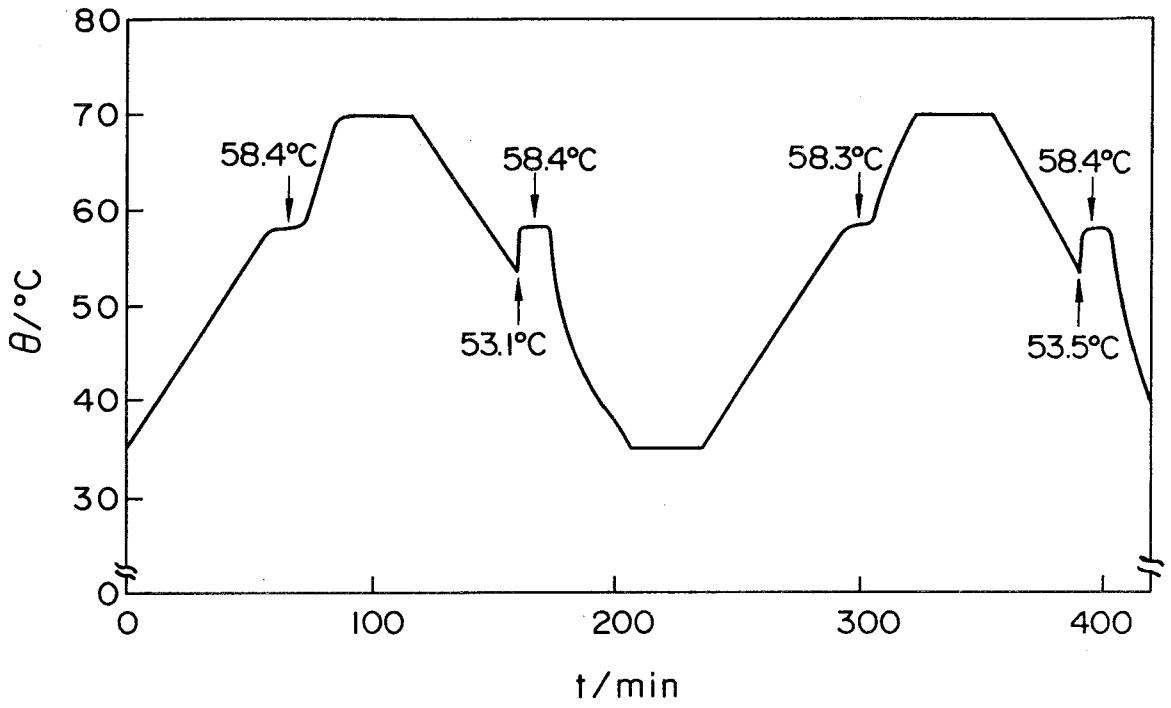

Fig. 12. Heating and cooling curve for a sample containing 30 g of $CH_3CO_2Na \cdot 3H_2O$ and 0.3 g of $Na_4P_2O_7 \cdot 10H_2O$.

of the sample rises to freezing point, 58.4°C. After maintaining for about 12 min, the temperature of the sample is down. In this case, supercooling, $\Delta\theta_c$, is −5.3°C.

The melting point, θ_m, and the temperature at which supercooling is broken θ_c, are protted in Fig. 13, against the number of cycles. As shown in Fig. 13, θ_c and θ_m are almost constant to be 53 and 58.4°C respectively. The slight scatter falls within a measuring error. The supercooling, $\Delta\theta_c (= \theta_c - \theta_m)$, is plotted in Fig. 14, using the result of Fig. 13. These are about −5°C over all the cycles. It is also found that $Na_4P_2O_7 \cdot 10H_2O$ works continuously as a nucleation catalyst for 1000 cycles. On the other hand, when $Na_4P_2O_7 \cdot 10H_2O$ powder was not added to $CH_3CO_2Na \cdot 3H_2O$ melt, supercooling was not broken down to about 35°C. These experimental results show that $Na_4P_2O_7 \cdot 10H_2O$ serves as a very effective nucleation catalyst for $CH_3CO_2Na \cdot 3H_2O$ whose melting point is scarcely lowered. In the case of using Na_2HPO_4, Na_2WO_4 or LiF as a nucleation catalyst, θ_m and θ_c are

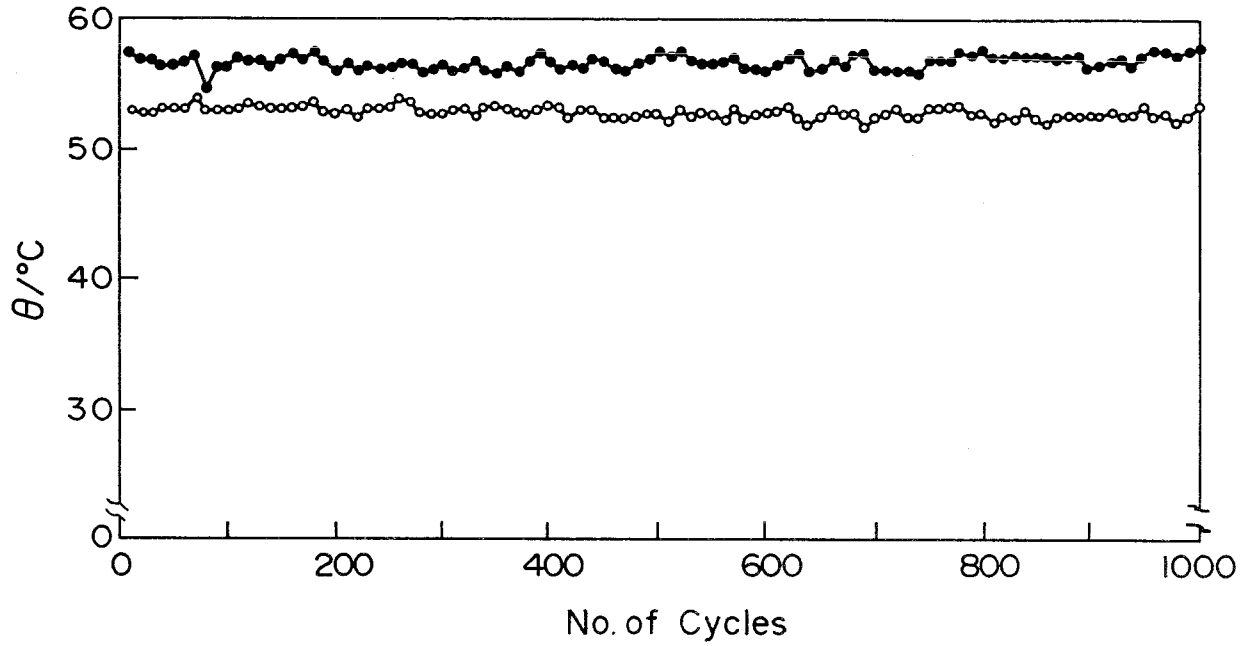

Fig. 13. Changes in melting point, θ_m, and the temperature at which supercooling is broken, θ_c, with cycling.
●: θ_m, ○: θ_c.

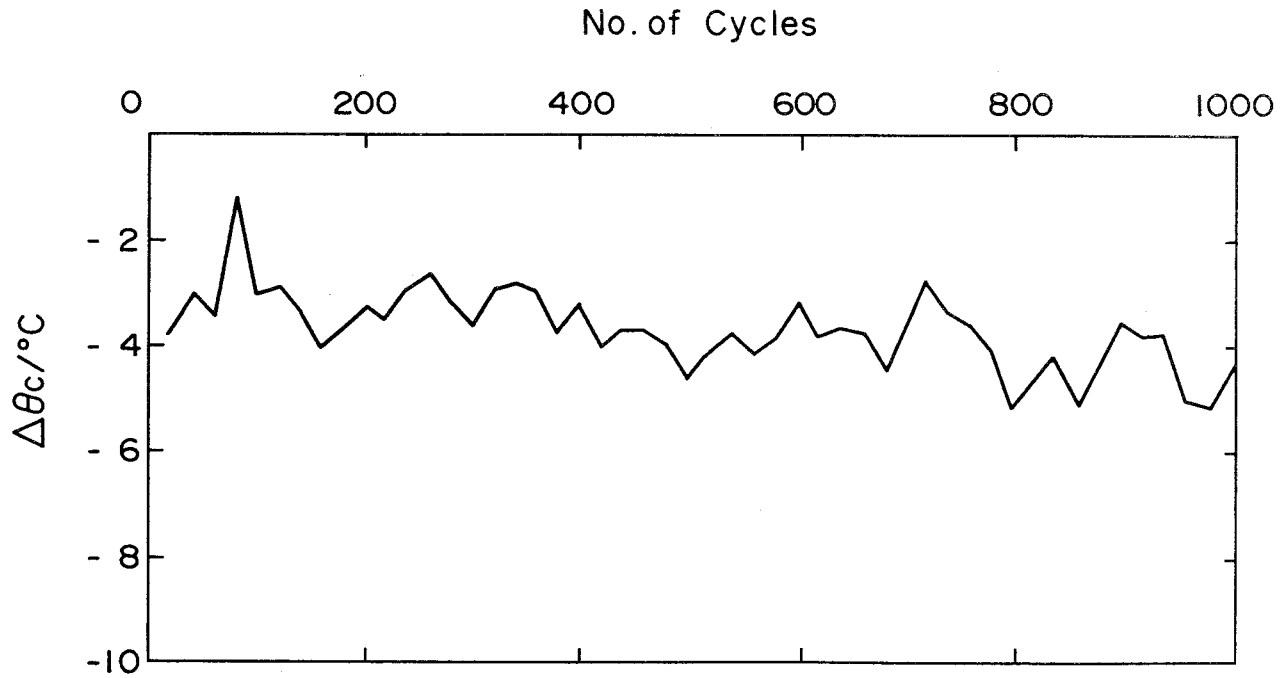

Fig. 14. Changes in supercooling, $\Delta\theta_c$, with cycling.

about 58°C and 53°C respectively and each $\Delta\theta_c$ is about −5°C. The values of $\Delta\theta_c$ in the case of using these nucleation catalysts are similar in magnitude to the previous case of $Na_4P_2O_7 \cdot 10H_2O$.

Figure 15 shows $CH_3CO_2Na \cdot 3H_2O$ crystals grown around a mass of the nucleation catalyst, $Na_4P_2O_7$. The white part indicates a mass of $Na_4P_2O_7$ and transparent crystals around it are $CH_3CO_2Na \cdot 3H_2O$. Figure 16 is a micro-photograph of $CH_3CO_2Na \cdot 3H_2O$ crystals grown around $Na_4P_2O_7$ particles. It is observed that $CH_3CO_2Na \cdot 3H_2O$ needles are radially grown from $Na_4P_2O_7$ particles. It is suggested that $CH_3CO_2Na \cdot 3H_2O$ crystallized as needles since it began to recrystallize at a temperature significantly below the melting point. This large supercooling, we suppose, results from a small amount of the sample in this experiment.

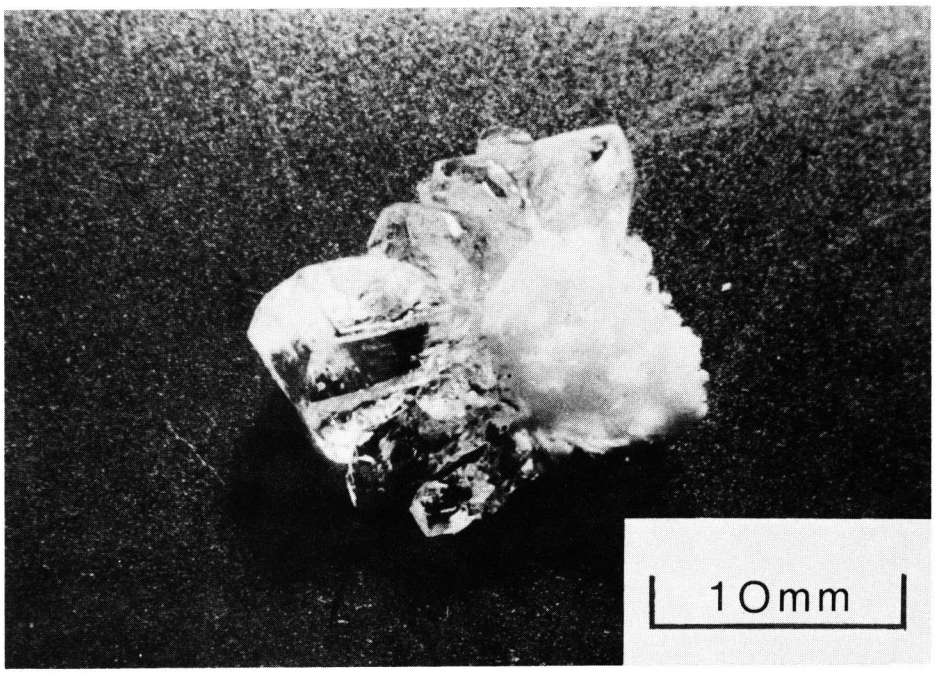

Fig. 15. Photograph of $CH_3CO_2Na \cdot 3H_2O$ crystals grown around a mass of $Na_4P_2O_7$ polycrystals.

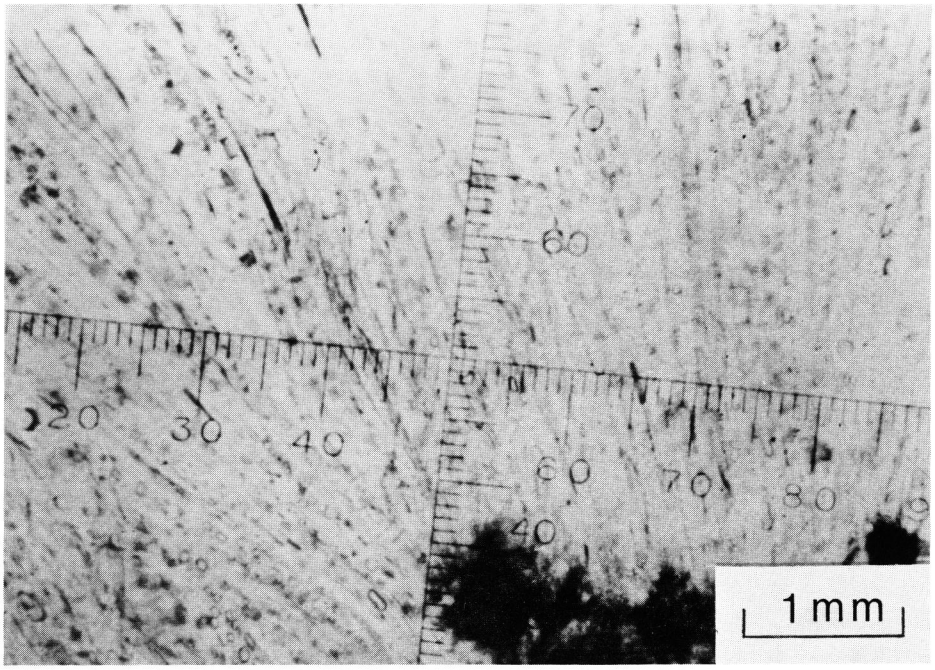

Fig. 16 Microphotograph of $CH_3CO_2Na \cdot 3H_2O$ grown around $Na_4P_2O_7$ particles.

III. 5. Preheating Effect on Crystallization of $CH_3CO_2Na \cdot 3H_2O$ from Aqueous Solution with an Addition of a Small Amount of the Nucleation Catalyst (I)

The liquid tends to supercool when it is preheated to the higher temperatures [27, 81, 82]. Richards [27] studied the preheating effect on crystallization of $CH_3CO_2Na \cdot 3H_2O$ from the aqueous solution. He used 20 sealed tubes each containing 3 g of 12 M (1 M = 1 mol dm^{-3}), about 50 wt%, CH_3CO_2Na aqueous solution and kept them at room temperature during intervals between preheating treatments. He reported that $CH_3CO_2Na \cdot 3H_2O$ was allowed to crystallize in 100, 35, or 5 % of the sample tubes respectively, when it was

preheated at a 2, 3.5, or 7°C higher temperature than the melting point.

This chapter reports the influences of preheating on crystallization of $CH_3CO_2Na \cdot 3H_2O$ from three kinds of CH_3CO_2Na aqueous solution, whose concentrations are 58.0, 60.3, and 62.8 wt%. The solutions have a small amount of the nucleation catalyst, $Na_4P_2O_7 \cdot 10H_2O$, Na_2HPO_4, Na_2WO_4 or LiF. It is found that the temperature at which the nucleation catalyst begins to get deactivated is a very important feature for the latent heat storage material containing it.

III. 5. 1 Experimental Procedure

$CH_3CO_2Na \cdot 3H_2O$, CH_3CO_2Na, $Na_4P_2O_7 \cdot 10H_2O$, Na_2HPO_4, Na_2WO_4 and LiF, used for the present experiment, were guaranteed grade reagents from Wako Pure Chemical Industries, Ltd. Eight grams of CH_3CO_2Na aqueous solution and 0.16 g of the nucleation catalyst were placed in a tube, and then sealed. The concentrations of the CH_3CO_2Na aqueous solution were 58.0 wt% (peritectic composition), 60.3 wt% ($CH_3CO_2Na \cdot 3H_2O$), and 62.8 wt%. It was 62.0 wt% instead of 62.8 wt%, in the case of using Na_2WO_4 or LiF as a nucleation catalyst. The sealed tubes were put into a water bath equipped with a gently-vibrating rack. Before subsequent steps, all aqueous solutions with a small amount of the nucleation catalyst were heated at 70°C for 1 h and then cooled to room temperature in order to force $CH_3CO_2Na \cdot 3H_2O$ to crystallize, with shaking if necessary. We kept the coagulum containing $CH_3CO_2Na \cdot 3H_2O$ and the nucleation catalyst for a duration longer than one week at room temperature, in order to obtain some steady reproducible deactivation temperature of the nucleation catalyst.

One hundred sealed tubes each containing a 60.3 wt% CH_3CO_2Na aqueous solution were heated to a predetermined temperature above the melting point of $CH_3CO_2Na \cdot 3H_2O$ for 3 h, and then cooled to 40°C at a rate of 5°C/h. This process was repeated with the

preheating temperature raised stepwise. In some of the 100 tubes preheated at a certain temperature, $CH_3CO_2Na \cdot 3H_2O$ failed in the crystallization on cooling to 40°C. Such tubes were excluded because all the nucleation catalyst in the tube should be deactivated. This deactivation possibility was supported by the observation that $CH_3CO_2Na \cdot 3H_2O$ scarcely crystallized in the excluded tubes during similar heating and cooling tests as mentioned above. The other two aqueous solutions were examined in the same manner as above. Thus, the influence of preheating temperature on the crystallization of $CH_3CO_2Na \cdot 3H_2O$ from aqueous solution was studied. The percentage of the tubes in which $CH_3CO_2Na \cdot 3H_2O$ did not crystallize on cooling down to 40°C was plotted against the temperature difference between the preheating temperature and the melting point to get Figs. 17-20. The ordinate in these figures, P/(%), indicates the deactivation probability of the nucleation catalyst.

III. 5. 2 Results

$Na_4P_2O_7 \cdot 10H_2O$ as a Nucleation Catalyst It is clear from Fig. 17 that the nucleation catalysts in the 60.3 wt% CH_3CO_2Na aqueous solution begin to get deactivated at 81°C, 23°C higher than the melting point of $CH_3CO_2Na \cdot 3H_2O$, until all of them are deactivated at about 89°C. The nucleation catalysts in the 58.0 and 62.8 wt% solutions begin to get deactivated at 77 and 85°C until all are deactivated at 85 and 89°C, respectively. In the 100 tubes each containing 8 g of 60.3 wt% CH_3CO_2Na aqueous soluton without nucleation catalyst, the cooling to 40°C preceded by the preheating at 60°C for 3 h did not crystallize $CH_3CO_2Na \cdot 3H_2O$ at all. The present CH_3CO_2Na aqueous solutions with no nucleation catalyst begin to get deactivated at a lower temperature than those in the Richards's experiment. This may be caused not only by differences in the CH_3CO_2Na concentration and experimental condition but also by the difference in purity of reagents

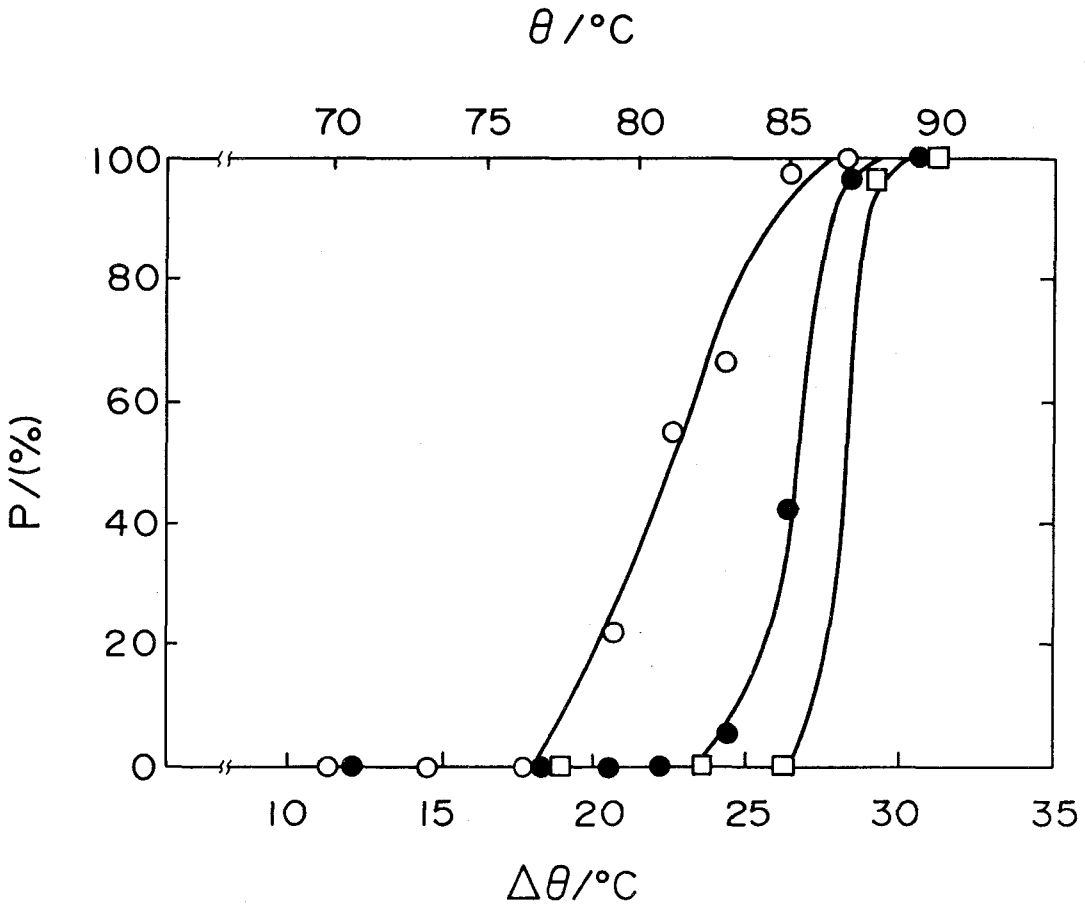

Fig. 17. **Influence of preheating temperature on the crystallization of $CH_3CO_2Na \cdot 3H_2O$ from the three kinds of aqueous solution with a small amount of $Na_4P_2O_7 \cdot 10H_2O$**
○: 58.0 wt% CH_3CO_2Na aqueous solution,
●: 60.3 wt% aqueous solution,
□: 62.8 wt% aqueous solution.

used. It is evident that the addition of $Na_4P_2O_7 \cdot 10H_2O$ to the CH_3CO_2Na aqueous solution is very effective in preventing the CH_3CO_2Na solution from supercooling.

It is understood from Fig. 17 that the temperature at which the catalyst begins to get deactivated is raised with increasing CH_3CO_2Na concentration of the solution containing the catalyst. The amount of the $Na_4P_2O_7 \cdot 10H_2O$ added is so small and, as explained later in this chapter, the solubility of $Na_4P_2O_7$ in the $CH_3CO_2Na \cdot 3H_2O$ melt is so low that

the lquidus lines for $CH_3CO_2Na \cdot 3H_2O$ and CH_3CO_2Na may be scarcely influenced by the addition of $Na_4P_2O_7 \cdot 10H_2O$. The figure indicates that the anhydrous CH_3CO_2Na is unstable above 58.4°C in the 58 wt% aqueous solution, the one is unstable above 78°C in the 60.3 wt% solution, and that the one is unstable above 97°C in the 62.8 wt% solution. The deactivation of the nucleation catalyst depends on the CH_3CO_2Na concentration of the solution containing it, but is not directly related to the existence of anhydrous CH_3CO_2Na in the solution, although Kumura [80] has pointed out that the existence of anhydrous CH_3CO_2Na played an important role in the heterogeneous nucleation of $CH_3CO_2Na \cdot 3H_2O$ from the solution.

Na_2HPO_4 as a Nucleation Catalyst It is clear from Fig. 18 that, the nucleation catalysts in the 60.3 wt% CH_3CO_2Na aqueous solution begin to get deactivated at 81°C, 23°C higher than the melting point of $CH_3CO_2Na \cdot 3H_2O$, until all of them are deactivated at about 88°C. These temperatures are in good agreement with the data obtained when $Na_4P_2O_7 \cdot 10H_2O$ was used as a nucleation catalyst. In 58.0 and 62.8 wt% solutions, the nucleation catalysts begin to get deactivated at 81 and 82°C, until all of them are deactivated at 88 and 89°C, respectively. It is understood from Fig. 18 that the deactivation temperature is slightly raised with increasing CH_3CO_2Na concentration of the solution. Such a phenomenon was similarly observed in the case of using $Na_4P_2O_7 \cdot 10H_2O$. The degree of concentration dependence of deactivation temperature is appreciably lower than in the previous case.

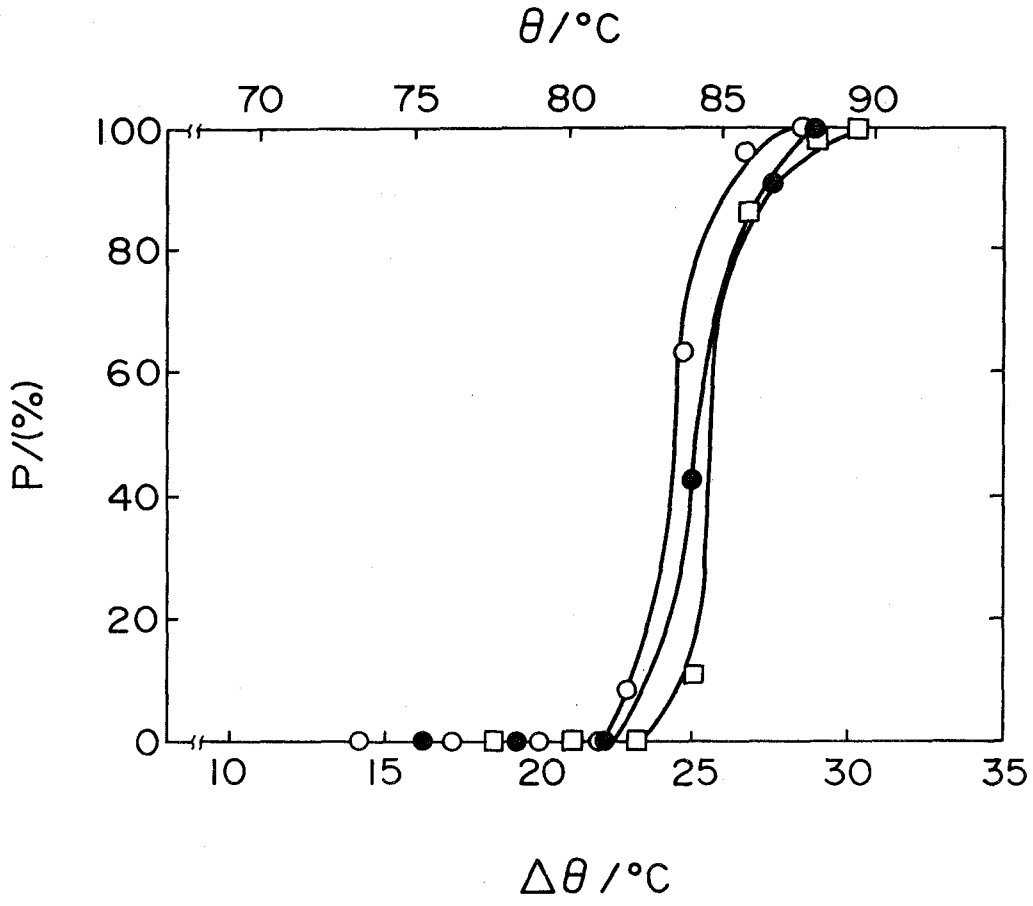

Fig. 18. **Influence of preheating temperature on the crystallization of $CH_3CO_2Na \cdot 3H_2O$ from the three kinds of aqueous solution with a small amount of Na_2HPO_4.**
○: 58.0 wt% CH_3CO_2Na aqueous solution,
●: 60.3 wt% aqueous solution,
□: 62.8 wt% aqueous solution.

Na_2WO_4 as a Nucleation Catalyst As shown in Fig. 19, the nucleation catalysts in the 60.3 wt% CH_3CO_2Na aqueous solution begin to get deactivated at 88°C, 30°C higher than the melting point of $CH_3CO_2Na \cdot 3H_3O$, until all of them are deactivated at about 92°C. These temperatures are higher than those in the case of using $Na_4P_2O_7 \cdot 10H_2O$ or Na_2HPO_4. In 58.0 and 62.0 wt% solutions, the nucleation catalysts begin to get deactivated at 86 and 90°C, until all are deactivated at 89 and 93°C respectively. The concentration

dependence of the deactivation temperature is qualitatively similar to that in the case of using $Na_4P_2O_7 \cdot 10H_2O$ or Na_2HPO_4 as a nucleation catalyst.

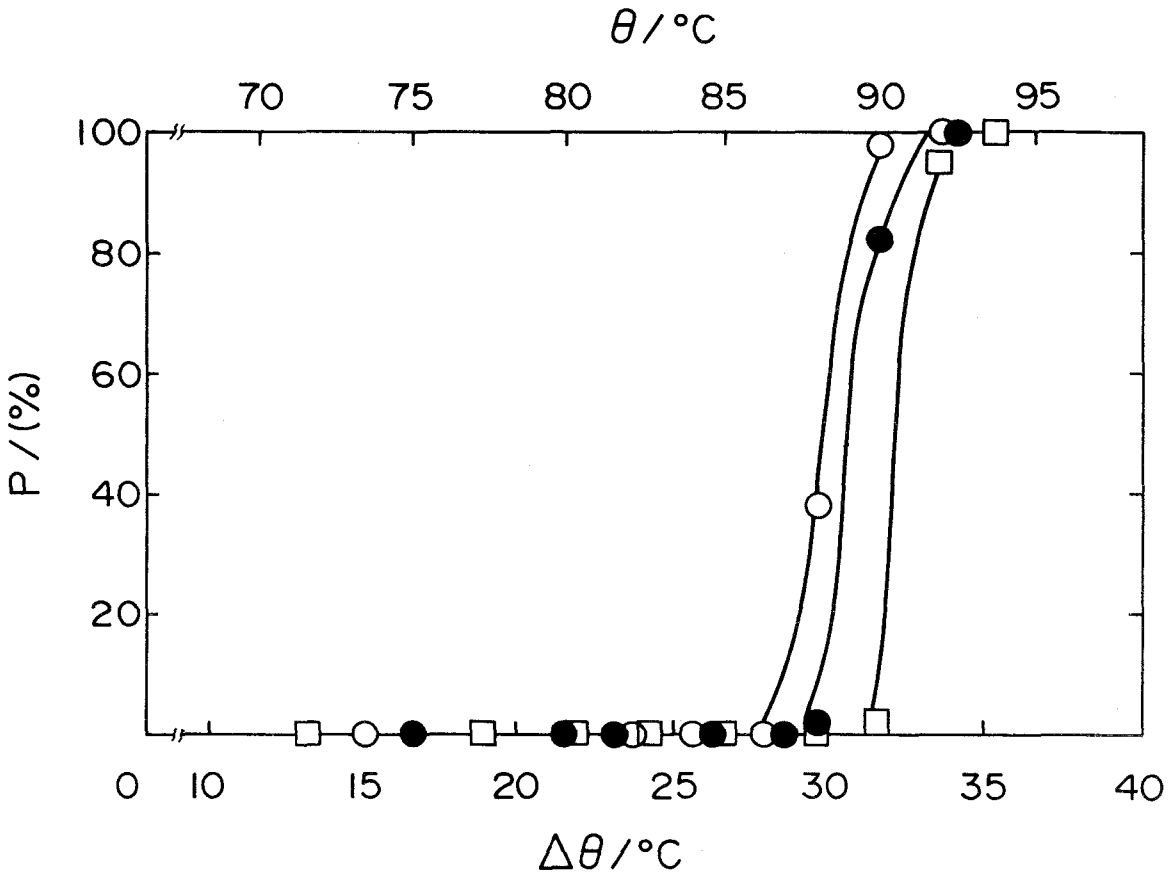

Fig. 19. **Influence of preheating temperature on the crystallization of $CH_3CO_2Na \cdot 3H_2O$ from the three kinds of aqueous solution with a small amount of Na_2WO_4,**
○: 58.0 wt% CH_3CO_2Na aqueous solution,
●: 60.3 wt% aqueous solution,
□: 62.8 wt% aqueous solution.

LiF as a Nucleation Catalyst As shown in Fig. 20, the nucleation catalysts in the 60.3 wt% CH_3CO_2Na aqueous solution begin to get deactivated at 92°C, 34°C higher than the melting point of $CH_3CO_2Na \cdot 3H_2O$, until all of them are deactivated at about 96°C. These temperatures are higher than the deactivation temperatures of the other cases. In

58.0 and 62.0 wt% solutions, the nucleation catalysts begin to get deactivated at 90 and 93°C, until all are deactivated at 94 and 97°C respectively. The concentration dependence of the deactivation temperature is qualitatively similar to that in the other cases.

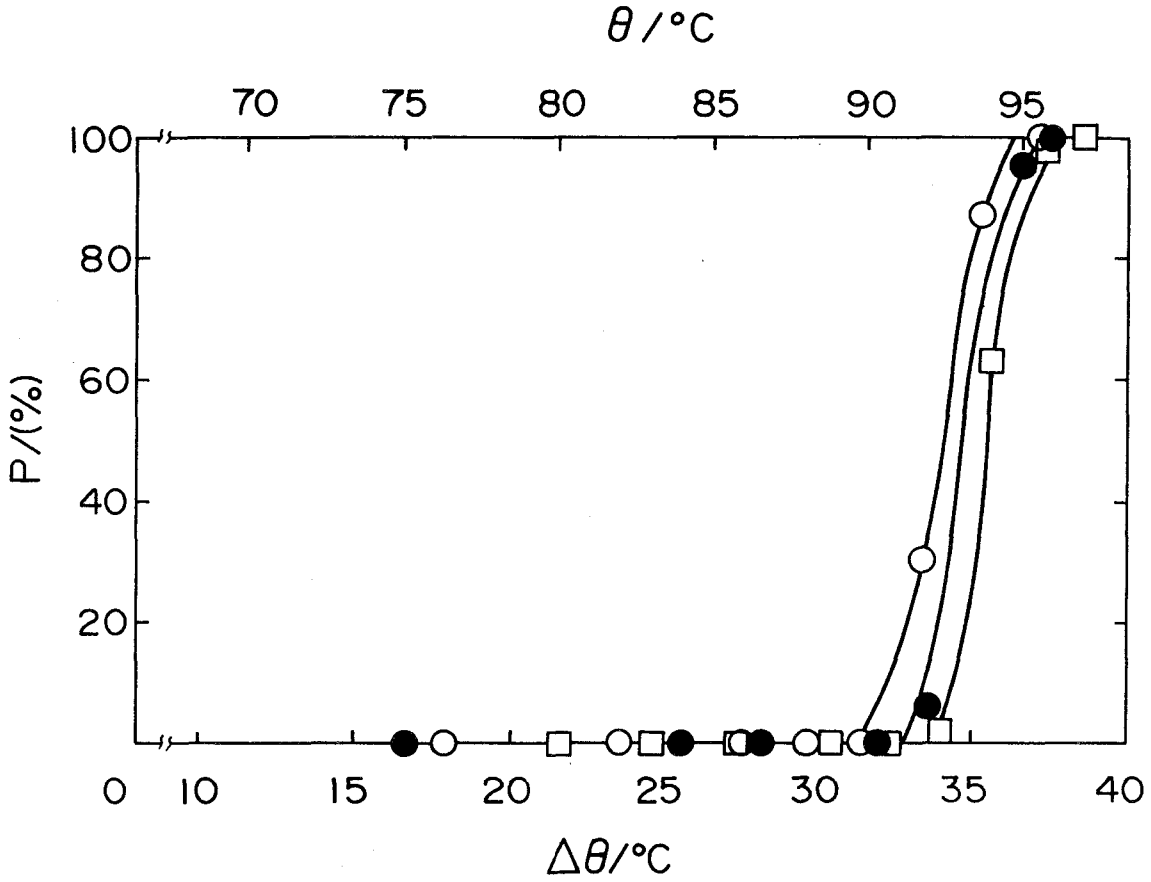

Fig. 20. **Influence of preheating temperature on the crystallization of $CH_3CO_2Na \cdot 3H_2O$ from the three kinds of aqueous solution with a small amount of LiF.**
○: 58.0 wt% CH_3CO_2Na aqueous solution,
●: 60.3 wt% aqueous solution,
□: 62.8 wt% aqueous solution.

III. 6 Preheating Effect on Crystallization of $CH_3CO_2Na \cdot 3H_2O$ from Aqueous Solution with an Addition of a Small Amount of the Nucleation Catalyst (II)

In the preceding paragraph, a influence of preheating temperature on crystallization of $CH_3CO_2Na \cdot 3H_2O$ from the CH_3CO_2Na aqueous solution containing the nucleation catalyst has been reported. This paragraph shows the influence of preheating temperature and time on crystallization of $CH_3CO_2Na \cdot 3H_2O$ form the melt with an addition of a small amount of the nucleation catalyst, LiF.

III. 6. 1 Experimental Procedure

$CH_3CO_2Na \cdot 3H_2O$ and LiF were guaranteed grade reagents from Wako Pure Chemical Industries Ltd. Eight grams of $CH_3CO_2Na \cdot 3H_2O$ and 0.16 g of LiF were placed in a container having thickness of about 3 mm. The container was made of four-layered laminate film: polyethylene terephthalate (12μm)/nylon (15μm)/aluminum film (9μm)/ polyethylene (70μm). The sample temperature was measured by a chromel-alumel thermocouple attatched to the outer wall of the container. The container was placed between plate heaters.

Before subsequent steps, all the containers were heated at 70°C for 1 h and then cooled to room temperature in order to force $CH_3CO_2Na \cdot 3H_2O$ to crystallize, with shaking if necessary. We kept these samples for a duration longer than one week at room temperature in order to obtain reproducible data.

Five containers were heated to a preheating temperature, θ_h, kept for a preheating time, Δt_h, and then cooled to 40°C at a rate of 30°C/h. Similar procedures were conducted with the variation of θ_h and Δt_h. In some of the five containers preheated at a certain temperature for a certain time, $CH_3CO_2Na \cdot 3H_2O$ failed in crystallization on cooling to

40°C. The nucleation catalysts in these containers must have been deactivated.

III. 6. 3 Results

The percentage of the containers in which $CH_3CO_2Na \cdot 3H_2O$ did not crystallize on cooling to 40°C is shown in Fig. 21. In this figure, the number on the ordinate indicates the preheating temperature, θ_h, and the number on the abscissa indicates the common logarithm of the preheating time, Δt_h. As shown in this figure, the temperatures at which the nucleation catalyst begins to get deactivated are 92°C for 1 h, 91°C for 4 h, 92°C for 8 h, 90°C for 30 h or 91°C for 100 h preheating. The results show that the deactivation temperature of the nucleation catalyst does not vary with preheating time, Δt_h. This characteristic of the nucleation catalyst is very important for practical use of latent heat storage material.

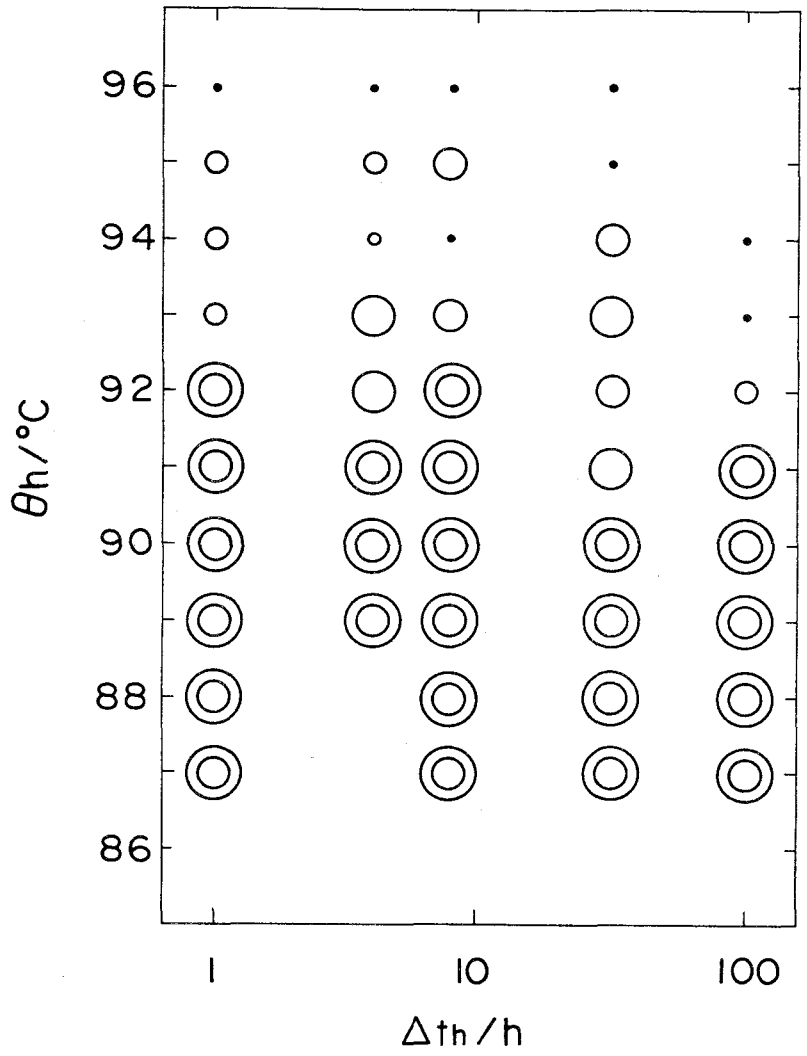

Fig. 21. Influence of preheating temperature and time on the crystallization of $CH_3CO_2Na \cdot 3H_2O$ from the melt containing a small amount of LiF.

◎ : all five samples were crystallized,
◯ : four samples were crystallized,
◯ : three samples were crystallized,
○ : two samples were crystallized,
○ : only one sample was crystallized,
● : any sample was not crystallized.

III. 7 The Relation Between Activation Process of Crystal Nucleation Catalysts and Their Deactivation Temperatures

In the previous paragraph (III. 5), it was reported that the nucleation catalysts were deactivated at an elevated temperature above the melting point of $CH_3CO_2Na \cdot 3H_2O$. However, the deactivation temperature varied widely. The reason for this variation has not yet been understood. In order to elucidate the cause of variation, the activation process of a nucleation catalyst was investigated in relation to the deactivation temperature. This paragraph presents the effect of aging of a nucleation catalyst preceded by forced crystallization of $CH_3CO_2Na \cdot 3H_2O$ from a melt containing the nucleation catalyst. The aging of the nucleation catalysts remarkably effects their deactivation temperatures.

III. 7. 1 Experimental Procedure

$CH_3CO_2Na \cdot 3H_2O$, $Na_4P_2O_7$, Na_2HPO_4, Na_2WO_4, and LiF were guaranteed grade reagents from Wako Pure Chemical Industries Ltd. Eight grams of $CH_3CO_2Na \cdot 3H_2O$ and 0.16 g of nucleation catalyst were placed in a container, having thickness of about 3 mm. The container was made of four-layered laminate film: polyethylene terephthalate (12μm)/nylon (15μm)/aluminum film (9μm)/polyethylene (70μm). The sample temperature was measured by a chromel-alumel thermocouple attached to the outer wall of the container. The container was placed between plate heaters.

Experimental runs were performed according to the temperature program shown in Fig. 22. Eight containers containing 8 g of $CH_3CO_2Na \cdot 3H_2O$ and 0.16 g of nucleation catalyst were heated at 95°C for 1 h (D→E) in order to deactivate the nucleation catalyst completely. Then, they were cooled to room temperature (E→F), and the supercooled melts were seeded (F); this is forced crystallization of $CH_3CO_2Na \cdot 3H_2O$. Immediately,

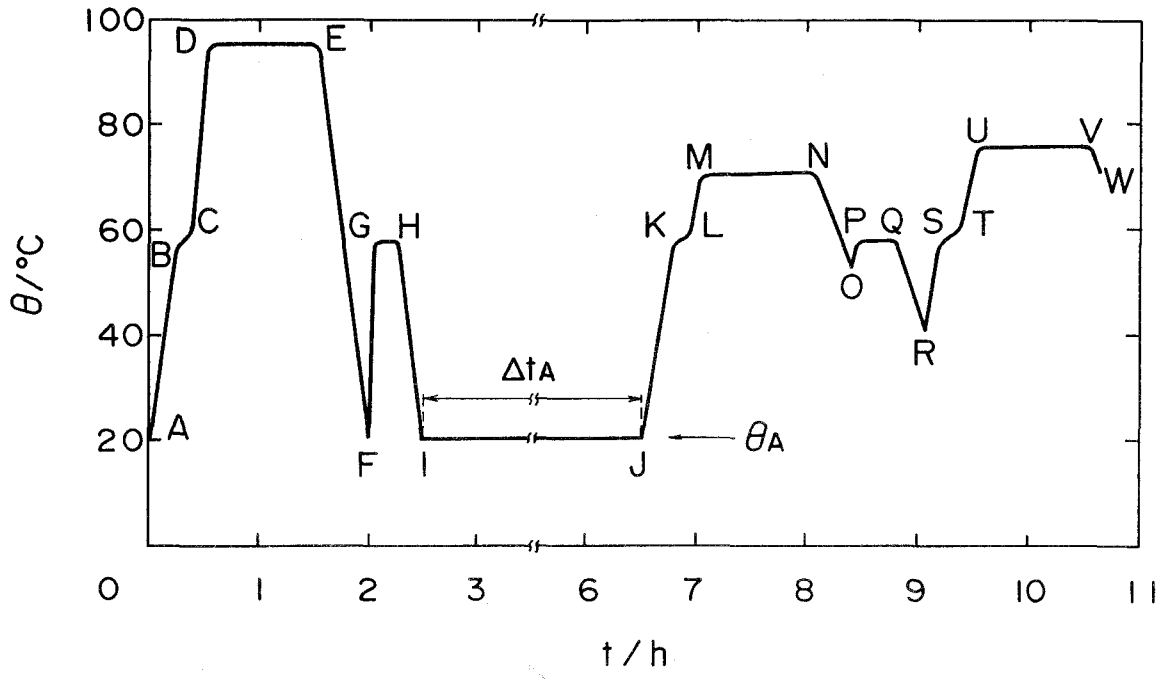

Fig. 22. **Temperature program of a typical sample. The nucleation catalyst is activated during the first crystallization of $CH_3CO_2Na \cdot 3H_2O$.**

the temperature was raised to the freezing point (F→G→H). Then they were cooled to the aging temperature in a thermostat (H→I) and kept there for the aging time (I→J). Then, the containers were heated to a predetermined temperature (J→M), kept for 1 h (M→N), and then cooled to 40°C at a rate of 30°C/h (N→R). In this cooling process, crystallization of $CH_3CO_2Na \cdot 3H_2O$ took place with a sudden rise in the temperature of the sample (O→P→Q). This process was repeated with the preheating temperature raised stepwise. In some of the eight containers preheated at a certain temperature, $CH_3CO_2Na \cdot 3H_2O$ failed to crystallize on cooling to 40°C. The nucleation catalyst in such containers must have been deactivated or degraded to lose nucleation ability. The percentage of the containers in which $CH_3CO_2Na \cdot 3H_2O$ did not crystallize on cooling was plotted against the difference ($\Delta\theta_h$) between the preheating temperature (θ_h) and the melting point of

$CH_3CO_2Na \cdot 3H_2O$ (58.4°C), as shown in Figs. 23-30. The ordinate in these figures, P/(%) indicates the deactivation possibility of the nucleation catalyst.

III. 7. 2 Results

$Na_4P_2O_7$ as a Nucleation Catalyst It is clear from Fig. 23 that the nucleation catalysts which were aged for 0.5 h at 20°C begin to get deactivated at 69°C, about 10°C

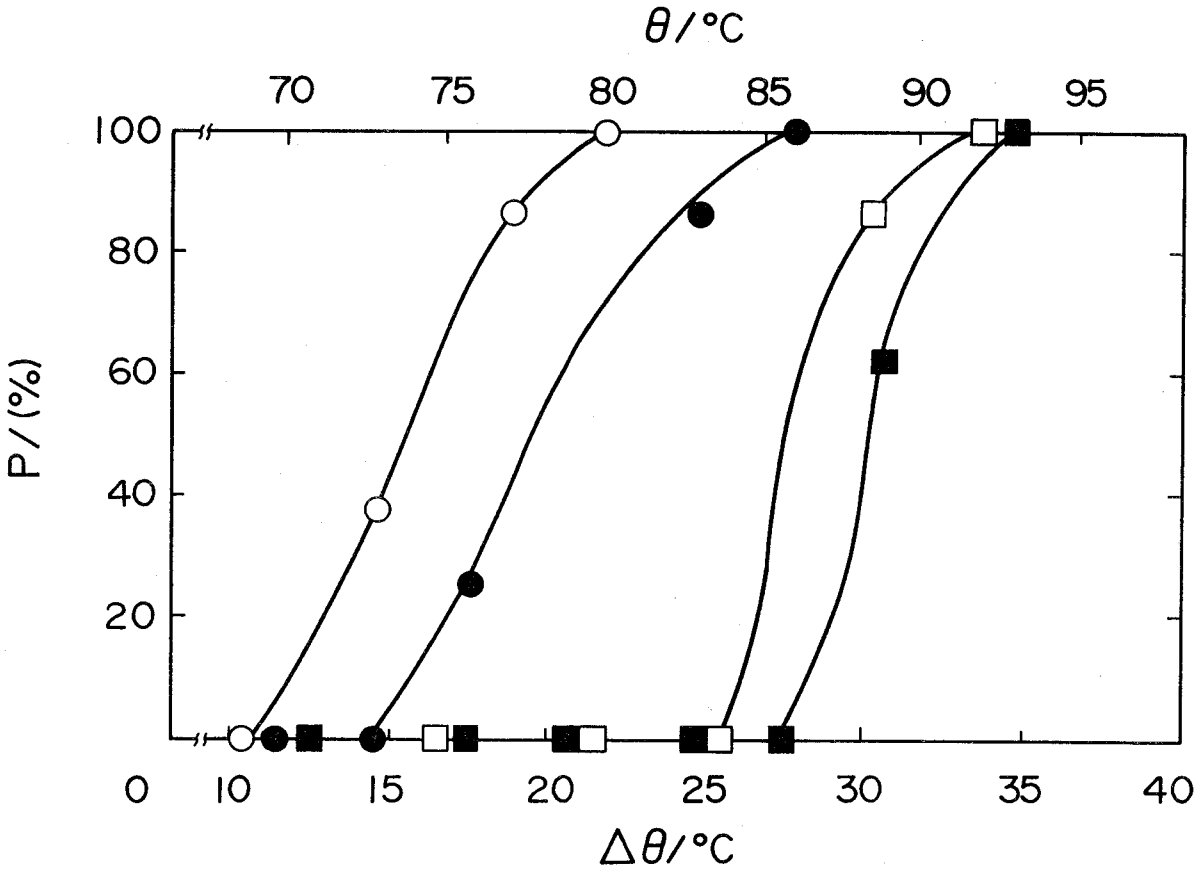

Fig. 23. Influence of preheating temperature on the crystallization of $CH_3CO_2Na \cdot 3H_2O$ from the melts containing a small amount of $Na_4P_2O_7$ as a nucleation catalyst which were aged at 20°C.
○: Δt_A (aging time) = 0.5 h, ●: Δt_A = 4.0 h,
□: Δt_A = 20 h, ■: Δt_A = 96 h.

higher than the melting point of $CH_3CO_2Na \cdot 3H_2O$, and that all of the catalysts are deactivated at about 80°C. The nucleation catalysts which were aged for 4, 20, and 96 h begin to get deactivated at 74, 84, and 86°C, and all of them are deactivated at 86, 92, and 93°C, respectively. It is understood from Fig. 23 that the deactivation temperature of nucleation catalyst is raised with length of aging time at a constant aging temperature. The deactivation behavior of the nucleation catalyst aged for 500 h at 20°C, which is not shown in Fig. 23, is almost the same as that of the nucleation catalyst aged for 96 h at 20°C. It is evident that the aging effect at 20°C is almost saturated within 96 h.

It can be seen from Fig. 24 that the nucleation catalysts aged for 96 h at −20°C begin to get deactivated at 76°C and that all of them are deactivated at about 83°C. The deactivation temperature of the nucleation catalyst aged for 96 h at −20°C is about 10°C lower than that of the nucleation catalyst aged for 96 h at 20°C. With the 8 samples which were aged for 96 h in liquid N_2, the cooling to 40°C preceded by the preheating at 65°C for 1 h caused no crystallization of $CH_3CO_2Na \cdot 3H_2O$. It is evident that, at lower temperatures, a longer aging time is required for the full againg effect on the nucleation catalyst.

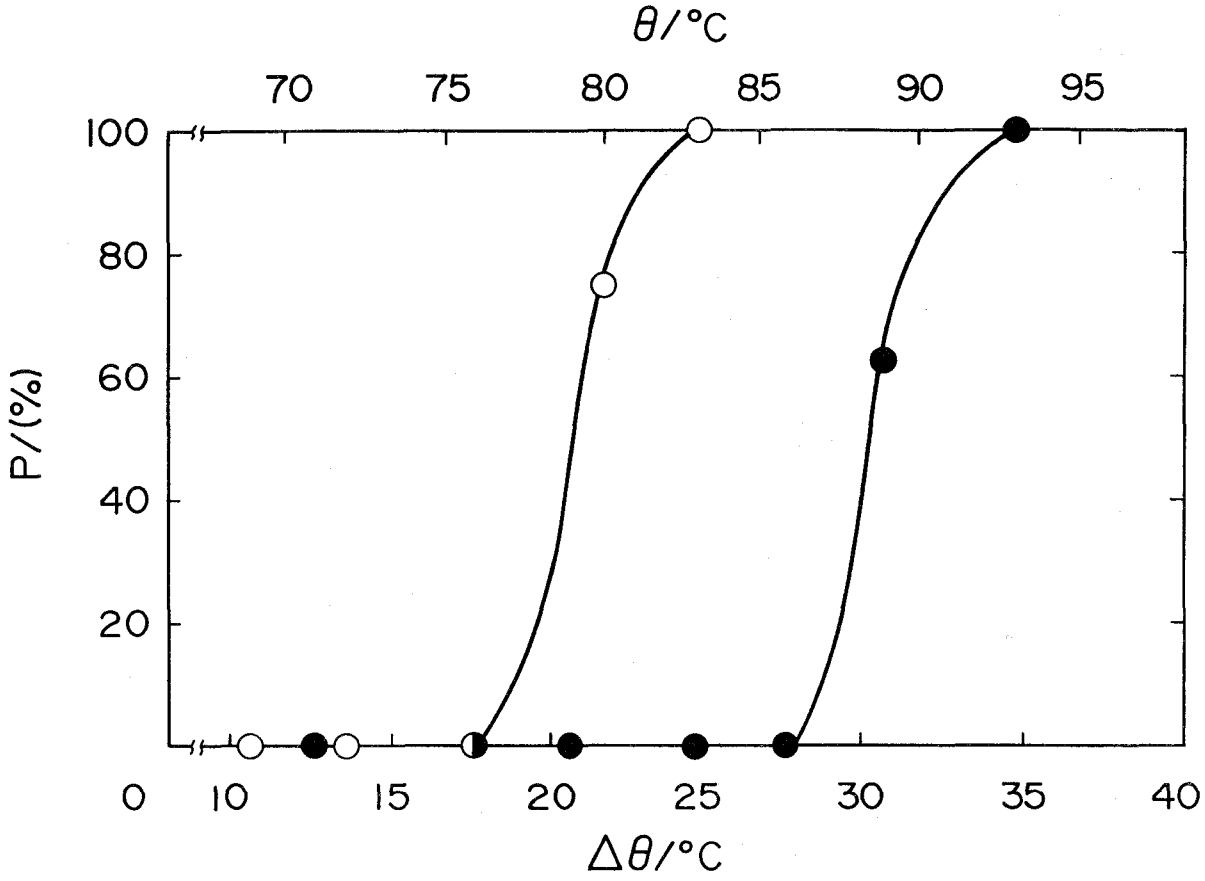

Fig. 24. **Influence of preheating temperature on the crystallization of $CH_3CO_2Na \cdot 3H_2O$ from the melts containing a small amount of $Na_4P_2O_7$ as a nucleation catalyst which were aged for 96 h.**
○: θ_A (aging temperature) = −20°C,
●: θ_A = 20°C.

Na_2HPO_4 as a Nucleation Catalyst It is clear from Fig. 25 that the nucleation catalysts aged for 0.5 h at 20°C begin to get deactivated at 81°C and that all of them are deactivated at about 88°C. The nucleation catalysts aged for 20 or 96 h begin to get deactivated at 84 or 86°C and all of them are deactivated at 89 or 91°C, respectively. It is understood from Fig. 25 that the deactivation temperature of the nucleation catalyst is raised with aging time a little. The deactivation behavior of the nucleation catalyst aged for

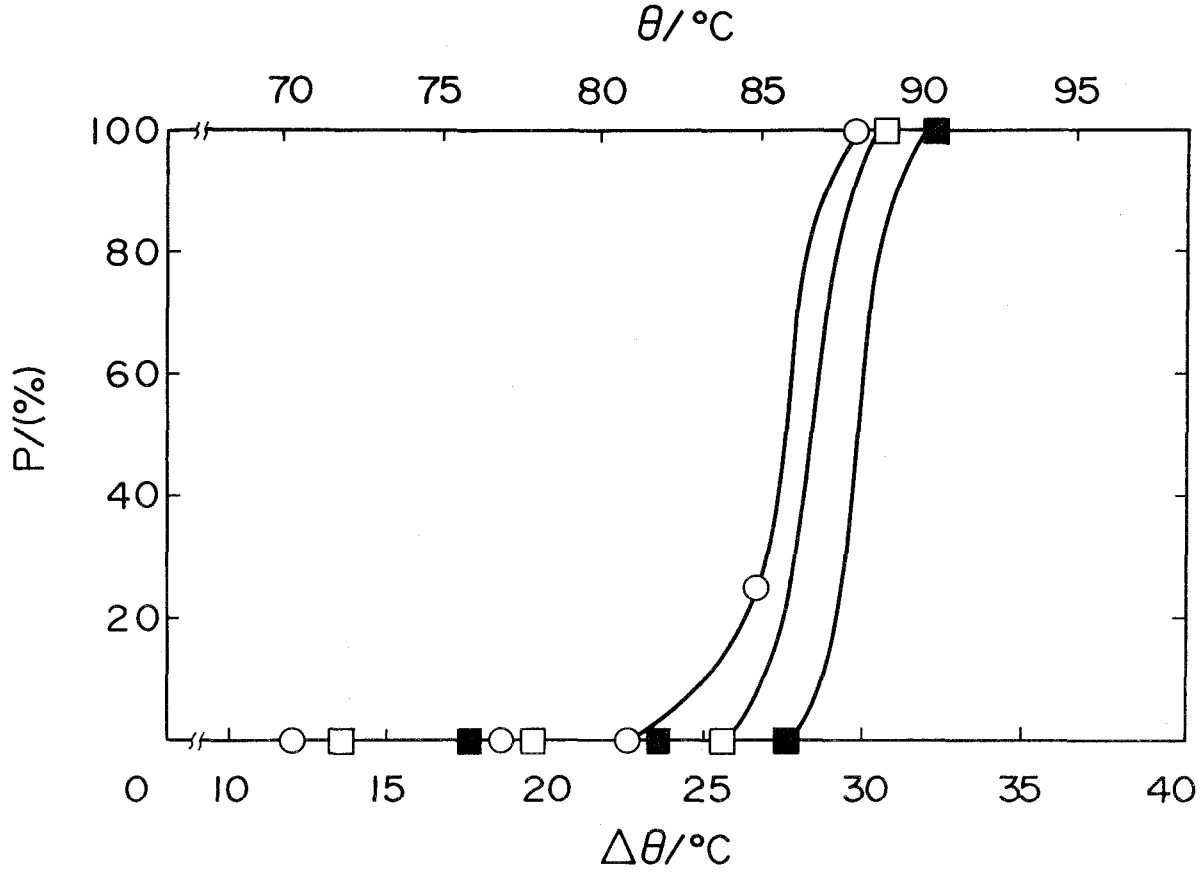

Fig. 25. Influence of preheating temperature on the crystallization of $CH_3CO_2Na \cdot 3H_3O$ from the melts containing a small amount of Na_2HPO_4 as a nucleation catalyst which were aged at 20°C.
○: Δt_A = 0.5 h, □: Δt_A = 20 h, ■: Δt_A = 96 h.

500 h at 20°C, which is not shown in Fig. 25, is almost the same as that of the nucleation catalyst aged for 96 h at 20°C. These phenomena are similar to those observed with $Na_4P_2O_7$ as a nucleation catalyst. The time required for saturation of the aging effect is much shorter than in the case of $Na_4P_2O_7$.

It can be seen from Fig. 26 that the nucleation catalysts aged for 96 h at −20°C begin to get deactivated at 84°C and that all of them are deactivated at 89°C. This deactivation temperature of the nucleation catalyst is a little lower than that of the nucleation catalyst

aged for 96 h at 20°C. These phenomena are also similar to those observed with $Na_4P_2O_7$. However, the aging-temperature dependence does not have so serious effect on the deactivation temperature as in the case of $Na_4P_2O_7$.

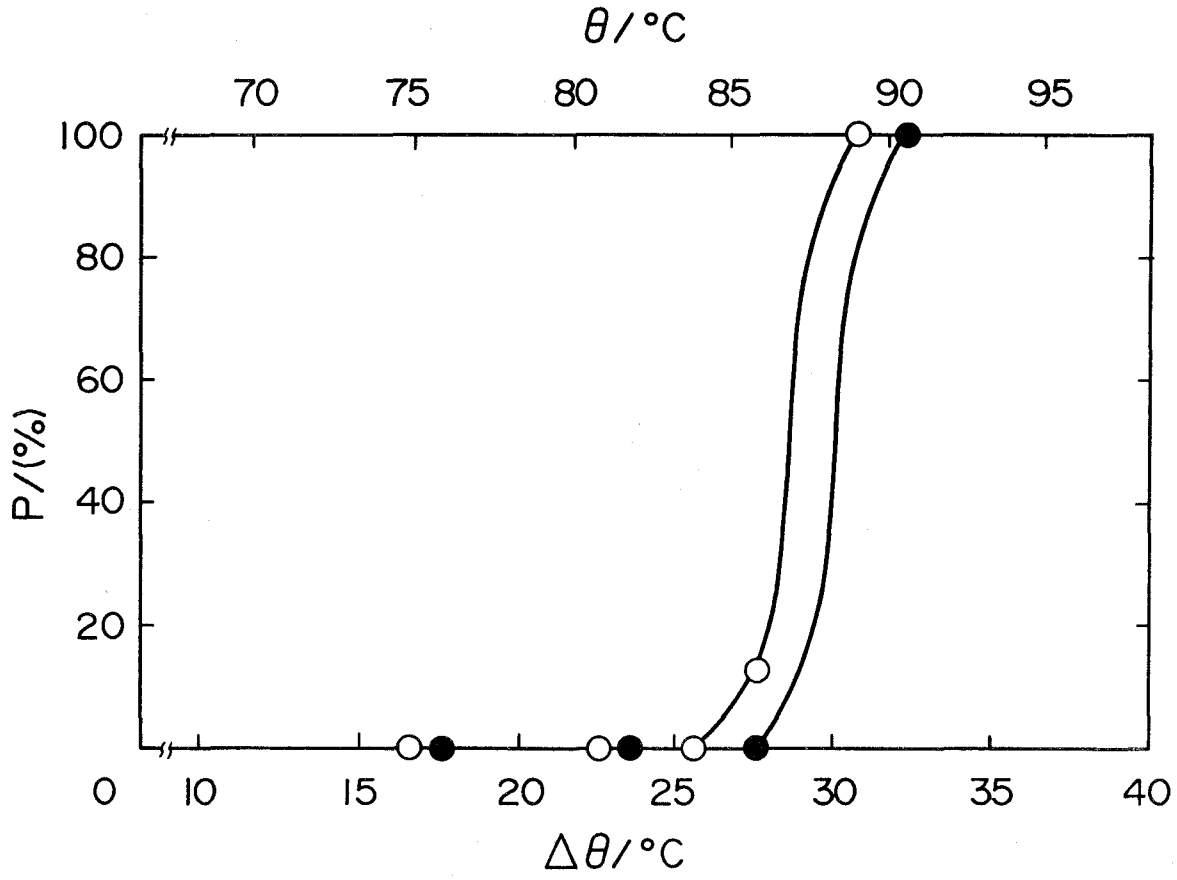

Fig. 26. **Influence of preheating temperature on the crystallization of $CH_3CO_2Na \cdot 3H_2O$ from the melts containing a small amount of Na_2HPO_4 as a nucleation catalyst which were aged for 96 h.**
○: $\theta_A = -20°C$, ●: $\theta_A = 20°C$.

Na_2WO_4 as a Nucleation Catalyst As shown in Fig. 27, the nucleation catalysts aged for 0.5 h at 20°C begin to get deactivated at 73°C and that all of them are deactivated at about 86°C. The nucleation catalysts aged for 3, 12 or 140 h begin to get deactivated at 75, 78 or 87°C and all of them are deactivated at 89, 92 or 94°C respectively. The deactivation temperature is raised with length of the aging time.

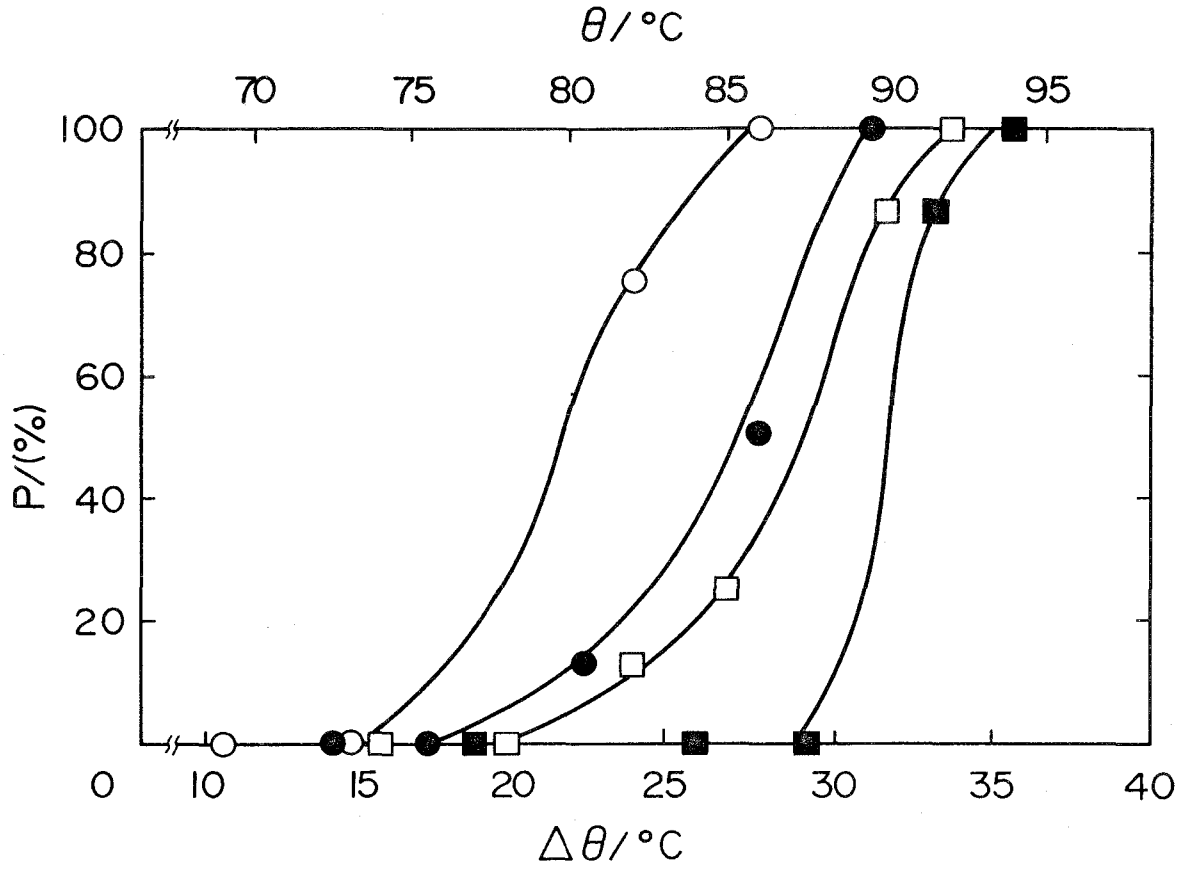

Fig. 27. Influence of preheating temperature on the crystallizatoin of $CH_3CO_2Na \cdot 3H_2O$ from the melts containing a small amount of Na_2WO_4 as a nucleation catalyst which were aged at 20°C.
○: Δt_A= 0.5 h, ●: Δt_A= 3 h, □: Δt_A= 12 h, ■: Δt_A= 140 h.

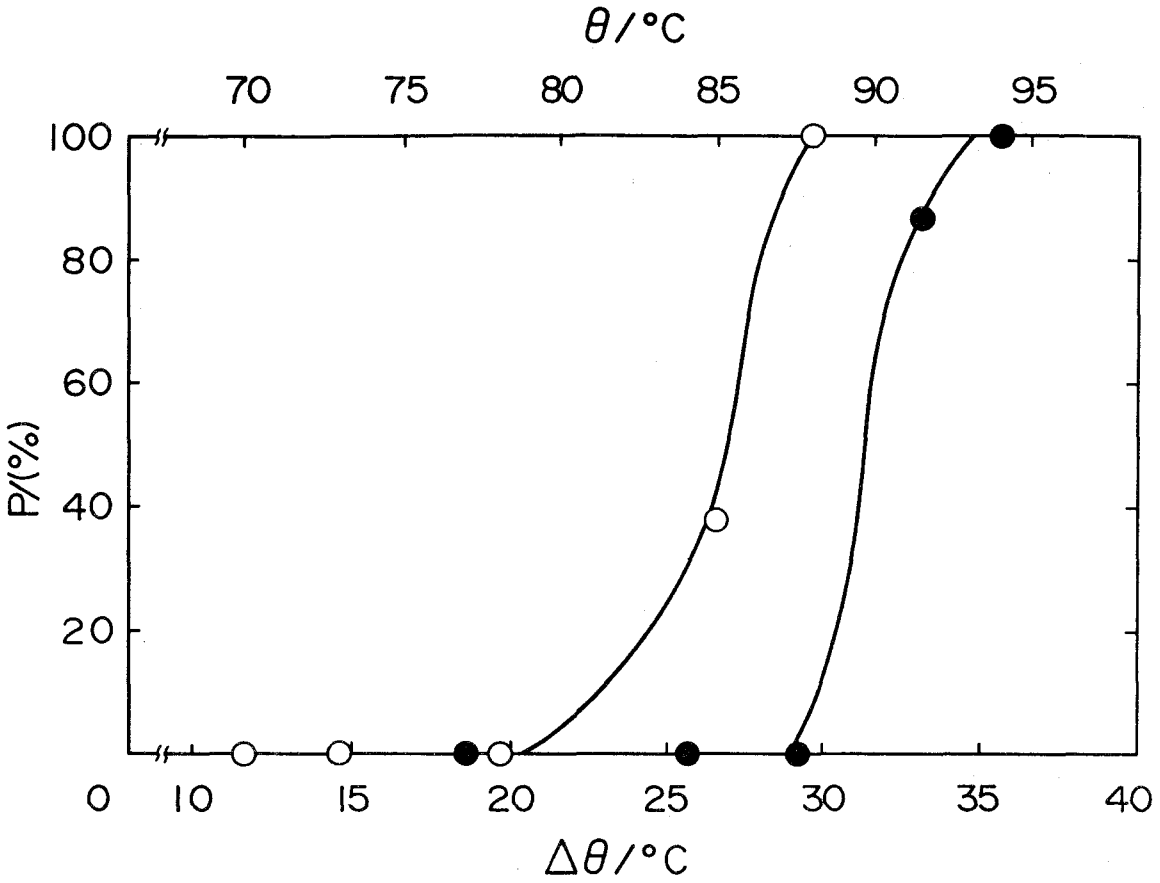

Fig. 28. **Influence of preheating temperature on the crystallization of $CH_3CO_2Na \cdot 3H_2O$ from the melts containing a small amount of Na_2WO_4 as a nucleation catalyst which were aged for 140 h.**
○: $\theta_A = -20°C$, ●: $\theta_A = 20°C$.

It can be seen from Fig. 28 that the nucleation catalysts aged for 140 h at −20°C begin to get deactivated at 78°C and that all of them are deactivated at 87°C. This deactivation temperature is lower than that of the nucleation catalyst aged for 140 h at 20°C. These phenomena are also qualitatively similar to those observed with the other nucleation catalyst. In this case, both aging-time dependence and aging-temperature dependence of the deactivation temperature are considerably pronounced.

LiF as a Nucleation Catalyst As shown in Fig. 29, the nucleation catalysts aged at 20°C begin to get deactivated at 85°C and that all of them are deactivated at about 95°C. The nucleation catalysts aged for 18 or 140 h begin to get deactivated at 90 or 92°C and all of them are deactivated at 96 or 98°C respectively. The deactivation temperature in the case is also raised with aging.

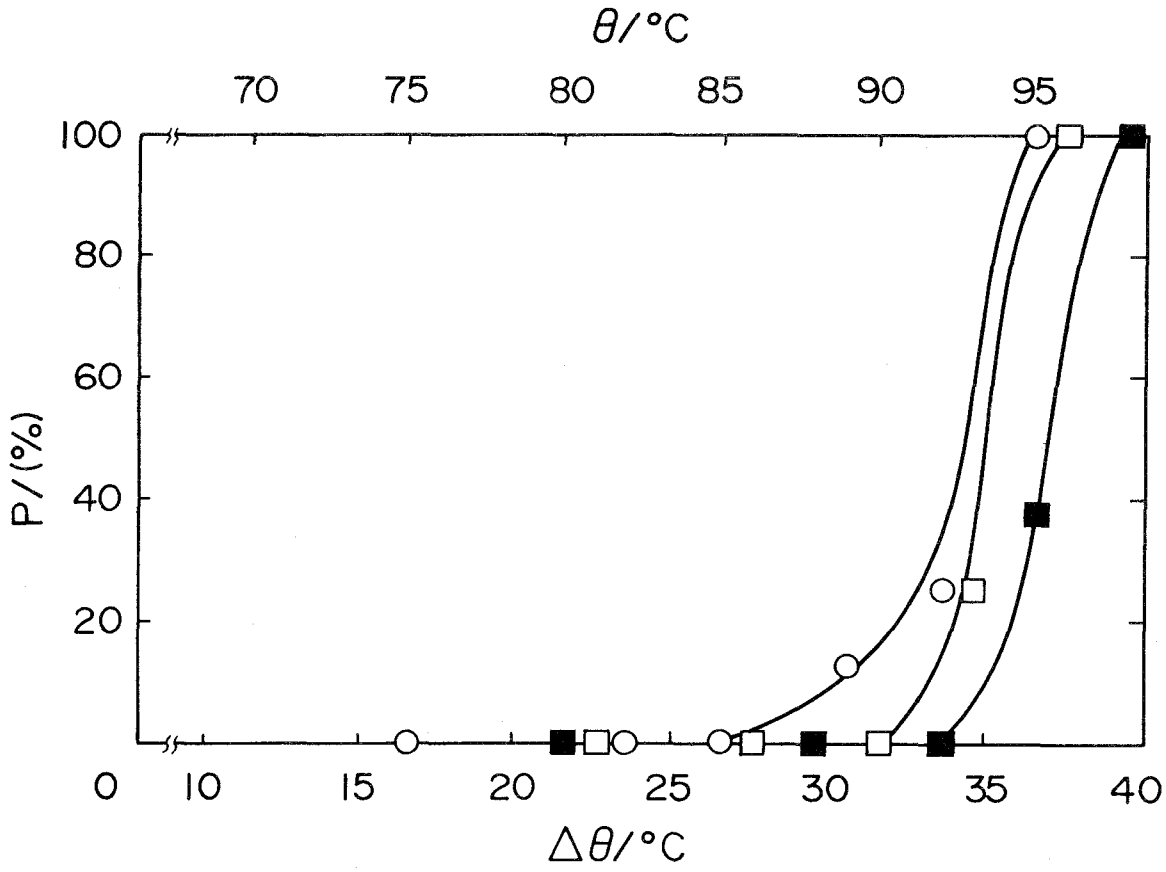

Fig. 29. Influence of preheating temperature on the crystallizaton of $CH_3CO_2Na \cdot 3H_2O$ from the melts containing a small amount of LiF as a nucleation catalyst which were aged at 20°C.
○: Δt_A = 0.5 h, □: Δt_A = 18 h, ■: Δt_A = 140 h.

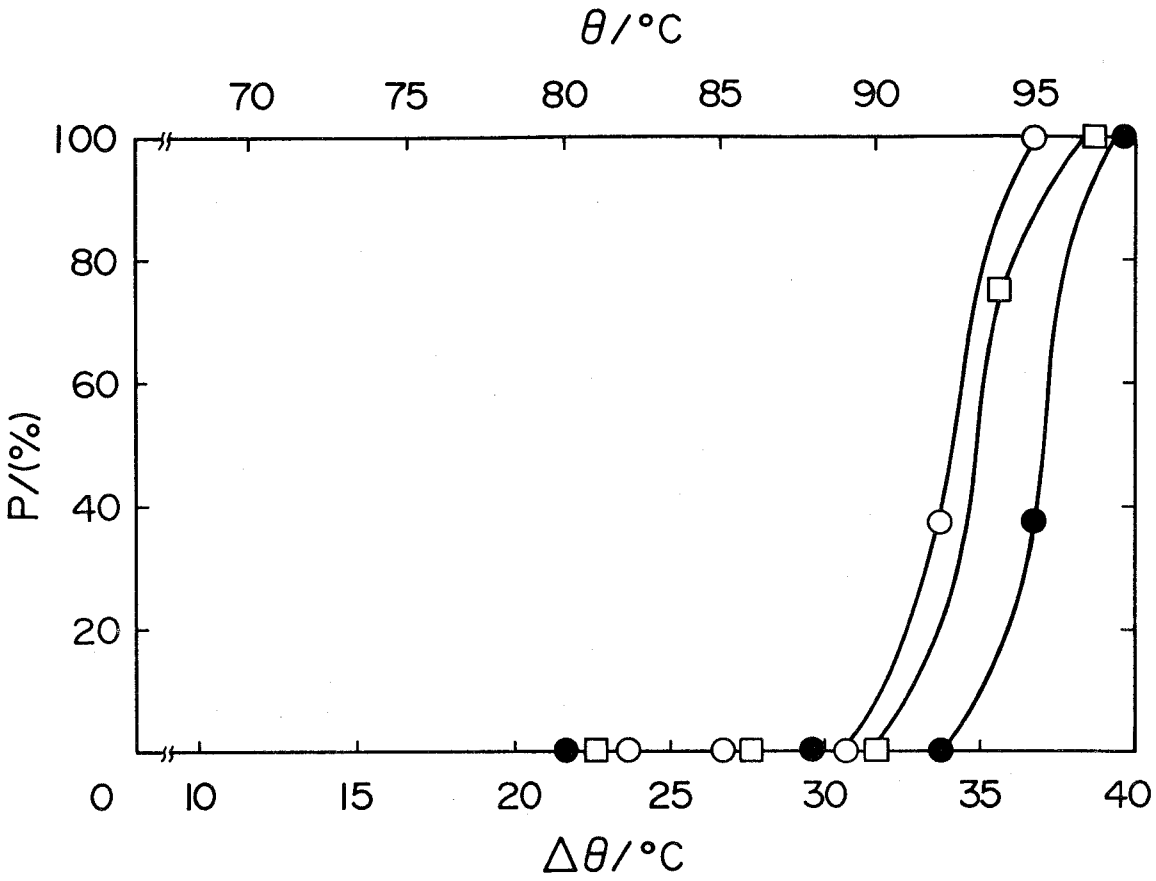

Fig. 30. **Influence of preheating temperature on the crystallization of $CH_3CO_2Na \cdot 3H_2O$ from the melts containing a small amount of LiF as a nucleation catalyst which were aged for 140 h.**
○: $\theta_A = -20°C$, ●: $\theta_A = 20°C$, □: $\theta_A = 40°C$.

It can be seen from Fig. 30 that the nucleation catalysts aged for 140 h at −20 or 40°C begin to get deactivated at 89 or 90°C and all of them are deactivated at 95 or 97°C respectively. The deactivation temperature of the nucleation catalyst aged for 140 h at 20°C is a little higher than those of the nucleation catalyst aged for 140 h at −20 and 40°C. In this case, both dependence of aging-time and aging temperature of the deactivation temperature are very small.

III. 8 Crystallization Temperature of $CH_3CO_2Na \cdot 3H_2O$ with an Addition of a Small Amount of the Nucleation Catalyst

Crystallization temperature of $CH_3CO_2Na \cdot 3H_2O$ with an addition of a small amount of the nucleation catalyst was measured by differential scanning calorimetry (DSC), in order to elucidate the thermal history upon the kinetics of crystallization. This paragraph deals with the relation between preheating temperature and crystallization temperature of $CH_3CO_2Na \cdot 3H_2O$.

III. 8. 1 Experimental Procedure

$CH_3CO_2Na \cdot 3H_2O$, $Na_4P_2O_7$, Na_2HPO_4, Na_2WO_4 and LiF were guaranteed grade reagents from Wako Pure Chemical Industries Ltd. Differential scanning calorimetry (DSC) was performed using an SSC 560S DSC (Dainiseikosha Co. Ltd.). Weighed quantities of samples were placed in a 15$\mu\ell$ silver crucible and the surface of the sample was covered with one drop of liquid paraffin to prevent water evaporation. Before subsequent steps, $CH_3CO_2Na \cdot 3H_2O$ with an addition of the nucleation catalyst was heated at 70°C and then cooled to room temperature to force $CH_3CO_2Na \cdot 3H_2O$ to crystallize, with seeding if necessary. The coagulum containing $CH_3CO_2Na \cdot 3H_2O$ and the nucleation catalyst was kept at room temperature for longer than one week in order to obtain some steady reproducible data. The sample was consecutively heated and cooled at the rate of 0.5°C/min between 40°C and predetermined temperature, θ_h, and maintained for 20 min respectively at 40°C and at θ_h. These thermal cycles were repeated for 5 times for each predetermined temperature. Melting temperature was obtained from the sample temperature curve at time corresponding to endothermal peak and the temperature at which supercooling was broken (crystallization temperature) was obtained from sample temperature curve at time corre-

sponding to the onset of exothermal peak. The crystallization temperature, θ_c, and the melting point, θ_m, were determined by averaging the 5 data. From these temperatures, supercooling, $\Delta\theta_c(=\theta_c-\theta_m)$, and preheating above the melting point, $\Delta\theta_h(=\theta_h-\theta_m)$, were calculated. This DSC system was calibrated by using ice (mp: 0.0°C), sodium sulfate decahydrate (mp: 32.4°C) and sodium acetate trihydrate (mp: 58.4°C) as standards.

III. 8. 2 Results

DSC curve of a smaple consisting of 18.3 mg of $CH_3CO_2Na\cdot 3H_2O$ and 3.7 mg of $Na_4P_2O_7$ is illustrated in Fig. 31. The difference between the temperature of the first

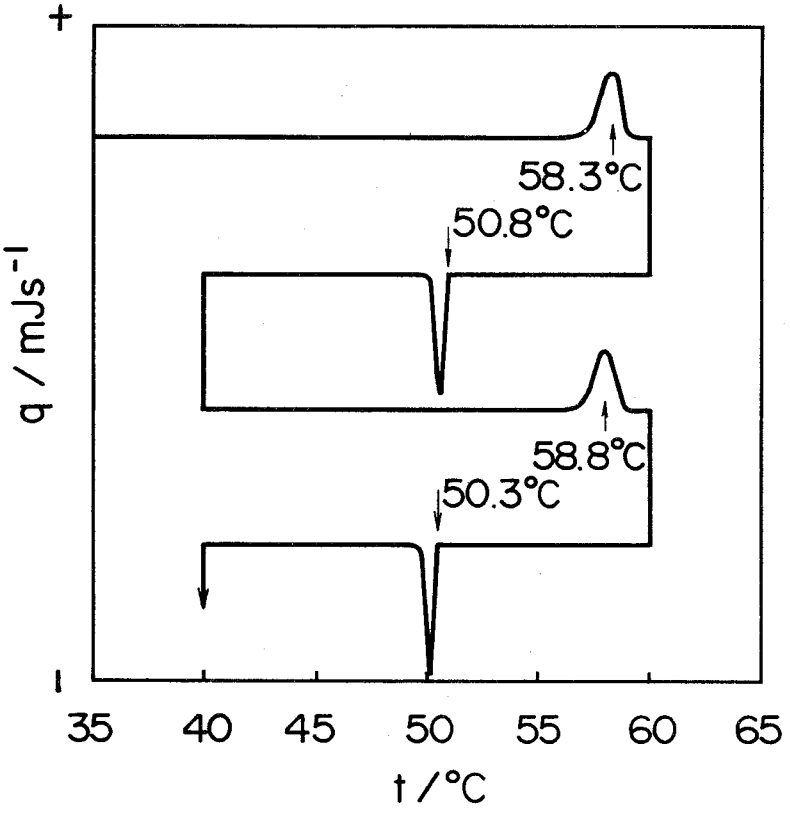

Fig. 31. DSC curve of a sample consisting of 18.3 mg of $CH_3CO_2Na\cdot 3H_2O$ and 3.7 mg of $Na_4P_2O_7$.

endothermal peak and that of the second is probably caused by measuring error. The supercooling, $\Delta\theta_c$, is determined by 5 continuous heating and cooling cycles. The $\Delta\theta_c$'s points are plotted against the preheating above the melting point, $\Delta\theta_h$, for each nucleation catalyst. They are shown in Figs. 32-35. In these figures, the scatter of data are also indicated by the vertical lines. In the case of using any nucleation catalyst, $CH_3CO_2Na \cdot 3H_2O$ melt supercooled serverely and frequently failed to crystallize on cooling to 40°C when samples were preheated above 70°C.

It is clear from Fig. 32 that the supercooling, $\Delta\theta_c$, of $CH_3CO_2Na \cdot 3H_2O$ melt containing $Na_4P_2O_7$ as a nucleation catalyst is about −8°C. This supercooling is negatively larger

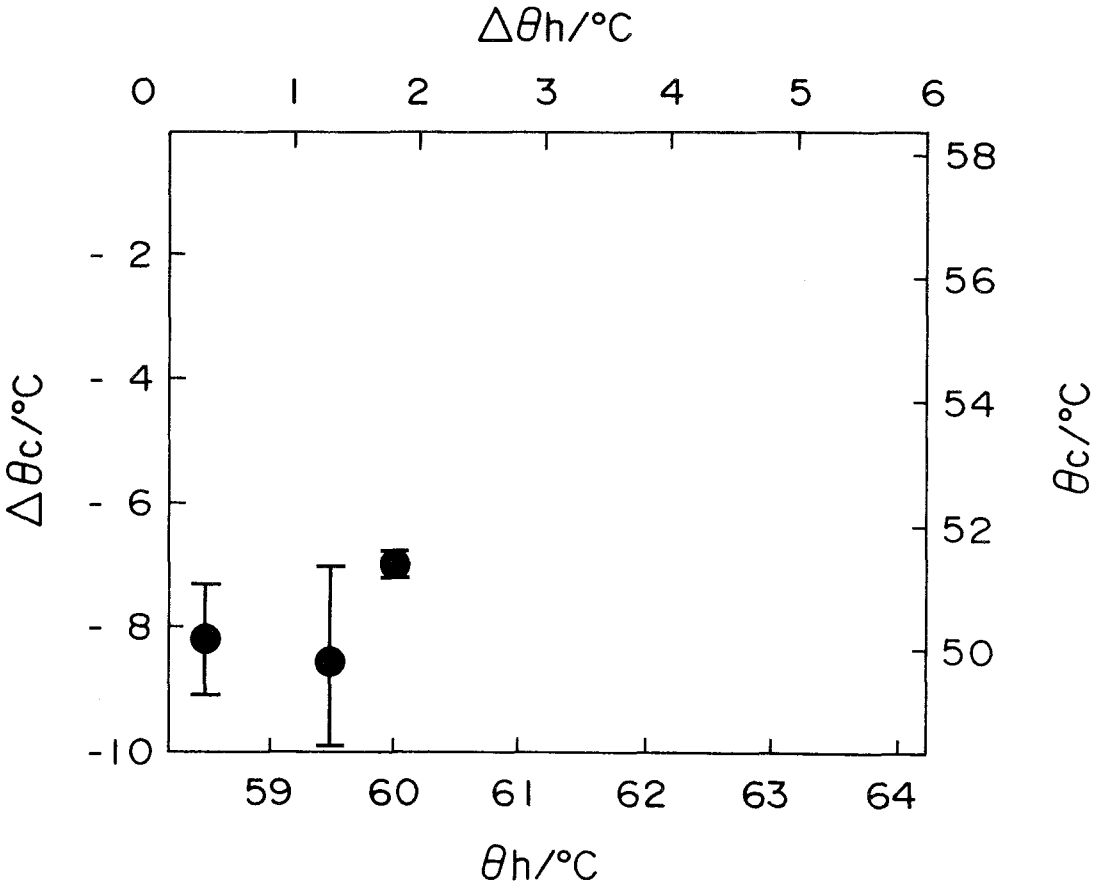

Fig. 32. Supercooling of $CH_3CO_2Na \cdot 3H_2O$ melt containing a small amount of $Na_4P_2O_7$ as a nucleation catalyst in relation to the preheating temperature.

than that of bulk sample (about $-6°C$) which is described in paragraph III. 4. The scatter of the data in this experiment is also larger than that of data for bulk sample. The crystallization behavior of $CH_3CO_2Na \cdot 3H_2O$ from the melt containing the nucleation catalyst is considered to depend upon the quantity of the sample.

In the case of using Na_2HPO_4 as a nucleation catalyst, the $\Delta\theta_c$ is about $-6°C$, which is in very good agreement with the data obtained with bulk sample preheated at 70°C. The scatter of the data is very small as well as with the bulk sample. It is understood from Fig. 33 that the $\Delta\theta_c$ is kept almost constant, about $-6°C$, when the sample is preheated below

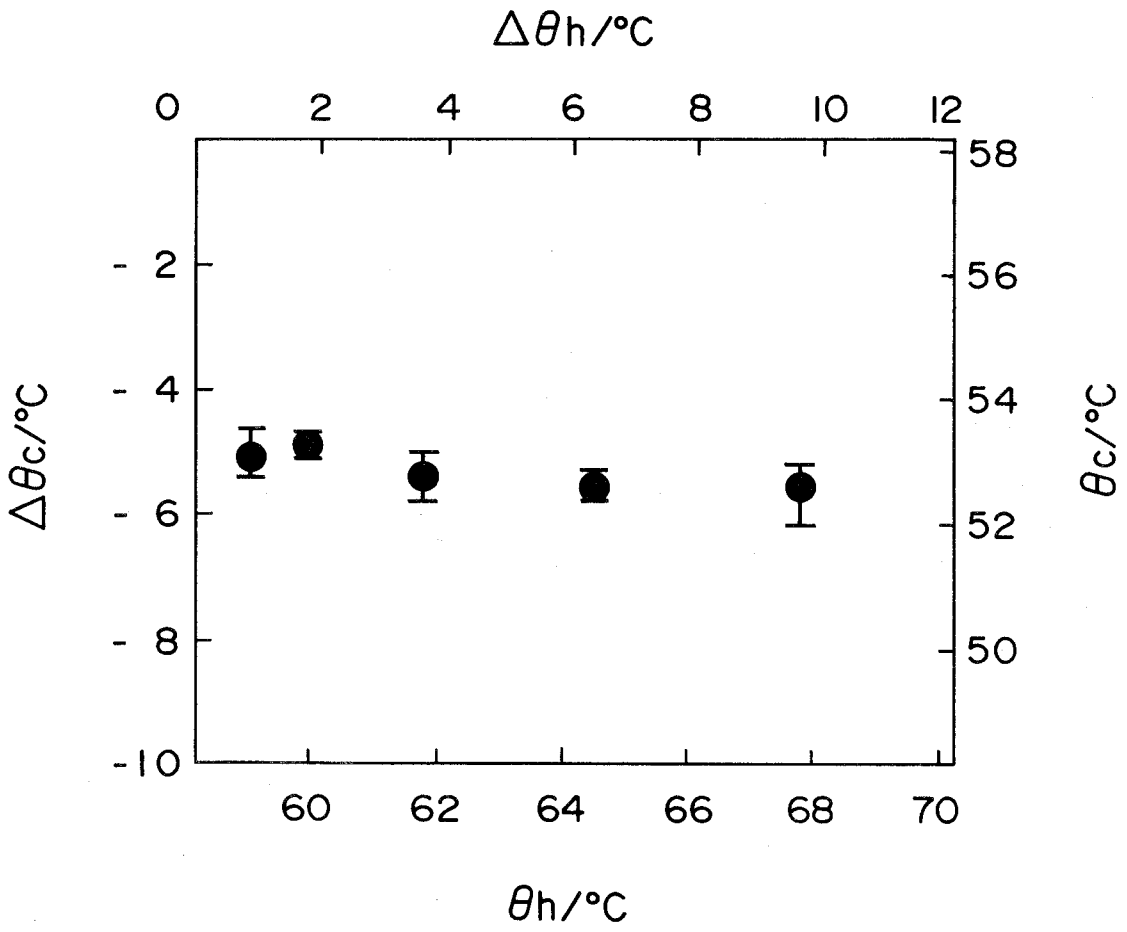

Fig. 33. Supercooling of $CH_3CO_2Na \cdot 3H_2O$ melt containing a small amount of Na_2HPO_4 as a nucleation catalyst in relation to the preheating temperature.

the deactivation temperature of the nucleation catalyst. This characteristic of the nucleation catalyst is very important in the discussion of the heterogeneous nucleation.

As shown in Figs. 34 and 35, the supercooling of $CH_3CO_2Na \cdot 3H_2O$ melt containing Na_2WO_4 or LiF as a nucleation catalyst is about $-6°C$. It is in good agreement with that of the bulk sample, as well as in the case of using Na_2HPO_4 as a nucleation catalyst. Their $\Delta\theta_c$s are also very close to the $\Delta\theta_c$ of the melt containing Na_2HPO_4 as a nucleation catalyst.

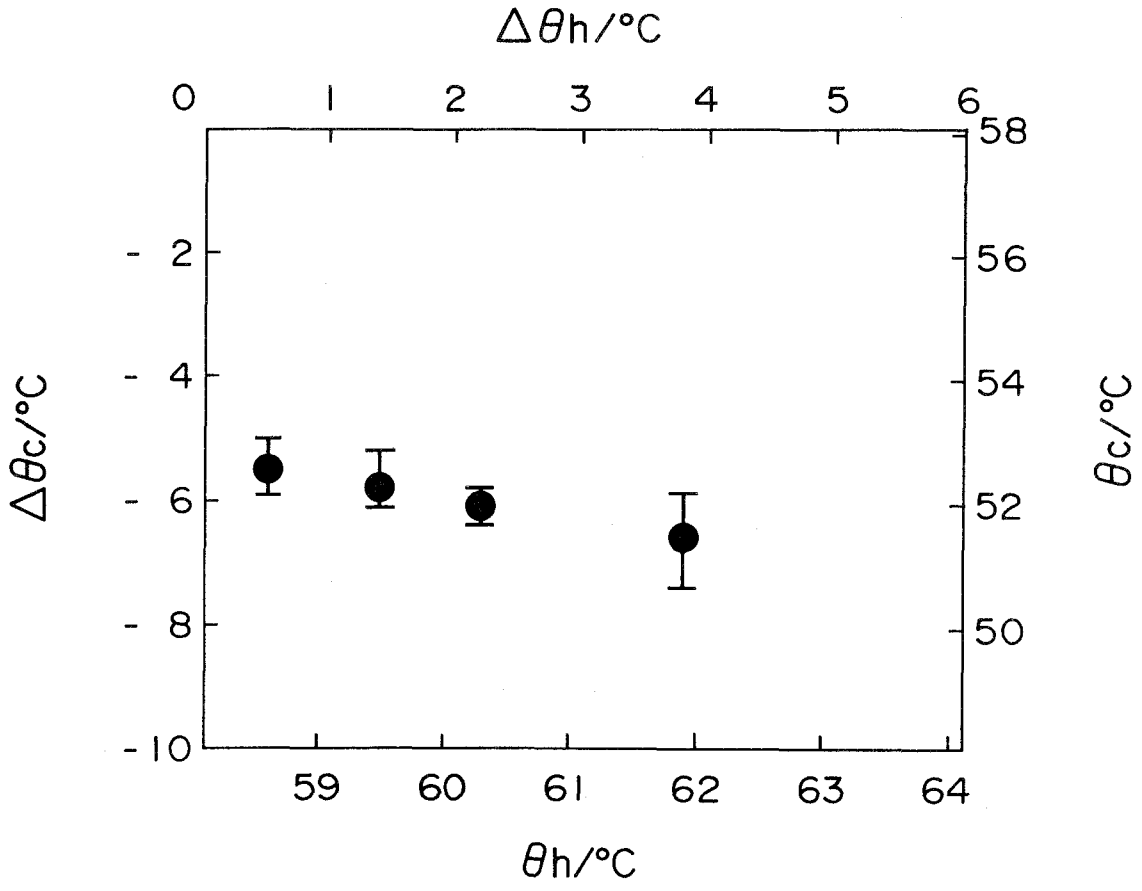

Fig. 34. **Supercooling of $CH_3CO_2Na \cdot 3H_2O$ melt containing a small amount of Na_2WO_4 as a nucleation catalyst in relation to the preheating temperature.**

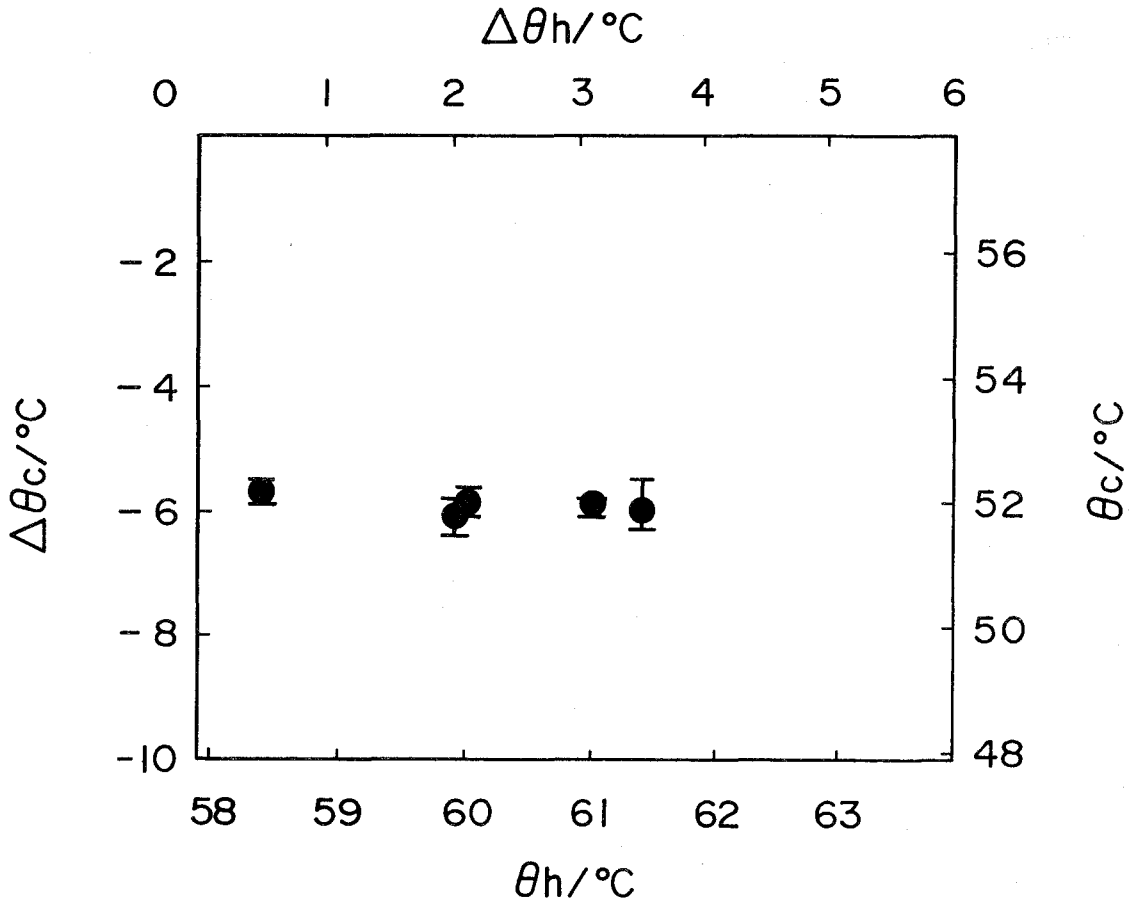

Fig. 35. Supercooling of $CH_3CO_2Na \cdot 3H_2O$ melt containing a small amount of LiF as a nucleation catalyst in relation to the preheating temperature.

III. 9 Catalytic Poison for the Nucleation Catalyst

It was found that, when a small amount of glycine ($H_2NCH_2CO_2H$) or calcium tartrate tetrahydrate ($C_4H_4O_6Ca \cdot 4H_2O$) was added to a CH_3CO_2Na aqueous solution with a nucleation catalyst, the catalyst was deactivated during thermal cycling, even if heating temperature is much lower than the deactivation temperature. The organic compounds, $H_2NCH_2CO_2H$ and $C_4H_4O_6Ca \cdot 4H_2O$ act as a catalytic poison for the nucleation catalyst. In this paragraph, the deactivation behavior of the nucleation catalyst is presented. In the

present experiment, Na_2HPO_4 is used as a nucleation catalyst.

III. 9. 1 Experimental Procedure

$CH_3CO_2Na \cdot 3H_2O$, Na_2HPO_4, $H_2NCH_2CO_2H$ and $C_4H_4O_6Ca \cdot 4H_2O$ were guaranteed grade reagents from Wako Pure Chemical Industries, Ltd. Mixtures of eight grams of 58 wt% CH_3CO_2Na aqueous solution, 0.16 g of Na_2HPO_4, and 0.16 g of $H_2NCH_2CO_2H$ or $C_4H_4O_6Ca \cdot 4H_2O$ were sealed in the tubes. The tubes were put into a water bath equipped with a gently vibrating rack. Before subsequent steps, all tubes were heated at 70°C for 1 h and then cooled to room temperature in order to force $CH_3CO_2Na \cdot 3H_2O$ to crystallize. Then the tubes were shaked if necessary. The tubes were kept for a duration longer than one week at room temperature in order to obtain some reproducible data.

Fifty tubes were heated to a constant preheating temperature for 3 h and then cooled to 40°C at the rate of 5°C/h. The preheating temperatures were 75 and 80°C. In some of 50 tubes preheated for a certain total time, $CH_3CO_2Na \cdot 3H_2O$ was failed to crystallize on cooling to 40°C. Such tubes were excluded because the nucleation catalyst in the tube must had been deactivated or degraded in its nucleation ability. The percentage of the tubes in which $CH_3CO_2Na \cdot 3H_2O$ did not crystallize on cooling over total tubes was plotted against the total preheating time to get Figs. 36 and 37. The ordinate in these figures, P/(%), corresponds to the deactivation probability of the nucleation catalyst. The nucleation catalyst in the presence of the catalytic poison deactivates in shorter time preheating.

III. 9. 2 Results

It can be seen from Fig. 36 that, in the 50 tubes each containing 8 g of 58 wt% CH_3CO_2Na aqueous solution, 0.16 g of Na_2HPO_4 and 0.16 g of $H_2NCH_2CO_2H$,

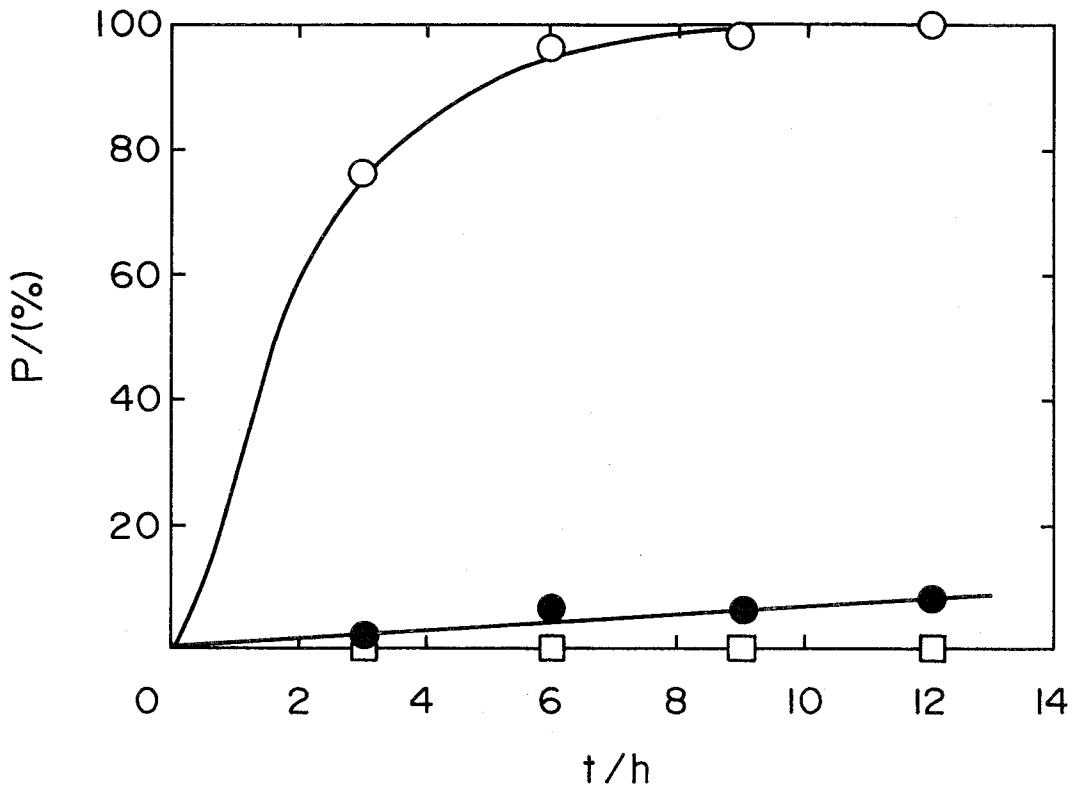

Fig. 36. **Influence of preheating time on the crystallization of $CH_3CO_2Na \cdot 3H_2O$ from the 58.0 wt% CH_3CO_2Na aqueous solutions containing a small amount of Na_2HPO_4 and the catalytic poison, which were preheated at 75°C.**
○: the catalytic poison is glycine,
●: the catalytic poison is calcium tartrate tetrahydrate,
□: the catalytic poison is not added.

$CH_3CO_2Na \cdot 3H_2O$ did not crystallize at all, even after the tubes had been preheated for 6 h at 75°C. In all tubes without catalytic poison, $CH_3CO_2Na \cdot 3H_2O$ crystallized after the tubes had been preheated for 12 h at 75°C. In the tubes containing $C_4H_4O_6Ca \cdot 4H_2O$, the nucleation catalyst also began to get deactivated for the preheating at 75°C. As also shown in Fig. 37, the nucleation catalyst in the tube containing $H_2NCH_2CO_2H$ or $C_4H_4O_6Ca \cdot 4H_2O$ was deactivated in a much shorter time for preheating at 80°C than that in the tube without a catalytic poison. It is clear from these results that the nucleation catalyst is inhibit-

ed by the presence of $H_2NCH_2CO_2H$ or $C_4H_4O_6Ca \cdot 4H_2O$. Then, these compounds are considered to be a catalytic poison for the nucleation catalyst such as Na_2HPO_4. The catalytic poison potency of $H_2NCH_2CO_2H$ is considered to be higher than that of $C_4H_4O_6Ca \cdot 4H_2O$, because, as shown in Fig. 36, the nucleation catalysts in the presence of $H_2NCH_2CO_2H$ were deactivated in shorter time for preheating at 75°C than those in the presence of $C_4H_4O_6Ca \cdot 4H_2O$. It is the common feature of these organic compound to have the COOH group, as well as in $CH_3CO_2Na \cdot 3H_2O$.

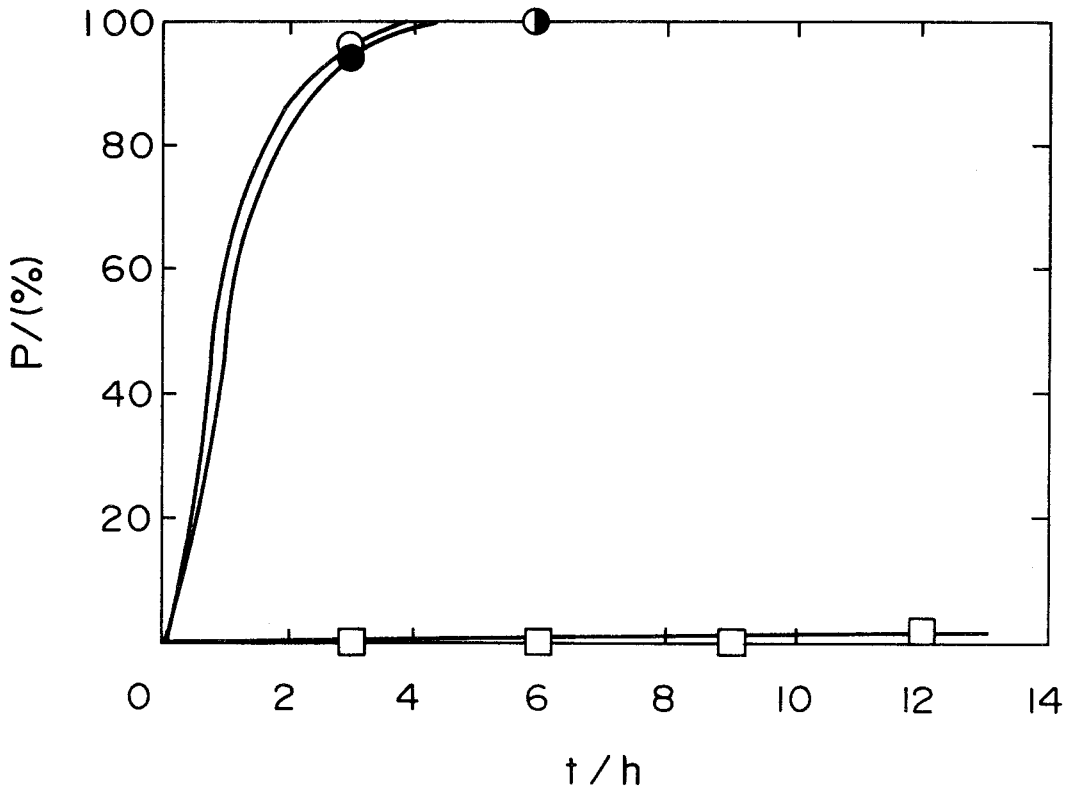

Fig. 37. **Influence of preheating time on the crystallization of $CH_3CO_2Na \cdot 3H_2O$ from the 58.0 wt% CH_3CO_2Na aqueous solutions containing a small amount of Na_2HPO_4 and the catalytic poison, which were preheated at 80°C.**
○: the catalytic poison is glycine,
●: the catalytic poison is calcium tartrate tetrahydrate,
□: the catalytic poison is not added.

III. 10 Phase Equilibria in the Aqueous System Containing CH_3CO_2Na and the Nucleation Catalyst, $Na_4P_2O_7$ or Na_2HPO_4

In an earlier paragraph, the addition of a small amount of nucleation catalyst to CH_3CO_2Na aqueous solution was shown to be very effective for heterogeneous nucleation of $CH_3CO_2Na \cdot 3H_2O$ from the solution. To promote the investigation, a knowledge is required of the aqueous system containing CH_3CO_2Na and the nucleation catalyst.

The phase diagrams of the binary systems, CH_3CO_2Na-H_2O, $Na_4P_2O_7$-H_2O and Na_2HPO_4-H_2O, based on the data from Seidell's compilation, are shown in Figs. 38-40. In these figures, W_a, W_p and W_q are the mass fractions of CH_3CO_2Na, $Na_4P_2O_7$ and Na_2HPO_4 respectively.

This paragraph reports the results from the investigation of $Na_4P_2O_7$ or Na_2HPO_4 together with CH_3CO_2Na aqueous solution.

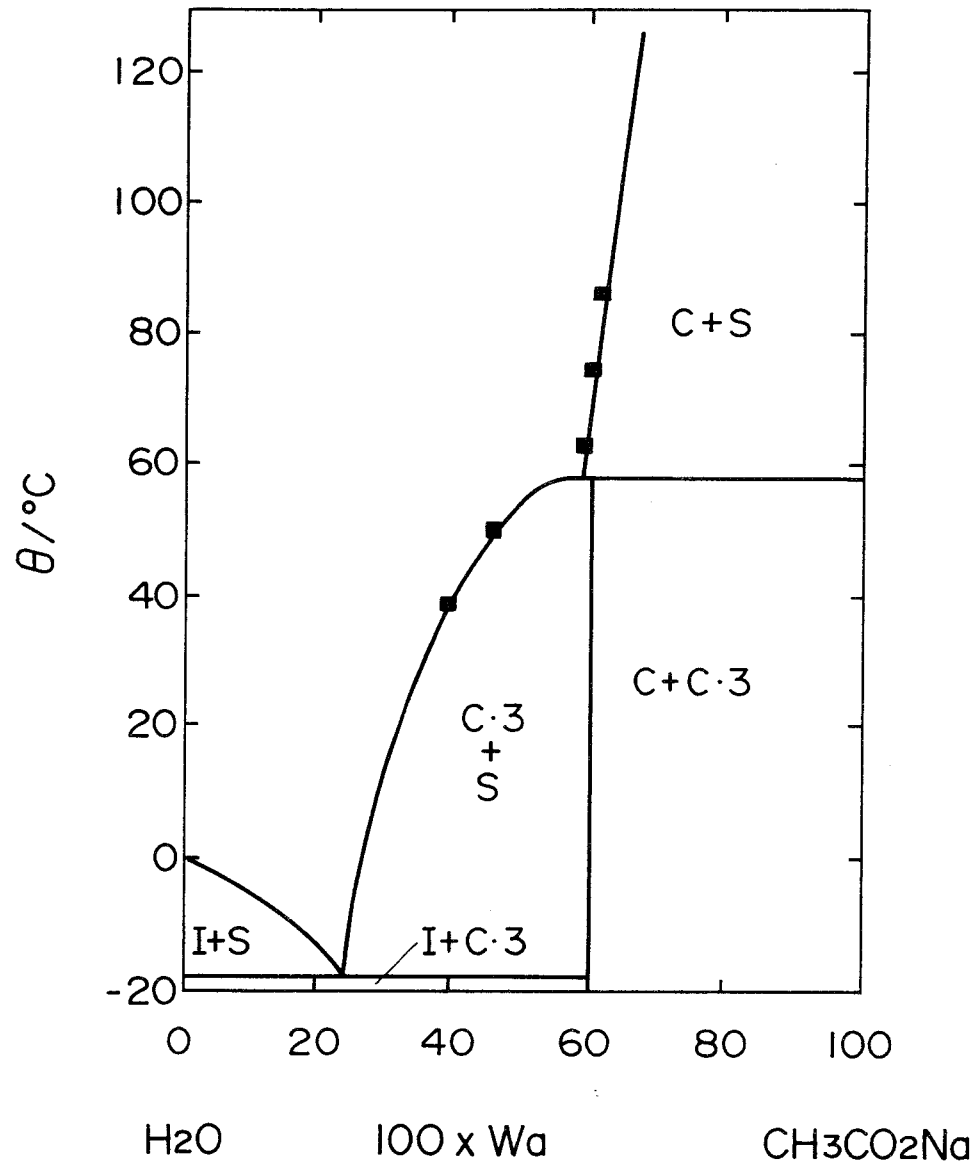

Fig. 38. The phase diagram of the binary system CH_3CO_2Na-H_2O.
■: the data obtained by the present experiment.
Symbols: C=CH_3CO_2Na, C·3=$CH_3CO_2Na \cdot 3H_2O$,
I=ice, S=solution.

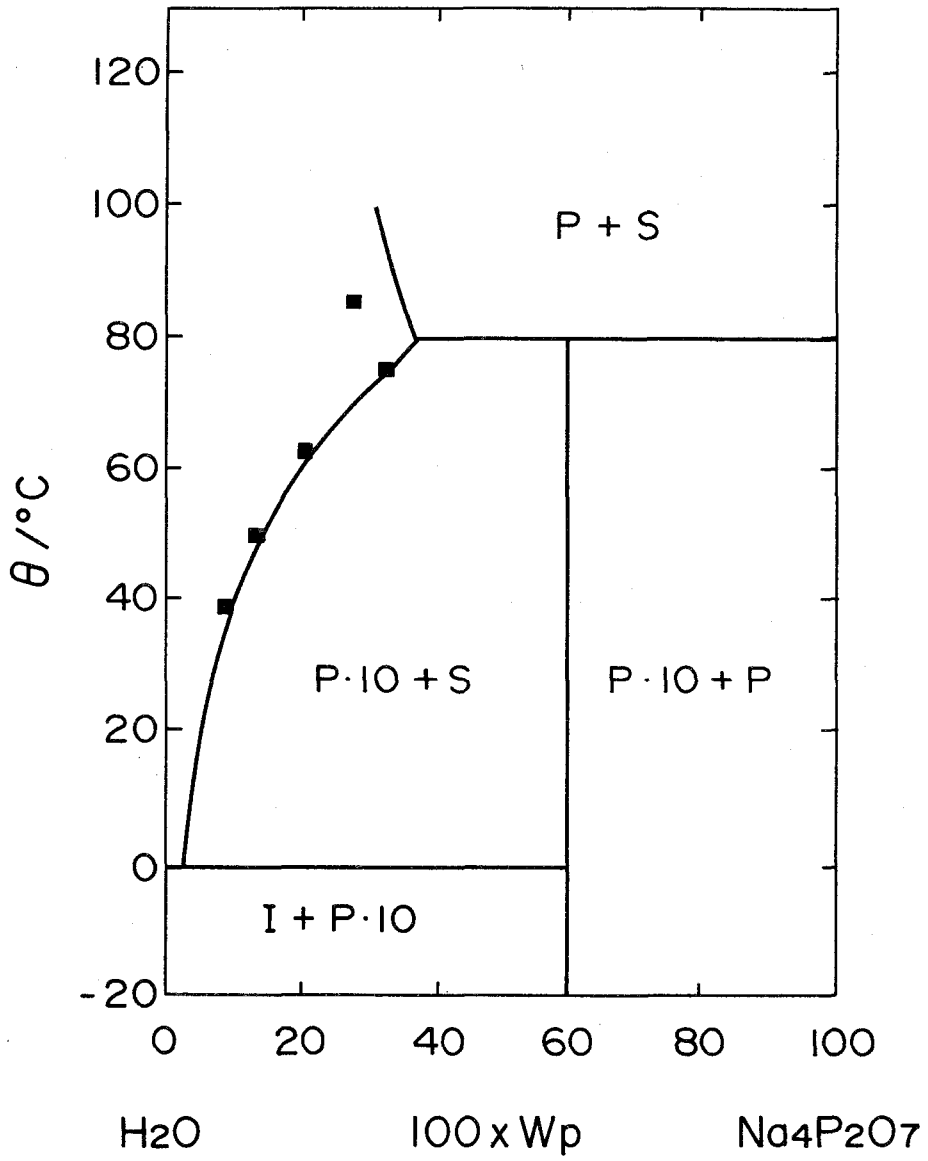

Fig. 39. The phase diagram of the binary system $Na_4P_2O_7$-H_2O.
■: the data obtained by the present experiment.
Symbols: P=$Na_4P_2O_7$, P·10=$Na_4P_2O_7 \cdot 10H_2O$.

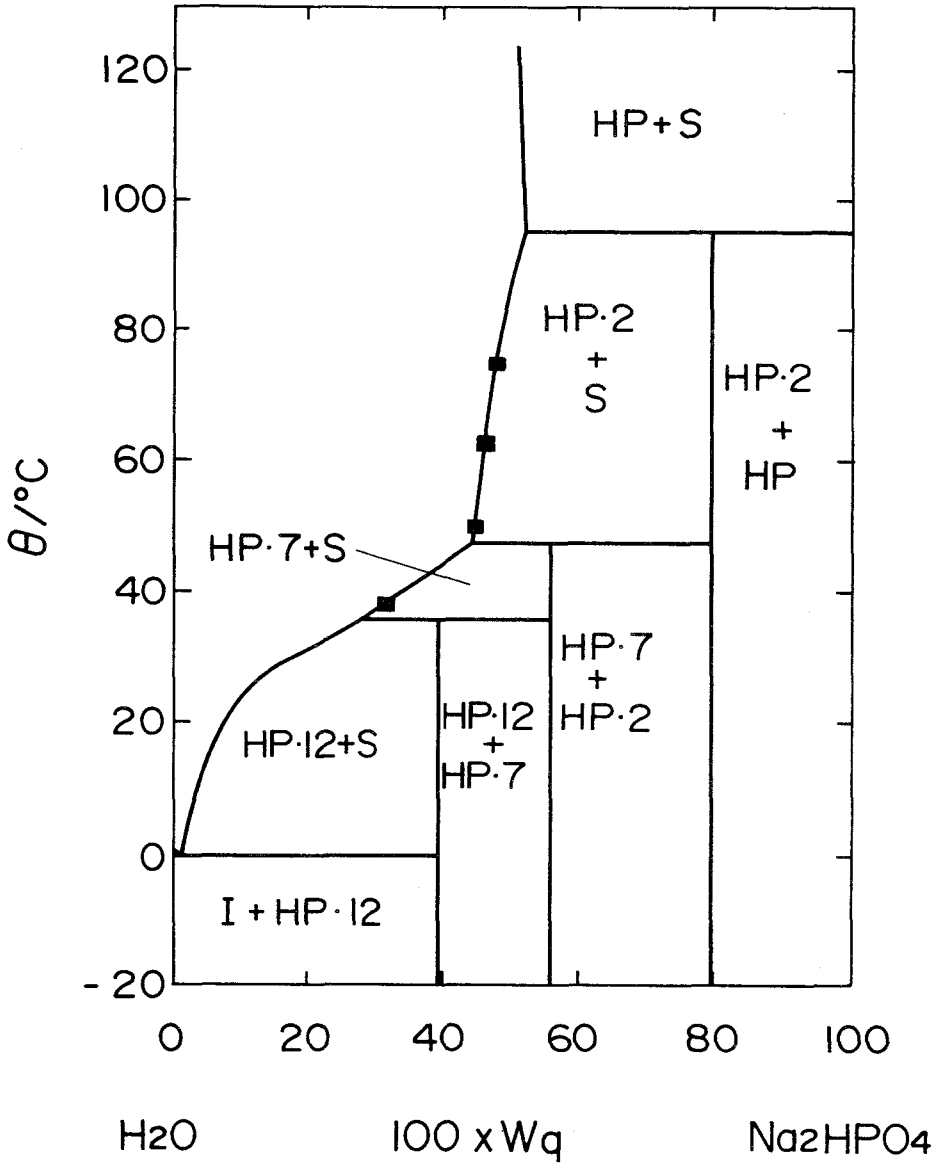

Fig. 40. The phase diagram of the binary system Na_2HPO_4-H_2O.
■: the data obtained by the present experiment.
Symbols: HP=Na_2HPO_4, HP·2=$Na_2HPO_4 \cdot 2H_2O$,
HP·7=$Na_2HPO_4 \cdot 7H_2O$, HP·12=$Na_2HPO_4 \cdot 12H_2O$.

III. 10. 1 Experimental Procedure

$CH_3CO_2Na \cdot 3H_2O$, anhydrous CH_3CO_2Na, $Na_4P_2O_7 \cdot 10H_2O$ and Na_2HPO_4 were guaranteed grade reagents. Weighed quantities of reagents and distilled water were placed in a glass vessel equipped with a stirrer bar. The glass vessel was sealed and immersed in a water bath, whose temperature was sealed and immersed in a water bath, whose temperature was controlled at the setting temperature within ±0.5°C. After stirring at a determined temperature for 6 h, the supernatant solution was pipetted off through the filter.

$Na_4P_2O_7$ or Na_2HPO_4 concentration was determined by the analysis of the supernatent solution. The supernatant solution was also dried at 120°C in an oven and the total salt concentration was determined. The sodium acetate concentration was calculated from the difference in concentration between the total salt and $Na_4P_2O_7$ or Na_2HPO_4. The residual solid in equilibrium with the saturated solution was separated and it was identified by X-ray diffraction.

The pyrophosphate ion concentration was measured colorimetrically. Concentrated nitric acid was added in the dilute supernatant solution and heated at 80°C for about 1 h in order to decompose a pyrophosphate ion into two orthophosphate ions. Dilute sulfuric acid was added furthermore. When ammonium molybdate aqueous solution was introduced into the solution, a yellow ammonium molybdophosphate was deposited. The precipitate was extracted with isobutyl methyl ketone. The extract was dried over anhydrous sodium sulfate. The absorbance of the extract was measured at 400 nm.

The hydrogenphosphate ion concentration was analyzed colorimetrically in a similar manner as the analysis of pyrophosphate ion concentration.

III. 10. 2 Results

III. 10. 2. 1 Ternary System CH_3CO_2Na-$Na_4P_2O_7$-H_2O

Table 5. Isotherms of the ternary system CH_3CO_2Na-$Na_4P_2O_7$-H_2O at 38, 50, 62, 75 and 85°C.

	Solution		Solid phase		Solution		Solid phase
	$100\times W_a$[a]	$100\times W_p$[b]			$100\times W_a$	$100\times W_p$	
38°C	0	8.5	P·10	62°C	39.9	0.10	P
	5.5	3.1	P·10		46.4	0.04	P
	11.1	1.1	P·10		51.3	0.03	P
	16.3	0.54	P·10		58.0	0.02	P+C
	21.0	0.28	P·10		58.2	0	C
	25.6	0.18	P·10	75	0	31.7	P·10
	29.9	0.14	P·10		2.5	26.0	P·10
	34.0	0.11	P·10		4.8	20.6	P·10+P
	37.9	0.10	P·10		9.4	11.1	P
	37.9	0.08	P·10+C·3		20.2	2.4	P
	38.5	0	C·3		29.3	0.55	P
50	0	12.9	P·10		36.9	0.13	P
	6.5	4.9	P·10		44.0	0.05	P
	13.4	1.6	P·10		50.1	0.03	P
	19.2	0.73	P·10		55.9	0.03	P
	25.0	0.47	P·10		59.2	0.02	P+C
	29.7	0.31	P·10		59.6	0	C
	34.0	0.24	P·10	85	0	27.4	P
	37.3	0.22	P·10+P		9.3	9.3	P
	41.6	0.10	P		18.9	1.9	P
	45.5	0.06	P+C·3		27.2	0.49	P
	45.4	0	C·3		34.2	0.18	P
62	0	20.4	P·10		40.9	0.09	P
	9.7	6.3	P·10		46.4	0.05	P
	19.5	2.1	P·10		51.9	0.02	P
	21.4	1.3	P·10+P		56.6	0.02	P
	24.7	1.1	P		60.8	0.02	P+C
	29.3	0.73	P		60.8	0	C
	35.5	0.24	P				

a) W_a is the mass fraction of CH_3CO_2Na in the system.

b) W_p is the mass fraction of $Na_4P_2O_7$ in the system.

c) Symbols: C= CH_3CO_2Na, C·3= $CH_3CO_2Na\cdot 3H_2O$, P= $Na_4P_2O_7$, P·10= $Na_4P_2O_7\cdot 10H_2O$.

Isotherms at five temperatures between 38 and 85°C are shown in Table 5. One of isotherms is illustrated in Fig. 41. In this figure, closed circle indicates isothermally invariant point. The solution at this point is in equillibirum with two solid phases (for point *a*, they are $Na_4P_2O_7$ and $Na_4P_2O_7 \cdot 10H_2O$). The solubilities of the binary systems, CH_3CO_2Na-H_2O and $Na_4P_2O_7$-H_2O, which are determined in the present experiments, are plotted in Figs. 38 and 39. From these figures, it is clear that the solubilities determined here are in good agreement with the reported data.

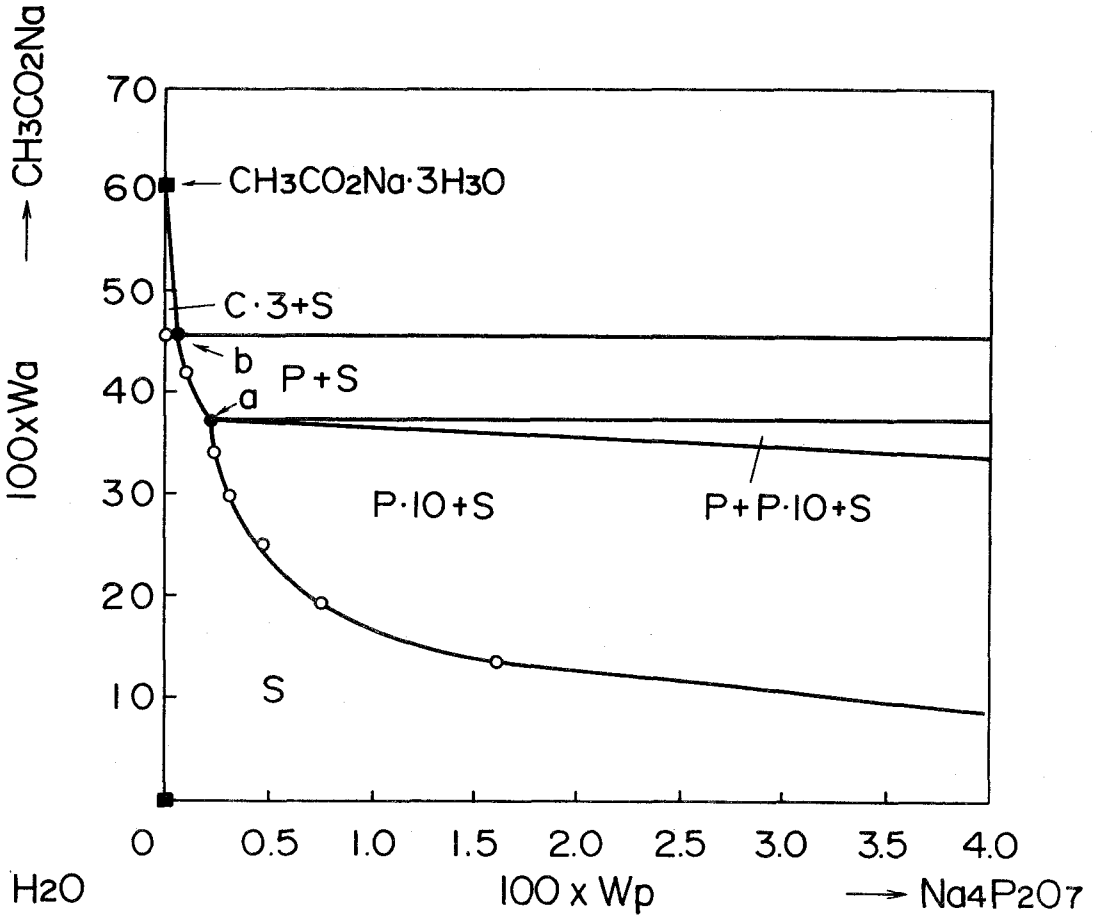

Fig. 41. **Isotherm of the ternary system CH_3CO_2Na-$Na_4P_2O_7$-H_2O at 50°C.**
○: isothermally univariant point,
●: isothermally invariant point.

The solids in equilibrium with the solution of the system include no double salt in the temperature range under investigation. The CH_3CO_2Na saturated solutions contain only a small amount of $Na_4P_2O_7$ and they have a very strong influence due to dehydration on the $Na_4P_2O_7 \cdot 10H_2O$. Accordingly, anhydrous $Na_4P_2O_7$ must be formed at temperatures which are low compared with the corresponding one in the pure aqueous system (79.5°C).

The isothermally invariant points below 85°C were plotted, with CH_3CO_2Na concentration as ordinate and $Na_4P_2O_7$ concentration as abscissa, as shown in Fig. 42. There, it is presumed that the solubility of $Na_4P_2O_7$ in CH_3CO_2Na solutions is insignificant below 0°C. This figure is informative for a survey of the formation field of the solid.

Isothermally invariant points were plotted with temperature as ordinate and $Na_4P_2O_7$ concentration as abscissa. The lowest formation temperature of anhydrous $Na_4P_2O_7$ is determined from the point of intersection of the curves on which the solution is in equilibrium with two solid phases and it is about 47°C.

It is understood from the transition temperature from $Na_4P_2O_7 \cdot 10H_2O$ to anhydrous $Na_4P_2O_7$ (47°C) and the crystallization temperature of $CH_3CO_2Na \cdot 3H_2O$ (53°C) that there are anhydrous $Na_4P_2O_7$ solid particles in the solution when $CH_3CO_2Na \cdot 3H_2O$ is heterogeneously nucleated.

In 20 tubes each containing 8 g of 58 wt% CH_3CO_2Na aqueous solution with 0.0001, 0.0005 or 0.001 g of $Na_4P_2O_7 \cdot 10H_2O$ added, $CH_3CO_2Na \cdot 3H_2O$ hardly crystallized on cooling down to 40°C after $Na_4P_2O_7 \cdot 10H_2O$ had been dissolved entirely in the CH_3CO_2Na solution by preheating at 70°C. It is understood from this experiment and the phase equilibria of ternary system, CH_3CO_2Na-$Na_4P_2O_7$-H_2O, that the presence of anhydrous $Na_4P_2O_7$ solid is required for the crystallization of $CH_3CO_2Na \cdot 3H_2O$ to occur from the solution near the transition temperature.

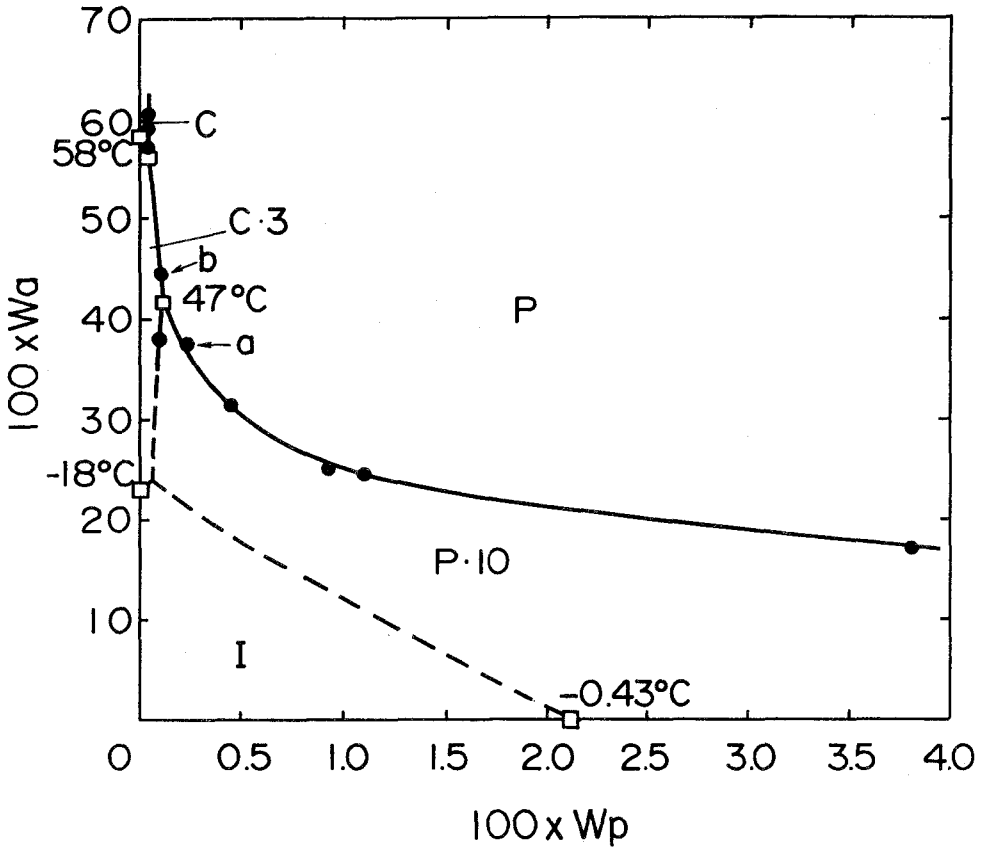

Fig. 42. Synopsis of the composition of the solution at the invariant and univariant equilibria of the ternary system CH_3CO_2Na-$Na_4P_2O_7$-H_2O. The symbols in this figure indicate the same phases as those in Figs. 38 and 39.
●: univariant point, □: invariant point.

III. 10. 2. 2 Ternary System CH_3CO_2Na-Na_2HPO_4-H_2O

Isotherms at the four temperatures between 38 and 75°C are shown in Table 6. One of isotherms is illustrated in Fig. 43. Solubilities of the binary system, Na_2HPO_4-H_2O, determined by the present experiment, are plotted in Fig. 40. From Fig. 40, it is clear that the solubilities determined here are in good agreement with the reported data.

Table 6. Isotherms of the ternary system CH_3CO_2Na-Na_2HPO_4-H_2O at 38, 50, 62 and 75°C.

	Solution		Solid phase		Solution		Solid phase
	$100\times W_a^{a)}$	$100\times W_q^{b)}$			$100\times W_a$	$100\times W_q$	
38°C	0	31.9	HP·7	62°C	0	45.4	HP·2
	5.3	24.2	HP·7		9.2	30.5	HP·2
	11.5	16.1	HP·7		21.0	14.7	HP·2
	18.0	10.3	HP·7		34.4	4.4	HP·2
	23.6	7.3	HP·7		40.4	2.5	HP·2
	27.9	6.0	HP·7		46.1	1.6	HP·2
	32.0	4.4	HP·7+HP·2		48.4	1.3	HP·2+HP
	34.0	3.6	HP·2		52.9	1.0	HP
	37.0	2.6	HP·2+C·3		57.5	0.69	HP+C
	38.5	0	C·3		58.2	0	C
50	0	44.4	HP·2	75	0	47.4	HP·2
	7.6	32.6	HP·2		9.1	32.6	HP·2
	12.1	22.7	HP·2		20.0	17.3	HP·2
	20.6	14.2	HP·2		32.1	6.5	HP·2
	29.6	6.3	HP·2		40.0	3.3	HP·2
	34.8	3.6	HP·2		42.2	2.8	HP·2+HP
	38.5	2.7	HP·2		48.1	1.6	HP
	42.3	1.7	HP·2		53.0	0.97	HP
	43.6	1.4	HP·2+C·3		59.2	0.60	HP+C
	44.5	0	C·3		59.6	0	C

a) W_a is the mass fraction of CH_3CO_2Na in the system.

b) W_q is the mass fraction Na_2HPO_4 in the system.

c) Symbols: C= CH_3CO_2Na, C·3= $CH_3CO_2Na\cdot 3H_2O$, HP= Na_2HPO_4, HP·2= $Na_2HPO_4\cdot 2H_2O$, HP·7= $Na_2HPO_4\cdot 7H_2O$.

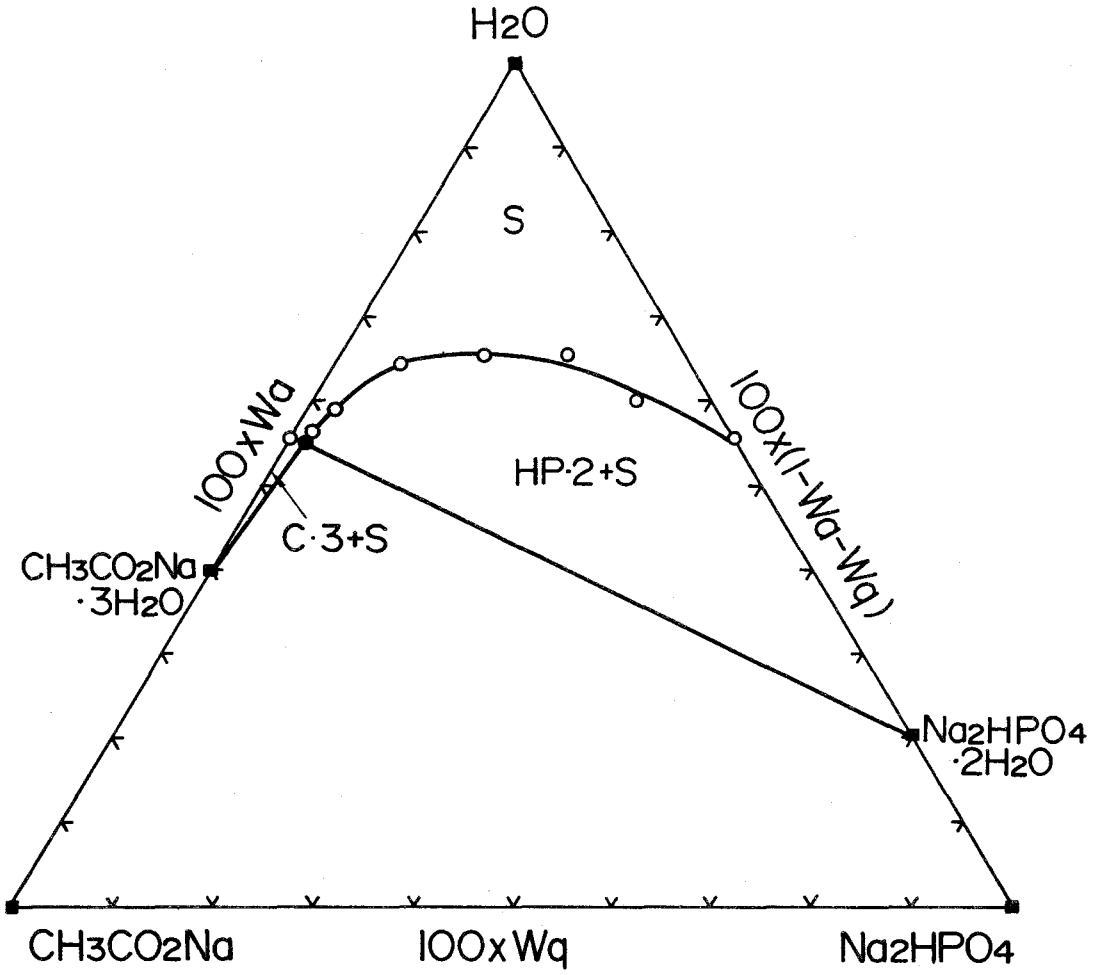

Fig. 43. **Isotherm of the ternary system CH_3CO_2Na-Na_2HPO_4-H_2O at 50°C.**
○: isothermally univariant point,
●: isothermally invariant point.

There is no formation of double salt in the present system between 38 and 75°C. It is noteworthy that the saturated CH_3CO_2Na solutions contain only a small amount of Na_2HPO_4 and that they have a very strong influence due to dehydration on the hydrous Na_2HPO_4 salts. Isothermally invariant points were plotted in a triangular diagram with some assumptions applied for lowest temperature as shown in Fig. 44. This figure gives a survey of the formation of the solid in this ternary system.

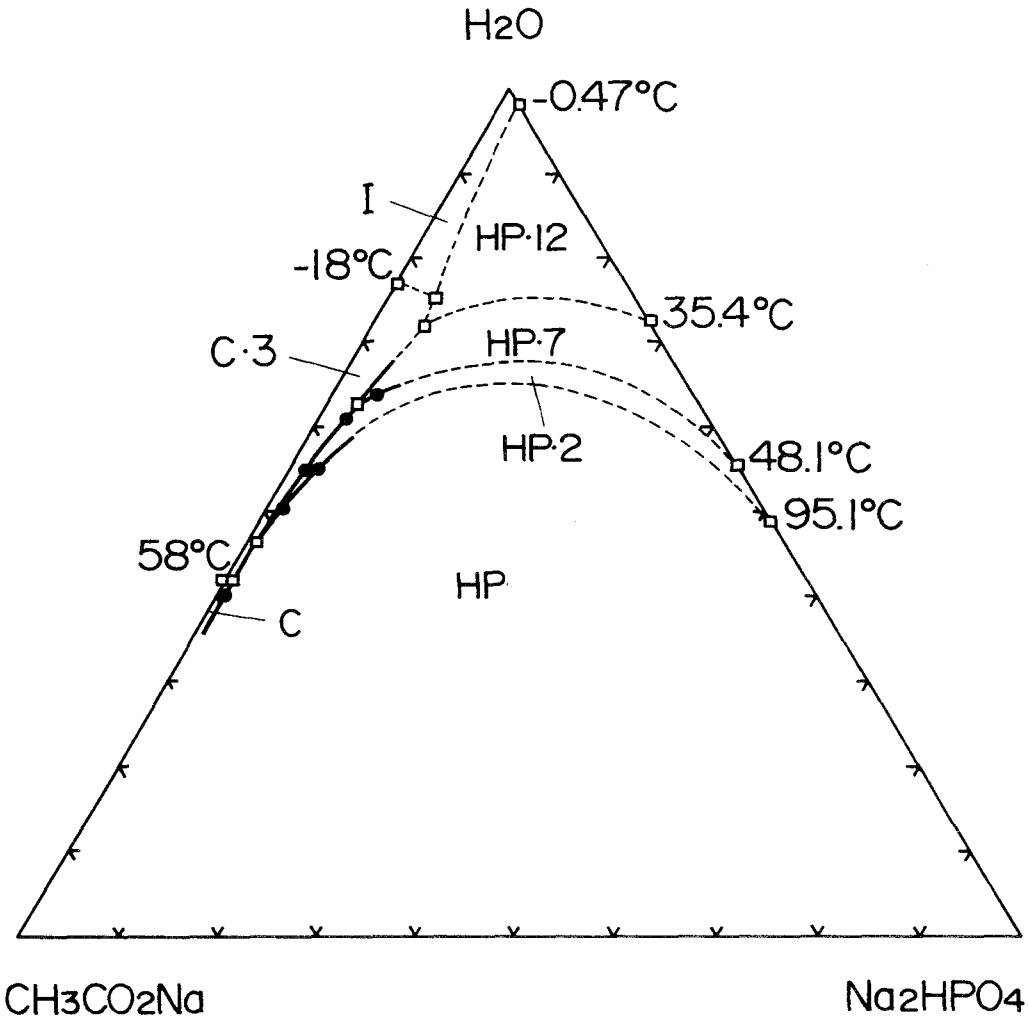

Fig. 44. **Synopsis of the composition of the solution at the invariant and univariant equilibria of the ternary system CH_3CO_2Na-Na_2HPO_4-H_2O. The symbols in this figure indicate the same phases as those in Figs. 38 and 40.**
●: univariant point, □: invariant point.

Isothermally invariant points were plotted with temperature as ordinate and Na_2HPO_4 concentration as abscissa. The lowest formation temperature for anhydrous Na_2HPO_4 is determined as about 57°C from the point of intersection of the curves on which the solution is in equilibrium with two solid phases.

It is understood from the transition temperature from $Na_2HPO_4 \cdot 2H_2O$ to Na_2HPO_4

(57°C) and the crystallization temperature of $CH_3CO_2Na \cdot 3H_2O$ that there are $Na_2HPO_4 \cdot 2H_2O$ solid particles in the solution when $CH_3CO_2Na \cdot 3H_2O$ is heterogeneously nucleated.

In 20 pieces of tubes each containing 8 g of 58 wt% CH_3CO_2Na aqueous solution with 0.001, 0.01 or 0.04 g of Na_2HPO_4 added, $CH_3CO_2Na \cdot 3H_2O$ hardly crystallized on cooling down to 40°C after Na_2HPO_4 had been dissolved entirely in the CH_3CO_2Na solution by the preheating at 70°C. It is understood from this experiment and the phase equilibria of ternary system, CH_3CO_2Na-Na_2HPO_4-H_2O, that the presence of $Na_2HPO_4 \cdot 2H_2O$ solid is required for the crystallization of $CH_3CO_2Na \cdot 3H_2O$ to occur from the solution near the transition temperature. A similar conclusion was drawn in the case of using $Na_4P_2O_7$ as a nucleation catalyst.

III. 11 Summary of the Results

Prior to the discussion, the results obtained were summarized briefly. These results are divided to two items. One (item A) is related to the nucleation catalyst of $CH_3CO_2Na \cdot 3H_2O$ and the other (item B) is related to the effect of thermal history upon the kinetics of heterogeneous nucleation of $CH_3CO_2Na \cdot 3H_2O$ from the solution with an addition of a small amount of the nucleation catalyst.

Item A

1) $Na_4P_2O_7 \cdot 10H_2O$ ($Na_4P_2O_7$), Na_2HPO_4, Na_2WO_4 or LiF acts as a crystal nucleation catalyst of $CH_3CO_2Na \cdot 3H_2O$.
2) In the case of adding $Na_4P_2O_7 \cdot 10H_2O$ to the CH_3CO_2Na aqueous solution, anhydrous $Na_4P_2O_7$ directly contributes to the heterogeneous nucleation of $CH_3CO_2Na \cdot 3H_2O$. In the case of adding Na_2HPO_4, $Na_2HPO_4 \cdot 2H_2O$ directly contributes to it.

3) When the nucleation catalyst is dissolved entirely in the CH_3CO_2Na solution, $CH_3CO_2Na \cdot 3H_2O$ hardly crystallizes from it.

Item B

1) Even if the nucleation catalyst such as $Na_4P_2O_7$ is added to CH_3CO_2Na aqueous solution, $CH_3CO_2Na \cdot 3H_2O$ hardly crystallizes from it, unless the nucleation catalyst is activated (memory effect).
2) The nucleation catalysts are deactivated at an elevated temperature above the melting point of $CH_3CO_2Na \cdot 3H_2O$. The deactivation temperature of the nucleation catalysts is dependent on varieties of them.
3) The deactivation temperature of the nucleation catalysts depends on the CH_3CO_2Na concentration of the solution and it is lowered with decreasing CH_3CO_2Na concentration of the solution.
4) The deactivation temperature of the nucleation catalysts scarecely varies with the duration of preheating time.
5) The deactivation temperature of the nucleation catalysts also depends on their activation process of them such as aging temperature and time. The deactivation temperature is raised with aging time at constant aging temperature.
6) In the case of using any nucleation catalyst, the supercooling of $CH_3CO_2Na \cdot 3H_2O$ melt, $\Delta\theta_c$, is about $-6°C$ and kept almost constant unless the melt containing the nucleation catalyst was preheated above its deactivation temperature.
7) In the presence of the catalytic poison such as $H_2NCH_2CO_2H$ or $C_4H_4O_6Ca \cdot 4H_2O$, the nucleation catalyst is deactivated for the preheating at much lower temperature than its normal deactivation temperature.

III. 12 Discussion

III. 12. 1 Effect of Thermal History upon the Kinetics of Heterogeneous Nucleation of $CH_3CO_2Na \cdot 3H_2O$

The effect of thermal history upon the kinetics of heterogeneous nucleation of $CH_3CO_2Na \cdot 3H_2O$ from the solution containing the nucleation catalyst is illustrated schematically in Fig. 45 from the summarized results. In this figure, $\Delta\theta_h (= \theta_h - \theta_m)$ is the temperature above the melting point to which the $CH_3CO_2Na \cdot 3H_2O$ melt is heated, and $\Delta\theta_c (= \theta_c - \theta_m)$ is the temperature that the melt must be subsequently supercooled in order for nucleation to occur at the lower temperature.

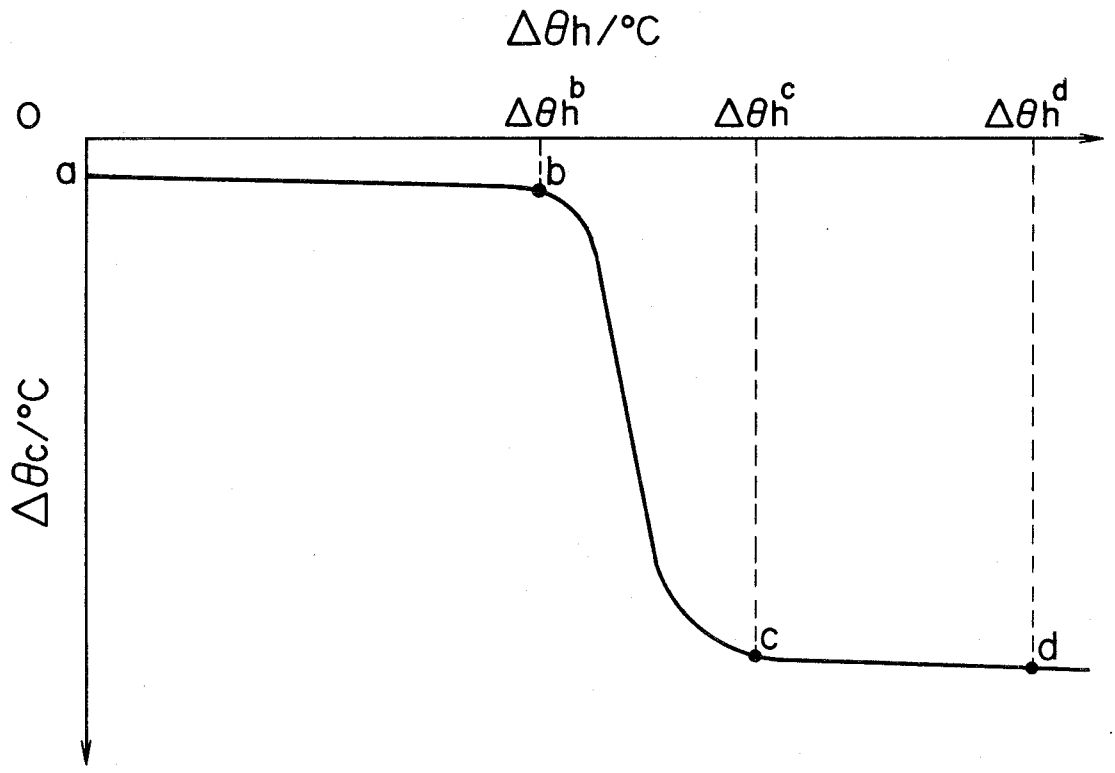

Fig. 45. Effect of thermal history on temperature of rapid nucleation in $CH_3CO_2Na \cdot 3H_2O$ melt containing the nucleation catalyst.

In the region of the curve *ab*, $\Delta\theta_c$ is scarcely dependent upon $\Delta\theta_h$. The nucleation catalyst keeps an activity in this temperature range, $0 \leqslant \Delta\theta_h \leqslant \Delta\theta_h^b$. The $\Delta\theta_h^b$ is the temper-

ature above the melting point at which the nucleation catalyst begins to be deactivated. The $\Delta\theta_h^b$ varies with several factors, for example, kind of the nucleation catalyst, concentration of the CH_3CO_2Na aqueous solution, or quantity of the sample, but it does not vary with preheating time, Δt_h. When the bulk $CH_3CO_2Na \cdot 3H_2O$ melt containing any nucleation catalyst is preheated at this temperature range, the supercooling of the sample, $\Delta\theta_c$, is about $-6°C$.

In the region *bc* in Fig. 45, $\Delta\theta_c$ is very strongly dependent upon $\Delta\theta_h$. The temperature range from $\Delta\theta_h^b$ to $\Delta\theta_h^c$ is usually narrow. When the $CH_3CO_2Na \cdot 3H_2O$ melt containing the nucleation catalyst is preheated at this temperature range, crystallization temperature of $CH_3CO_2Na \cdot 3H_2O$ usually varies very widely, though it is shown by a smooth curve in Fig. 45.

In the region *cd*, $\Delta\theta_c$ is virtually independent of $\Delta\theta_h$ and it is in good agreement with the supercooling of $CH_3CO_2Na \cdot 3H_2O$ melt without the nucleation catalyst, which was described in Chapter II. When the melt containing the nucleation catalyst is preheated in the region *cd*, the nucleation catalyst entirely loses its activity. Figure 45 has two characteristics in comparison with Fig. 6 showing the effect of the thermal history upon the kinetics of many liquid-solid transformations. One is that $\Delta\theta_c$ scarcely depends upon $\Delta\theta_h$ for the preheating below $\Delta\theta_h^b$. Another is that the supercooling is not $0°C$ but about $-6°C$, for the preheating at the temperature infinitesimal above the melting point.

III. 12. 2 Mechanism of Heterogeneous Nucleation of $CH_3CO_2Na \cdot 3H_2O$ (I)

As shown in paragraph III. 2, two explanations have applied to the memory effect of heterogeneous nucleation. One is cavity model proposed by Turnbull [70].

The cavity model explains the effect of the thermal history upon the kinetics of many liquid-solid transformations, shown in Fig. 6. However, this model can not explain the

observation of heterogeneous nucleation of $CH_3CO_2Na \cdot 3H_2O$, which is clarified in the present experiment. As shown in Fig. 45, the nucleation catalysts of $CH_3CO_2Na \cdot 3H_2O$ were deactivated for preheating at much higher temperature than the melting point of $CH_3CO_2Na \cdot 3H_2O$ (the $\Delta\theta_h^b$ is much higher). The temperature range from $\Delta\theta_h^b$ to $\Delta\theta_h^c$ is considerably narrow. The high deactivation temperature of the fully aged nucleation catalyst requires a very small fissures or cavities retaining the $CH_3CO_2Na \cdot 3H_2O$ crystals. The narrow temperature range from $\Delta\theta_h^b$ to $\Delta\theta_h^c$ requires a sharp limit of the geometry of these small cavities. Usual cavities can not fulfill these requirements.

In addition, the supercooling, $\Delta\theta_c$ is about $-6°C$ for the preheating infinitesimal above the melting point, although the cavity model expects it to be about $0°C$. Furthermore, the theory is considered to be unable to explain the aging effect on the nucleation catalyst, as described in paragraph, III. 7.

Another explanation applied to the memory effect is the crystalline adsorption model, proposed by Richards [27]. According to this model, $\Delta\theta_h$ dependence of $\Delta\theta_c$, shown in Fig. 45, is well explained. As shown in Fig. 10, crystalline adsorbate transforms to the liquid adsorbate at a higher temperature than the melting point of $CH_3CO_2Na \cdot 3H_2O$. The crystalline adsorbate contributes to the nucleation of $CH_3CO_2Na \cdot 3H_2O$ and the liquid adsorbate does not contribute to it. The high deactivation temperature of the nucleation catalyst is explained satisfactorily on the basis of this crystalline adsorption model. The narrow temperature range from $\Delta\theta_h^b$ to $\Delta\theta_h^c$, shown in Fig. 45, is possibly due to the irregular surface of the adsorbent.

The structure of crystalline adsorbate is considered to be resemble to that of $CH_3CO_2Na \cdot 3H_2O$ crystal but the crystalline adsorbate is not a real $CH_3CO_2Na \cdot 3H_2O$ crystal. Therefore, $CH_3CO_2Na \cdot 3H_2O$ melt containing the nucleation catalyst must be supercooled to about $53°C$ ($\Delta\theta_c \approx 5°C$), even if the melt is preheated at a little higher temperature than the melting point of $CH_3CO_2Na \cdot 3H_2O$.

The effect of addition of the catalytic poison for the nucleation catalysts is also explained satisfactorily. A part of the added catalytic poison is dissolved in the $CH_3CO_2Na \cdot 3H_2O$ melt. $H_3N^+CH_2COO^-$ and $CH(OH)(COO^-) \cdot CH(OH)(COO^-)$ ions in the solution presumably adsorb easily on the surface of $CH_3COONa \cdot 3H_2O$ crystalline adsorbate, because both ions have COO^- group similarily to $CH_3CO_2Na \cdot 3H_2O$. $H_3N^+CH_2COO^-$ or $CH(OH)(COO^-) \cdot CH(OH)(COO^-)$ ion is considered to cover the surface of the crystalline adsorbate during preheating. Therefore, the nucleation catalyst is deactivated for the preheating at much lower temperature than its normal deactivation temperature.

As mentioned above, the effect of thermal history upon the kinetics of heterogeneous nucleation of $CH_3CO_2Na \cdot 3H_2O$ is well explained according to the crystalline adsorption model. However, the aging effect of the nucleation catalyst can not be explained by this model. In the next paragraph, the crystalline adsorption model is improved in order to explain the aging effect.

III. 12. 3 Mechanism of Heterogeneous Nucleation of $CH_3CO_2Na \cdot 3H_2O$ (II)

Recently, the monolayer adsorbed on substrate has been studied extensively. From this study, possible phase diagrams of the adsorbed monolayer on substrate such as that shown in Fig. 46 [81] are postulated [82, 83]. The competition of adsorbate-adsorbate interaction with adsorbate-substrate lateral periodic potential can produce a sturcture which is either commensurate or incommensurate with the substrate, depending on the fitness between substrate and natural adsorbate lattice spacing; the fitness depends on both temperature and chemical potential (concentration of the solution or vapor pressure). In Fig. 46, the low-dimensional (where the ratio of the periodicity of substrate to that of adsorbed monolayer is very simple) commensurate solid adsorbate is transformed directly into the

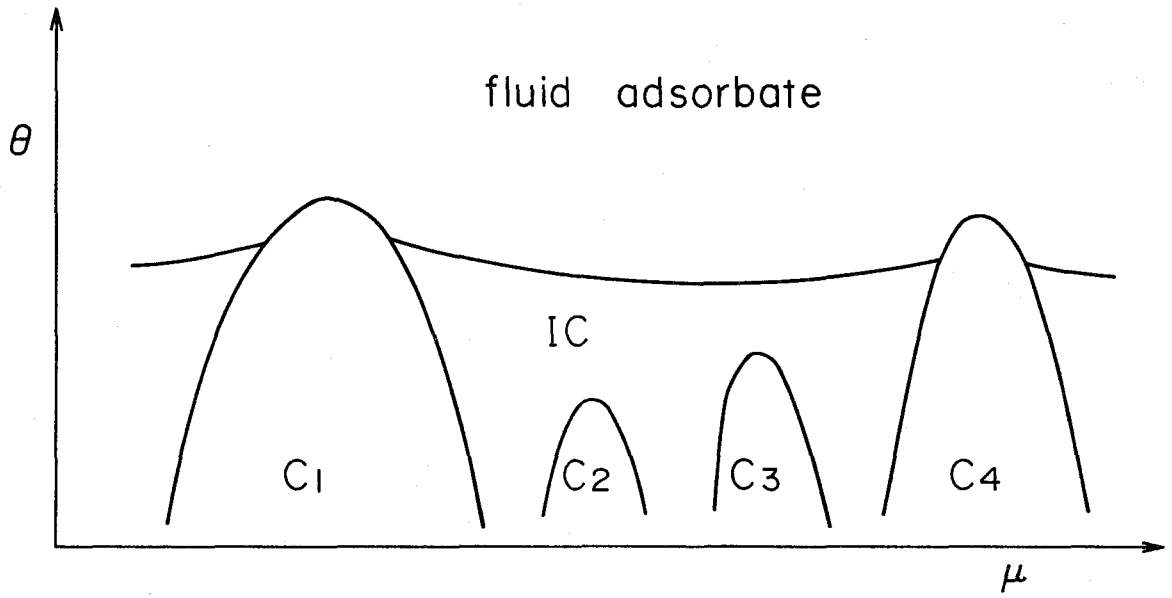

Fig. 46. **Shematic phase diagram of the monolayer on the substrate as a function of temperature (ordinate) and chemical potential (abscissa). C_n: commensurate solid adsorbate (crystalline adsorbate), IC: incommensurate solid adsorbate.**

fluid (liquid) adsorbate with rise in temperature (order-disorder transition), and the high-dimentional commensurate solid adsorbate is transformed into the fluid adsorbate through the incommensurate solid adsorbate with rise in temperature. Jaubert et al. [84] evidenced the existence of a uniaxial commensurate-incommensurate transition in a solid monolayer of xenon adsorbed on the (110) face of copper by low-energy electron diffraction and Auger electron spectroscopy. Shematic representation of atomic arrangement in Cu (110)-Xe system is shown in Fig. 47. The crystalline adsorption model, shown in Fig. 10, may be modified by considering the commensurate-incommensurate transition into solid adsorbate, as shown in Fig. 48. The results obtained in the present experiment will be discussed on the basis of this modified crystalline adsorption model.

In crystalline adsorption model proposed by Richards, the crystalline adsorbate is considered to be formed on the nucleation catalyst as soon as $CH_3CO_2Na \cdot 3H_2O$ is forced

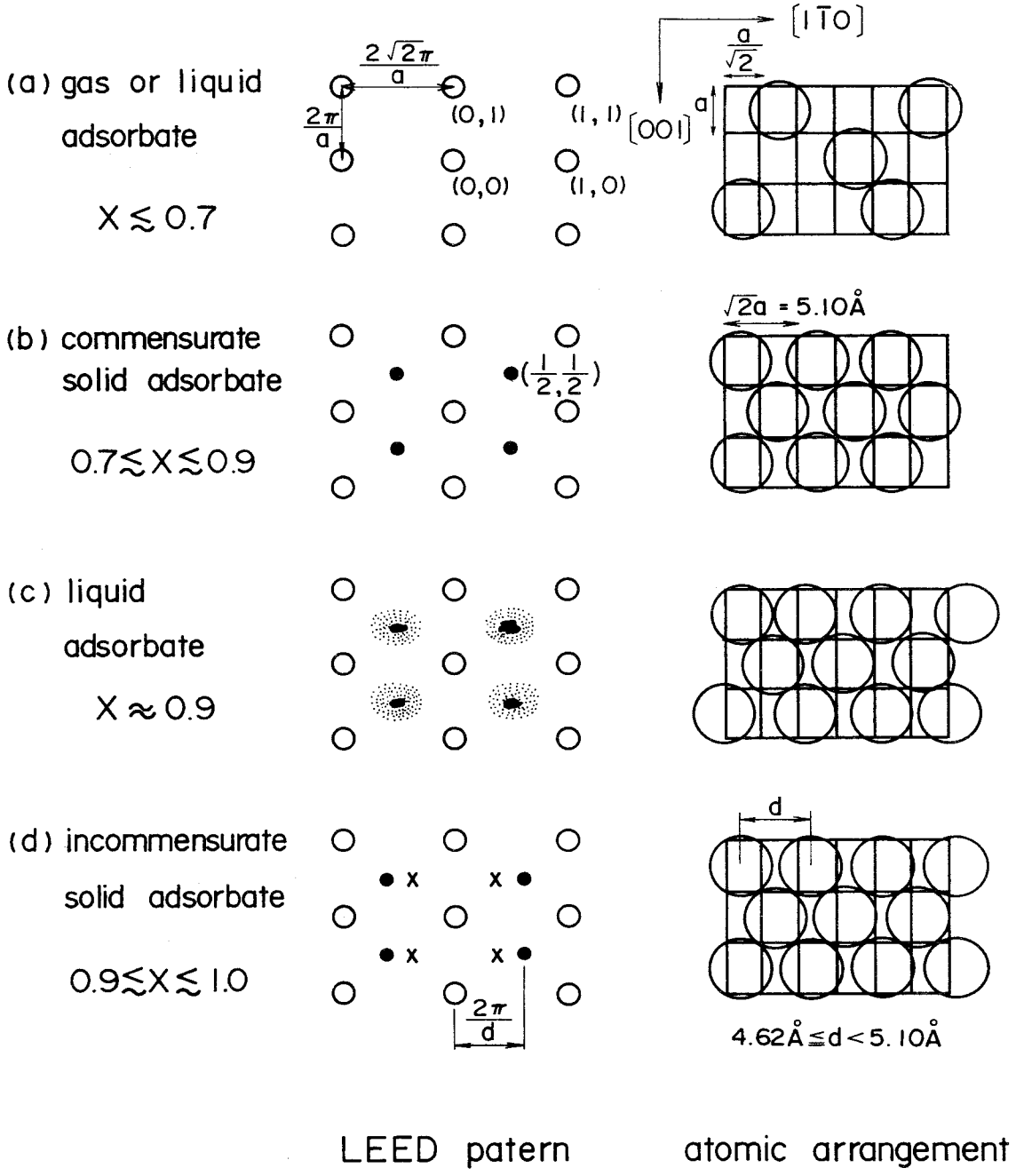

Fig. 47. Shematic representation of the commensurate-incommensurate transition in Cu(110)-Xe system at 77 K. An uniaxial compression of layer occurs along [1$\bar{1}$0] with increasing coverage.

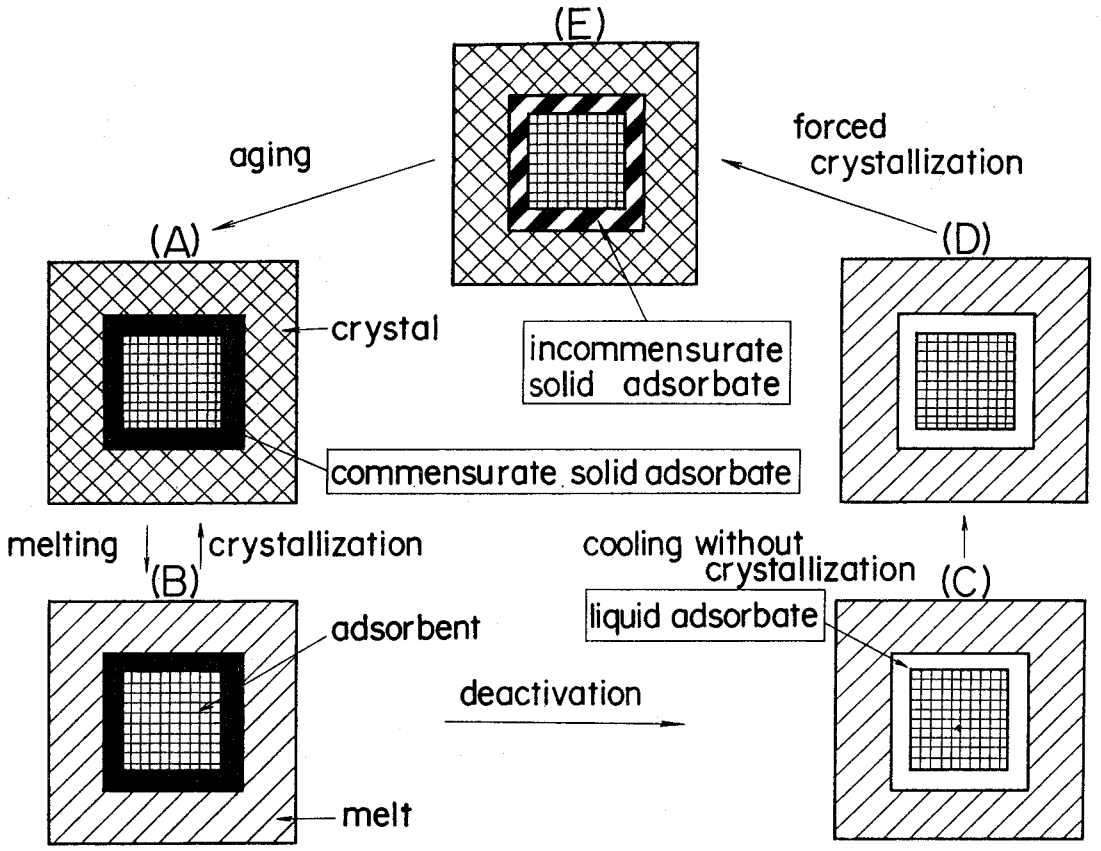

Fig. 48. **Modified adsorption model for heterogeneous nucleation. (A): crystalline state with commensurate solid adsorbate, (B): melting state with commensurate solid adsorbate, (C): melting state with fluid adsorbate, (D): supercooled state, (E): crystalline state with incommensurate solid adsorbate.**

to crystallize from a supercooled melt. However, $CH_3CO_2Na \cdot 3H_2O$ solid adsorbate, which is formed as soon as $CH_3CO_2Na \cdot 3H_2O$ is forced to crystallize from a supercooled melt containing a nucleation catalyst (adsorbent), is considered to be incommensurate with the adsorbent, because the crystallization of $CH_3CO_2Na \cdot 3H_2O$ is independent of the nucleation catalyst in the melt. The negative heat of adsorption of metastable incommensurate solid adsorbate on the nucleation catalyst is not so large as that of liquid (fluid) adsorbate.

Therefore, the incommensurate solid adsorbate melts near the bulk melting point of $CH_3CO_2Na \cdot 3H_2O$ and thus the incommensurate solid adsorbate little contributes to the nucleation of $CH_3CO_2Na \cdot 3H_2O$ from the melt.

The incommensurate solid adsorbate is transformed into the commensurate solid adsorbate (crystalline adsorbate) with elapse of time, because incommensurate solid adsorbate is considered to be a metastable phase. Commensurate solid adsorbate contributes to the nucleation of $CH_3CO_2Na \cdot 3H_2O$. The negative heat of adsorption of commensurate solid adsorbate on the adsorbent is considered to be much larger than that of liquid adsorbent. Therefore, the commensurate solid adsorbate does not melt near the bulk melting point of $CH_3CO_2Na \cdot 3H_2O$ and thus the deactivation temperature of the fully aged nucleation catalyst is much higher.

The transformation of incommensurate into commensurate solid adsorbate is considered to proceed with atomic (ionic) diffusion, because the rate of transformation is dependent on aging temperature. In the modified adsorption model illustrated in Fig. 48 as well as the crystalline adsorption model shown in Fig. 7, the commensurate solid adsorbate is transformed directly into the liquid adsorbate at an elevated temperature.

According to the modified crystalline adsorption model, a satisfactory, though qualitative, explanation has been given to the observations on the heterogeneous nucleation of $CH_3CO_2Na \cdot 3H_2O$, including the aging effect on the nucleation catalysts. The modified crystalline adsorption model is expected to apply to the heterogeneous nucleation of other salt hydrates such as $CaCl_2 \cdot 6H_2O$ [80]. In order to give some quantitative explanations for these crystal nucleation catalytic actions, the discussion is required from the structural point of view.

III. 12. 4 Crystallographic Point of View

In the case of using $Na_4P_2O_7 \cdot 10H_2O$ or Na_2HPO_4 as a nucleation catalyst, $Na_4P_2O_7$ or $Na_2HPO_4 \cdot 2H_2O$ directly contributes to the nucleation of $CH_3CO_2Na \cdot 3H_2O$ as described in paragraph III. 10. In the case of using Na_2WO_4 or LiF, it is not clear which phase directly relates to the nucleation of $CH_3CO_2Na \cdot 3H_2O$, because the phase equilibria of the ternary system CH_3CO_2Na-Na_2WO_4-H_2O and that of the reciprocal salt pair system CH_3CO_2Na-LiF-H_2O are not known yet. The phase diagram of the binary system Na_2WO_4-H_2O, based on data from Seidell's compilation [16, 85], is shown in Fig. 49. It is plausible from this phase diagram that $Na_2WO_4 \cdot 2H_2O$ directly relates to the nucleation of $CH_3CO_2Na \cdot 3H_2O$, because the transition point between $Na_2WO_4 \cdot 2H_2O$ and Na_2WO_4 is much higher than the crystallization temperature of $CH_3CO_2Na \cdot 3H_2O$ from the solution.

The solubility of LiF in H_2O is very small and the hydrates containing LiF does not occur [16, 86]. Therefore, it is also plausible that LiF directly contributes to the nucleation of $CH_3CO_2Na \cdot 3H_2O$. This is confirmed by analyzing the solid by X-ray diffraction, which is in equilibrium with the saturated solution near above the crystallization temperature of $CH_3CO_2Na \cdot 3H_2O$ (about 55°C).

The crystallographic data of $CH_3CO_2Na \cdot 3H_2O$, $Na_4P_2O_7$, $Na_2HPO_4 \cdot 2H_2O$, $Na_2WO_4 \cdot 2H_2O$ and LiF are shown in Table 7. The crystal structures of these compounds are shown in Fig. 50. As explained in paragraph III. 3, the crystal system of $CH_3CO_2Na \cdot 3H_2O$ is monoclinic. In the crystal structure of $CH_3CO_2Na \cdot 3H_2O$, Na^+ ion has distorted octahedral coordination with six oxygen atoms which consist of one acetate oxygen and five water molecules, and adjacent octahedra share an edge and form a continuous chain along the c axis. As shown in Table 7, the crystal system of $Na_4P_2O_7$, $Na_2HPO_4 \cdot 2H_2O$ and $Na_2WO_4 \cdot 2H_2O$ is orthorhombic and that of LiF is cubic [78, 87-90]. In the crystal structure of $Na_4P_2O_7$, two of the four Na^+ ions are coordinated to five oxygen atoms, while the

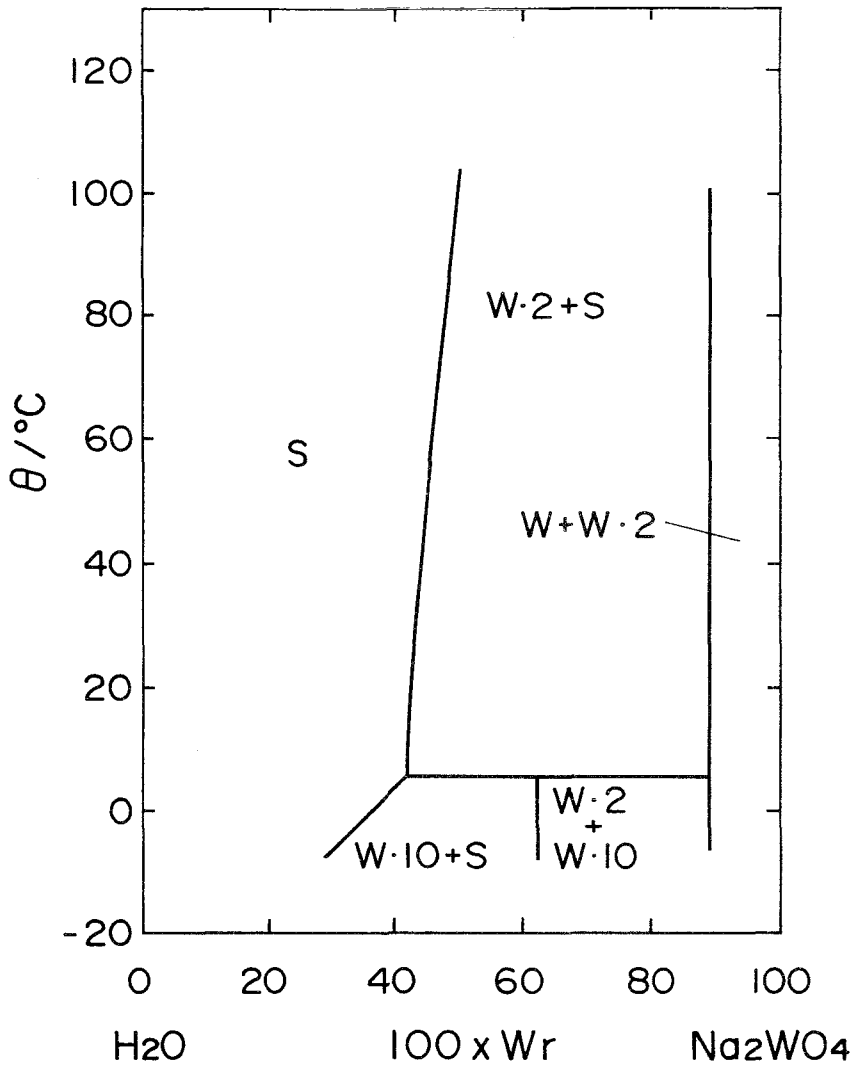

Fig. 49. **Phase diagram of the binary system Na_2WO_4-H_2O.**
Symbols: W= Na_2WO_4, W·2= $Na_2WO_4 \cdot 2H_2O$,
W·10= $Na_2WO_4 \cdot 10H_2O$.

remainders are coordinated to six oxygen atoms. The structure contains chains of cations with four nearly collinear Na^+ per cell paralleling the c axis. The crystal structure of $Na_2HPO_4 \cdot 2H_2O$ contains PO_4H tetrahedra joined along c axis by hydrogen bonding directly and via one of the water molecules and Na^+ ions have two independent coordinations. In the crystal structure of $Na_2WO_4 \cdot 2H_2O$, each Na^+ ion is surrounded by six

Table 7. Crystallographic data for $CH_3CO_2Na \cdot 3H_2O$, $Na_4P_2O_7$, $Na_2HPO_4 \cdot 2H_2O$, $Na_2WO_4 \cdot 2H_2O$ and LiF

	$CH_3CO_2Na \cdot 3H_2O$	$Na_4P_2O_7$	$Na_2HPO_4 \cdot 2H_2O$	$Na_2WO_4 \cdot 2H_2O$	LiF
Crystal System	monoclinic	orthorhombic	orthorhombic	orthorhombic	cubic
Space Group	C2/c	P 2,2,2,	Pbca	Pbca	Fm3m
Unit-cell parameter					
a/Å	12.353	9.367	16.872	8.454	4.0173
b/Å	10.466	5.390	10.359	10.598	
c/Å	10.401	13.480	6.599	13.895	
β/°	111.69				

oxygen atoms, two of which belong to water molecules. The crystal structure of LiF is a rock salt type. Li^+ ion is surrounded by six F^- ions.

As mentioned above, $CH_3CO_2Na \cdot 3H_2O$ does not resemble $Na_4P_2O_7$, $Na_2HPO_4 \cdot 2H_2O$, $Na_2WO_4 \cdot 2H_2O$ or LiF in the crystal structure. Therefore, the catalytic action of these compounds can not be explained from the crystal structure resemblance.

The studies on the heterogeneous nucleation in the solution or melt have disregarded the molecular process, by which crystalline solid grows on nucleating substrate (surface of the nucleation catalyst), and in particular have overlooked the important process by which the first monolayer of crystalline solid develops. In other system such as evaporating thin crystalline films onto substrate, the early stage of growth can be studied by low-energy electron diffraction (LEED), reflection high-energy electron diffraction (RHEED), Auger electron spectroscopy (AES), ultraviolet photoelectron spectroscopy (UPS), electron micros-

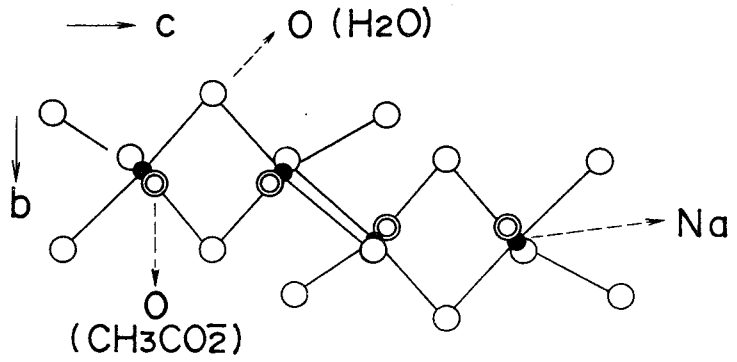

(a) The sodium ion environment as see down a axis in $CH_3CO_2Na \cdot 3H_2O$

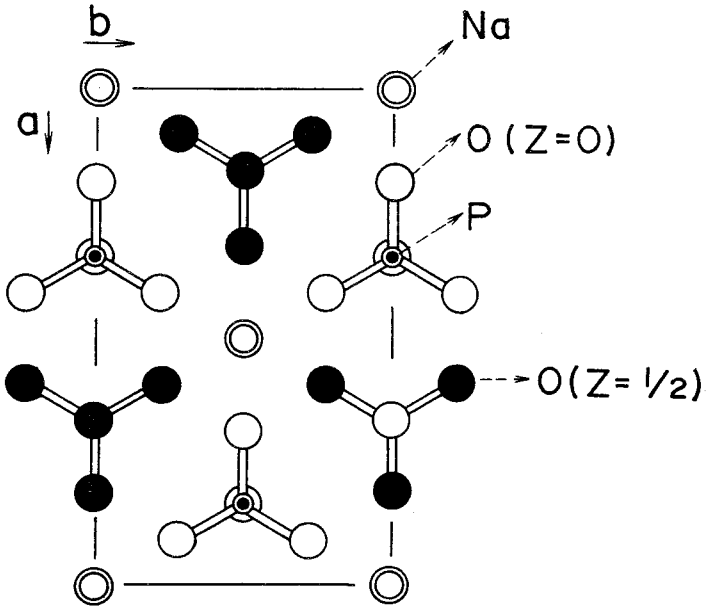

(b) The idealzed structure of $Na_4P_2O_7$ projected on to the a b plane

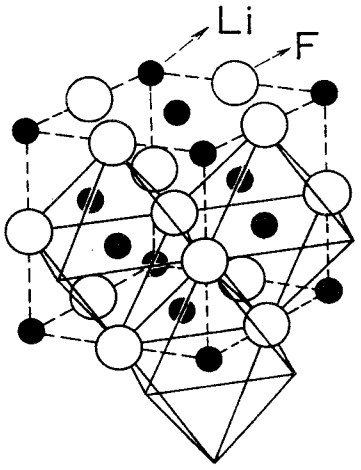

(c) The crystal structure of Li F

Fig. 50. Crystal structures of $CH_3CO_2Na \cdot 3H_2O$ and some nucleation catalysts for it.

copy and so on. By these methods, it has been shown that the first monolayer develops as separate patches possesing two dimentional structure [82, 91]. It is to be expected that the nucleation of crystalline $CH_3CO_2Na \cdot 3H_2O$ on the surface of the nucleation catalyst is an analogous process. However, the nucleation in the solution or melt can not be analyzed by these methods of vacuum physics. In addition, the problem of the epitaxy in the field of thin film physics has not been solved clearly even by the development of the techniques analyzing the surface of the solid [92].

At present, the structure of the crystalline adsorbate or liquid adsorbate on the surface of the nucleation catalyst can not be analyzed and can not be calculated theoretically. Therefore, we can not relate the nucleation catalysts to $CH_3CO_2Na \cdot 3H_2O$ from the structural point of view. At present, the difference in the characteristics of the nucleation catalysts, $Na_4P_2O_7$, $Na_2HPO_4 \cdot 2H_2O$, $Na_2WO_4 \cdot 2H_2O$ and LiF, can not be also explained at all.

CHAPTER IV HEAT STORAGE CAPACITY OF $CH_3CO_2Na \cdot 3H_2O$ DURING THERMAL CYCLING

IV. 1 Introduction

$CH_3CO_2Na \cdot 3H_2O$ melts incongruently and severely supercools. In the previous chapter, it was shown that the addition of the nucleation catalyst to $CH_3CO_2Na \cdot 3H_2O$ satisfactorily solved the problem concerning the supercooling. The problem caused by incongruent melting of $CH_3CO_2Na \cdot 3H_2O$ still remains.

Telkes [8, 93] studied Glauber's salt ($Na_2SO_4 \cdot 10H_2O$) for latent heat storage and found that addition of a thickening agent such as attapulgite clay was effective for suspending the Na_2SO_4 particles homogeneously in the melt and prevented $Na_2SO_4 \cdot 10H_2O$ from forming a metastable condition where the undissolved Na_2SO_4 particles coexisted with newly formed $Na_2SO_4 \cdot 10H_2O$ crystals and excess solution. Marks [37, 94] measured the heat storage capacity of $Na_2SO_4 \cdot 10H_2O$ thickened by using attapulgite clay during thermal cycling and showed that the addition of attapulgite clay was a little useful for solving the problem caused by incongruent melting.

In order to investigate the decreasing of heat storage capacity of $CH_3CO_2Na \cdot 3H_2O$ during thermal cycling, we performed calorimetric measurements on three kinds of sample. Samples, *a*, *b* and *c*, were respectively guaranteed grade $CH_3CO_2Na \cdot 3H_2O$, technical grade $CH_3CO_2Na \cdot 3H_2O$ and technical grade $CH_3CO_2Na \cdot 3H_2O$ thickened by using polyvinyl alcohol.

IV. 2 Experimental Procedure

Guaranteed grade $CH_3CO_2Na \cdot 3H_2O$, $Na_4P_2O_7 \cdot 10H_2O$, polyvinyl alcohol (degree of polymerization, n≈500), acetone and liquid paraffin were obtained from Wako Pure Chemical Industries. Technical grade $CH_3CO_2Na \cdot 3H_2O$ was obtained from Nippongosei-kagaku Co., Ltd. The thickened mixture was prepared by mixing technical grade $CH_3CO_2Na \cdot 3H_2O$ with polyvinyl alcohol, acetone, liquid paraffin and water at 70°C for 30 min. Table 8 shows the initial composition of the three kinds of sample.

Table 8. Composition of the samples

sample name	component	percent by weight
sample *a*	guaranteed grade $CH_3CO_2Na \cdot 3H_2O$	99.0
	$Na_4P_2O_7 \cdot 10H_2O$	1.0
sample *b*	technical grade $CH_3CO_2Na \cdot 3H_2O$	99.0
	$Na_4P_2O_7 \cdot 10H_2O$	1.0
sample *c*	technical grade $CH_3CO_2Na \cdot 3H_2O$	93.0
	H_2O	3.5
	polyvinyl alcohol	1.0
	acetone	0.5
	liquid paraffin	1.0
	$Na_4P_2O_7 \cdot 10H_2O$	1.0

About 80 g of $CH_3CO_2Na \cdot 3H_2O$ or thickened mixture and 0.8 g of $Na_4P_2O_7 \cdot 10H_2O$ were placed in a stainless steel vessel, 30 mm inner diameter, 100 mm height and 1 mm wall thickness. This vessel was sealed and put into a water bath. The sample was consecutively heated and cooled at the rate of 5°C/min between 70 and 40°C, and kept for 60 min at both 70 and 40°C. At various times the sample was taken out of the water bath and calorimetric measurement was performed on it.

Heat storage capacity was measured by the standard calorimetric technique in which the heat evolved by the sample was equated to the heat absorbed by the calorimeter's water. A molten sample whose mass and temperature were known was quickly placed into water whose temperature was recorded as a function of time. Prior to the measurement, the sample was brought to a uniform temperature above its melting point, about 60°C.

Calorimetric measurement provides a precise and direct measure of the heat storage capacity of the sample. The total stored heat is the sum of sensible heat and latent heat of fusion. The latent heat storage capacity was computed by subtracting the contributing of the specific heat of $CH_3CO_2Na \cdot 3H_2O$ { C_p(cryst)= 1.7 J/gK, C_p(melt)= 2.9 J/gK } from measured heat storage capacity. It was assumed that only $CH_3CO_2Na \cdot 3H_2O$ contributed to the measured heat storage capacity because heat storage capacity of the nucleation catalyst and the thickener was very small compared to that of $CH_3CO_2Na \cdot 3H_2O$.

IV. 3 Results and Discussion

The decreasing of latent heat storage capacity of sample *a* with increase in the number of thermal cycles is shown in Fig. 51. In this fugure, ΔH_i is the latent heat of fusion of $CH_3CO_2Na \cdot 3H_2O$. The latent heat storage capacity of this sample is initially 254 J/g; after 30 cycles declines to 200 J/g; and after 400 cycles declines to 160 J/g.

The decreasing of latent heat capacity of sample *b* with increase in the number of

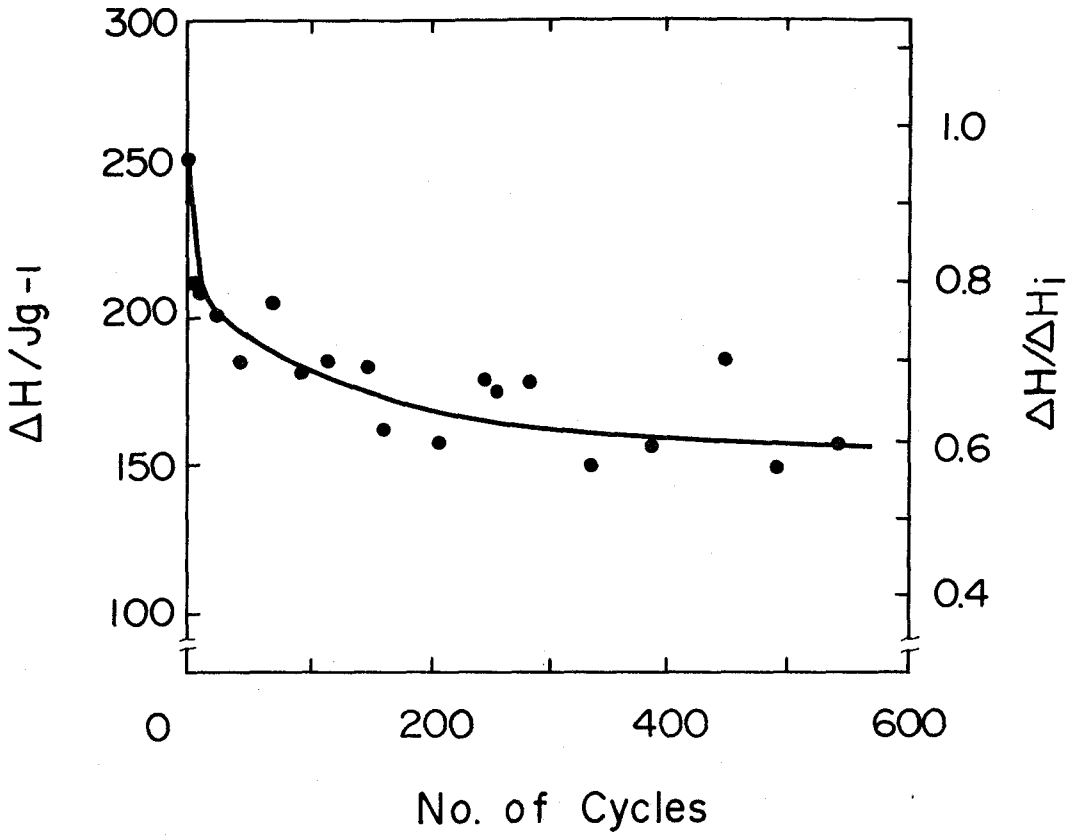

Fig. 51. Decreasing of latent heat storage capacity of sample *a* with increase in number of cycles.

thermal cycles is shown in Fig. 52. The latent heat storage capacity of this sample is initially 259 J/g; after 30 cycles declines to 235 J/g; and after 400 cycles declines to 200 J/g.

From Figs. 51 and 52, it is clear that the heat storage capacity of sample *b* decreases much more slowly than that of sample *a* during thermal cycling.

Apparent change of the phases present in sample *a* comprising guaranteed grade $CH_3CO_2Na \cdot 3H_2O$ during thermal cycling is illustrated in Fig. 53. In molten state, the upper layer is liquid paraffin preventing water evaporation, the intermediate layer is CH_3CO_2Na solution and the lower layer is the mixture of CH_3CO_2Na solution and anhydrous CH_3CO_2Na particles settling to the bottom of the graduated cylinder. In frozen

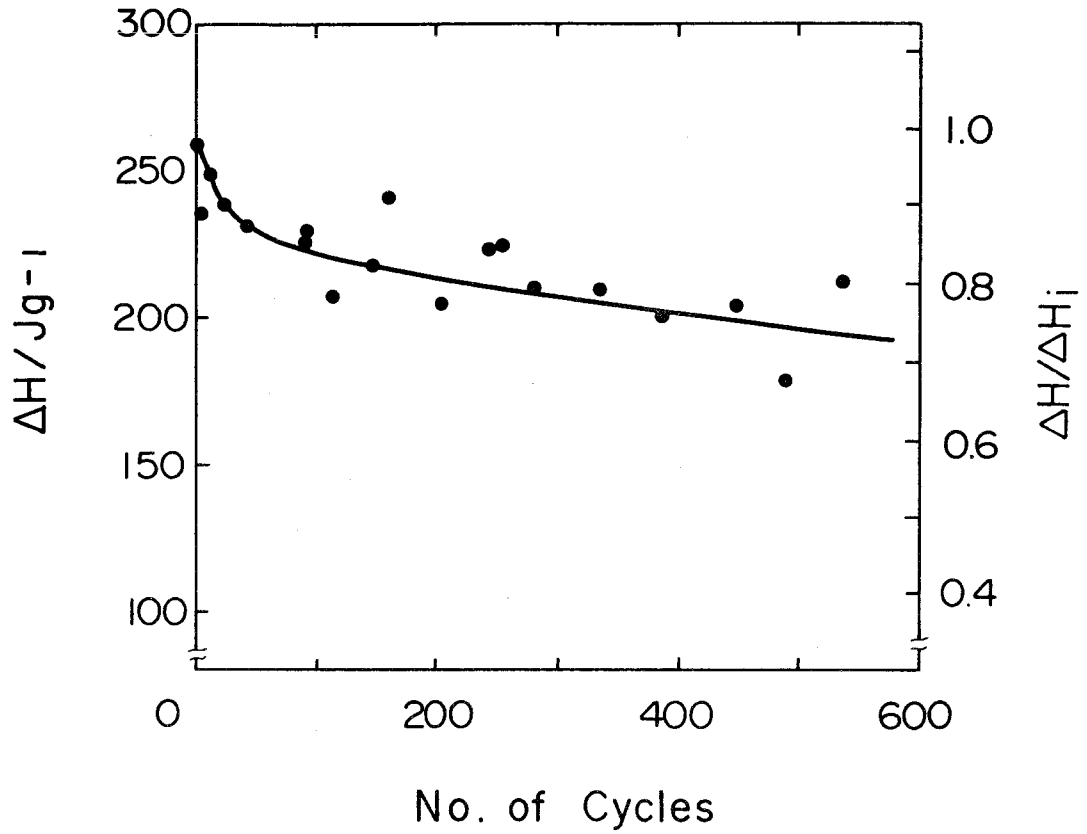

Fig. 52. **Decreasing of latent heat storage capacity of sample *b* with increase in number of cycles.**

state, the upper layer is also liquid paraffin, the intermediate layer is unfrozen CH_3CO_2Na solution and the lower layer is the mixture of $CH_3CO_2Na \cdot 3H_2O$ crystals and anhydrous CH_3CO_2Na particles. Apparent change of the phases present in sample *b* comprising technical grade $CH_3CO_2Na \cdot 3H_2O$ is also illustrated in Fig. 54. Whichever grade $CH_3CO_2Na \cdot 3H_2O$ is used, it is observed from Figs. 53 and 54 that the extent of settling of anhydrous CH_3CO_2Na particles in molten state and the volume of unfrozen CH_3CO_2Na solution in frozen state increase during thermal cycling, respectively. It is also clear that anhydrous CH_3CO_2Na particles in the melt of sample *b* settle more slowly than that of sample *a* and, accordingly, the volume of unfrozen CH_3CO_2Na solution in frozen sample *b*

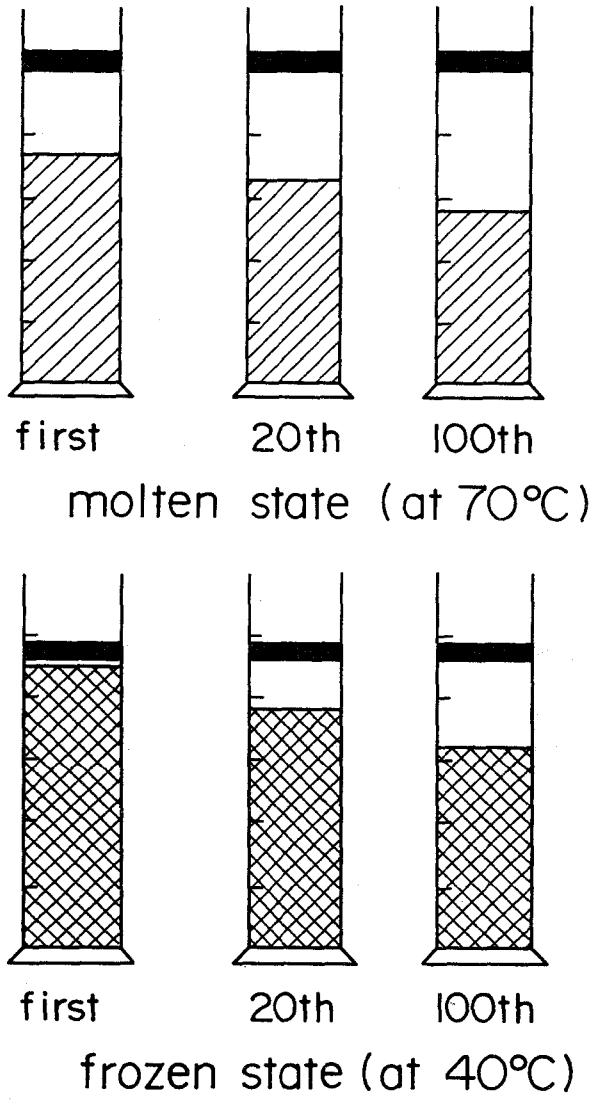

Fig. 53. Apparent change of phases in sample *a*.

increases more slowly than that of sample *a*. This result is in good agreement with the result of calorimetric measurement mentioned above.

The differences between sample *a* and sample *b* are considered to come from the impurities (NaCl, $MgCl_2$, HCO_2Na and so on) contained in technical grade $CH_3CO_2Na \cdot 3H_2O$.

Impurities such as HCO_2Na are supposed to be adsorbed onto the surface of anhydrous CH_3CO_2Na particles in the melt and prevent anhydrous CH_3CO_2Na particles from growing (which is due to an Ostwald ripening process where fine CH_3CO_2Na particles dissolve preferentially and several large anhydrous CH_3CO_2Na particles grow) and from sintering together (anhydrous CH_3CO_2Na particles bonding together to form solid mass). Such impurity effect is indicated in Glauber's salt by Marks [94]. He

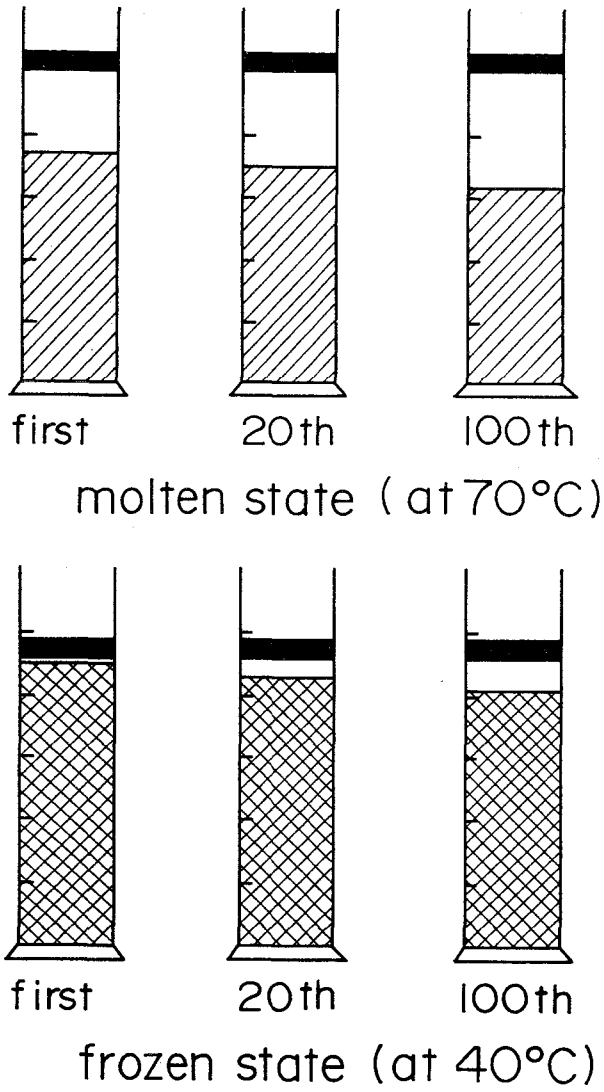

Fig. 54. Apparent change of phases in sample *b*.

called such impurities "crystal habit modifiers".

The latent heat storage capacity of sample *c* with number of cycles is shown in Fig. 55. The latent heat storage capacity of this sample is about 230 J/g, and this latent heat storage capacity scarcely decreases during all thermal cycling. The addition of thickening agent considerably improves latent heat storage capacity after many cycles. The addition of thickening agent has greatly retarded the decline in heat storage capacity of $CH_3CO_2Na \cdot 3H_2O$, because the thickener prevents anhydrous CH_3CO_2Na particles from settling to the bottom of the container. The thickener used in this experiment comprises polyvinyl alcohol, acetone and liquid paraffin but the action of these components cannot be well understood.

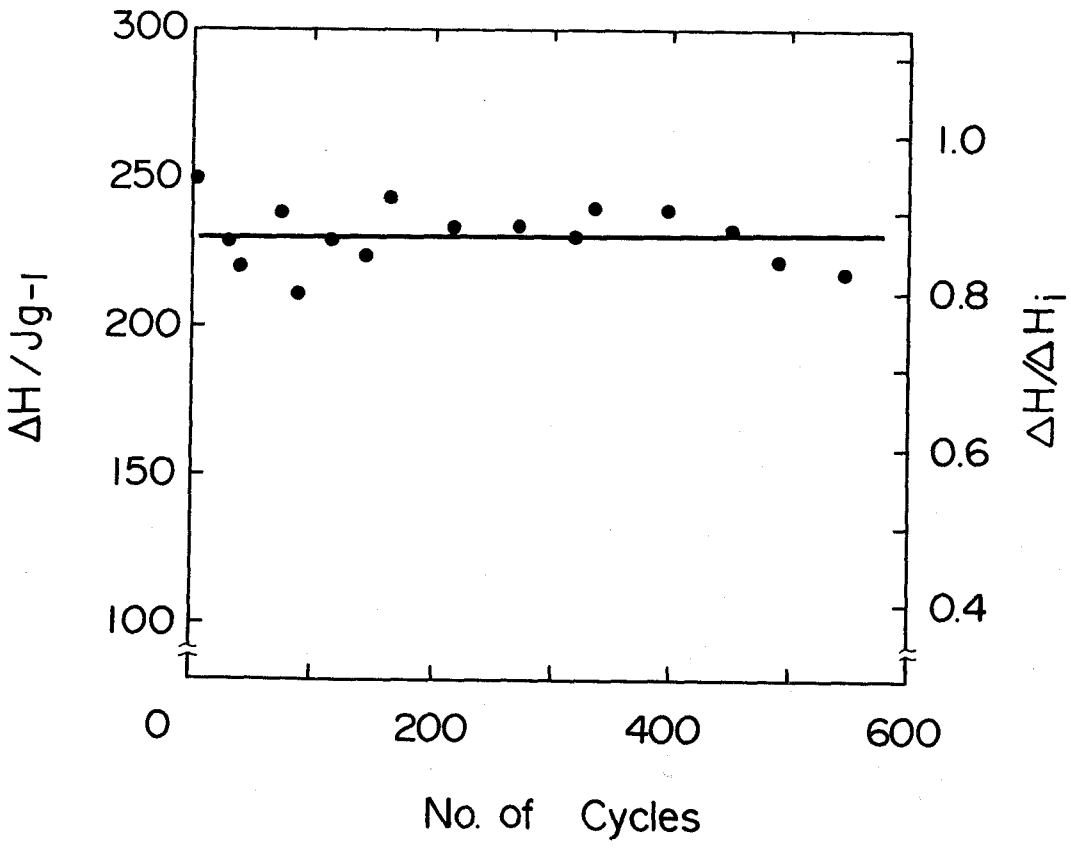

Fig. 55. Latent heat storage capacity of sample *c* with number of cycles.

CHAPTER V CONTROLLING THE MELTING POINT OF $CH_3CO_2Na \cdot 3H_2O$

V. 1 Introduction

Recently, some mixtures containing salt hydrate have been studied in order to develop latent heat storage materials. Böer et al. [40] used a eutectic mixture of system $Na_2SO_4 \cdot 10H_2O$-NH_4Cl-NaCl as a heat storage material for a solar house, which is called as "solar one." Yoneda and Takanashi [41] studied on mixtures of a system $Mg(NO_3)_2 \cdot 6H_2O$-$MgCl_2 \cdot 6H_2O$ and found that the eutectic mixture of this system melted at 59.1°C and that its heat of fustion was 144 J/g.

In contrast, no mixtures of salt hydrate and organic compound have been studied yet. In this study, mixtures of pseudo-binary system $CH_3CO_2Na \cdot 3H_2O$ and organic compound $CO(NH_2)_2$ or $HCONH_2$ were subjected to measurements using differential scanning calorimetry (DSC). From these measurements, the partial phase diagrams of ternary systems CH_3CO_2Na-$CO(NH_2)_2$-H_2O and CH_3CO_2Na-$HCONH_2$-H_2O at ambient pressure were constructed. The values were determined for the heat of fusion of the eutectic mixture of the pseudo-binary system $CH_3CO_2Na \cdot 3H_2O$-$CO(NH_2)_2$ and that of the addition compound of $CH_3CO_2Na \cdot 3H_2O$ and $HCONH_2$. Crystallization behavior of these pseudo-binary systems each containing $CH_3CO_2Na \cdot 3H_2O$ was studied in a similar manner as in the case of the binary system CH_3CO_2Na-H_2O, described in Capter II. In the pseudo-binary system $CH_3CO_2Na \cdot 3H_2O$-$CO(NH_2)_2$, the linear velocity of crystallization from the pseudo-binary molten mixture was measured and the microstructure of the mixtures was observed.

V. 2 Experimental Procedure

Materials $CH_3CO_2Na \cdot 3H_2O$, CH_3CO_2Na, $CO(NH_2)_2$, $HCONH_2$ and $Na_4P_2O_7 \cdot 10H_2O$ were guaranteed grade reagent purchased from Wako Pure Chemical Industry Ltd.

Differential Scanning Colorimetry for Construction of the Phase Diagram Differential scanning calorimetry (DSC) was performed with an SSC 560U DSC (Dainiseikosha Co.). Weighed quantities of $CH_3CO_2Na \cdot 3H_2O$, $CO(NH_2)_2$, and so on were heated and mixed to a homogeneous melt. One drop of this melt was placed in a 15 μl silver crucible and was solidified. After the crucible was closed, the sample was heated at a rate of 0.5°C/min from 10 to 90°C. The melting temperature of the sample was obtained from the endothermic peak on the sample temperature curve. The heat of fusion was obtained from the endothermic peak area. This DSC system was calibrated by using ice (mp: 0.0°C; ΔH_m : 335 J/g), sodium sulfate decahydrate (mp: 32.4°C), and sodium acetate trihydrate (mp: 58.4°C) as standards.

Crystallization Behavior Crystallization temperature on slow cooling from a melt (t_c), glass transition temperature (T_G), and crystallization temperature on slow heating from a quenched vitrified solid (T_c) were measured in a similar manner as in the case of the binary system CH_3CO_2Na-H_2O, which has been already described in Chapter II.

Microscopic and Microphotographic Studies For microscopic and microphotographic studies, sample's slides were prepared and examined under a microscope. A very small drop of melt was placed on a slide glass and covered with a cover glass. Nucleation was started from one side.

Linear Velocity of Crystallization The experimental technique for determining the linear velocity of crystallization was similar to that adopted by Dietz et al. [20]. Measurement was made in a pyrex glass tube, 500 mm in length, 1 mm in wall thickness, and 8 mm in inner diameter, provided with two right-angled bends. The tube was placed in

a water bath thermostated to ±0.1°C. The melt was seeded at one end and the time required for the crystal boundary to move a definite distance was measured by a stopwatch. The linear velocity of crystallization was determined for various degrees of supercooling in this manner.

V. 3 Results and Discussion

V. 3. 1 Pseudo-binary system $CH_3CO_2Na \cdot 3H_2O$-$CO(NH_2)_2$

V. 3. 1. 1 Phase Diagram

DSC curves for some mixtures of pseudo-binary system $CH_3CO_2Na \cdot 3H_2O$-$CO(NH_2)_2$ are illustrated in Fig. 56. Considering the phase diagram of the system CH_3CO_2Na-H_2O shown in Fig. 1, we understand that the peak at 58.4°C on the DSC curve for $CH_3CO_2Na \cdot 3H_2O$ corresponds to the melting of $CH_3CO_2Na \cdot 3H_2O$ and that the change at 77.8°C in the DSC curve for $CH_3CO_2Na \cdot 3H_2O$ corresponds to the entire dissolution of the anhydrous CH_3CO_2Na in the water of crystallization.

The pseudo-binary section in ternary system CH_3CO_2Na-$CO(NH_2)_2$-H_2O at ambient pressure, which is constructed from such DSC curves, is shown in Fig. 57. This pseudo-binary section is confirmed by the cooling method adopted by Carlson et al. [14]. In this figure, W_X shows the mass fraction of $CO(NH_2)_2$, so the quantity on the abscissa, $100 \times W_X$, indicates the weight percentage of $CO(NH_2)_2$ in the system. From this figure, it is clear that pseudo-binary system $CH_3CO_2Na \cdot 3H_2O$-$CO(NH_2)_2$ forms a eutectic mixture without forming any new addition compound. The eutectic mixture of this system, containing 0.6 mass fraction of $CH_3CO_2Na \cdot 3H_2O$ and 0.4 mass fraction of $CO(NH_2)_2$, melts congruently at 31.5°C.

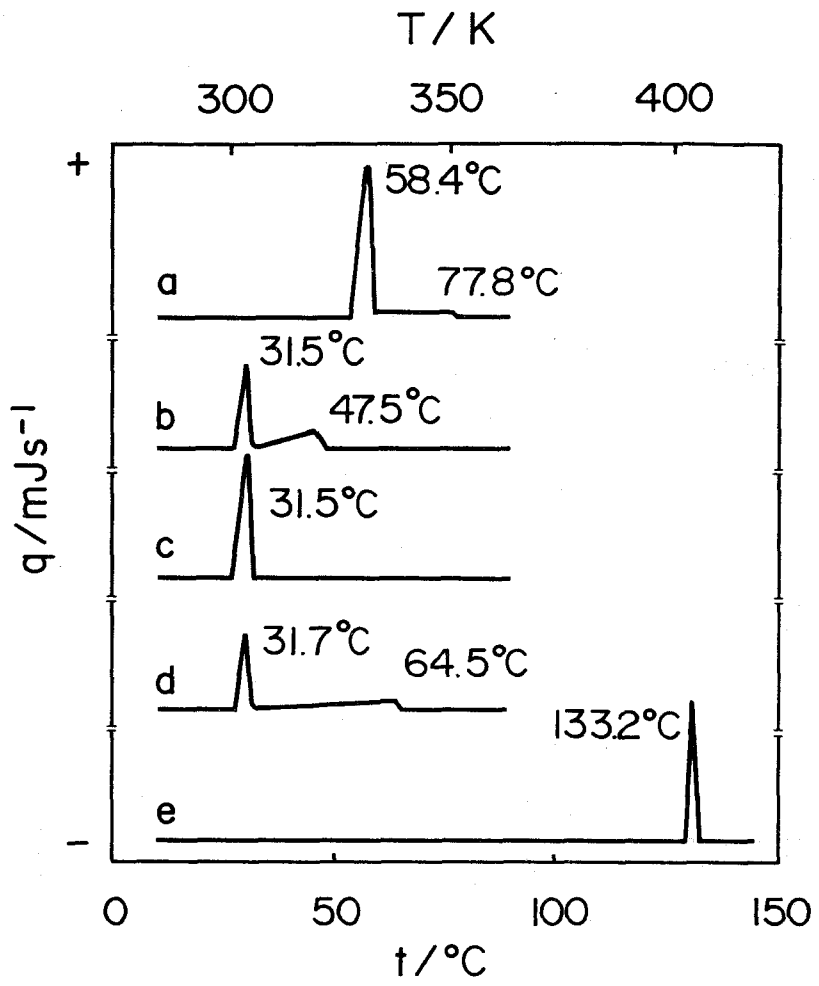

Fig. 56. **DSC curves of mixture of the pseudo-binary system $CH_3CO_2Na \cdot 3H_2O$-$CO(NH_2)_2$.**
a: $CH_3CO_2Na \cdot 3H_2O$, b: 0.2 mass fraction of $CO(NH_2)_2$, c: 0.4 mass fraction of $CO(NH_2)_2$, d: 0.6 mass fraction of $CO(NH_2)_2$, e: $CO(NH_2)_2$.

Melting-point diagrams at ambient pressure for the system CH_3CO_2Na-$CO(NH_2)_2$-H_2O, in which the mass fraction of $CO(NH_2)_2$ is kept constant, are plotted in Fig. 58. In this figure, W_a shows the mass fraction of CH_3CO_2Na and W_b shows the mass fraction of H_2O. The quantity on the abscissa, $100 \times W_a/(W_a + W_b)$, is the weight percentage of CH_3CO_2Na in the system without $CO(NH_2)_2$. The melting-point diagram for the system CH_3CO_2Na-H_2O without $CO(NH_2)_2$ is in good agreement with previous data [18]. It is

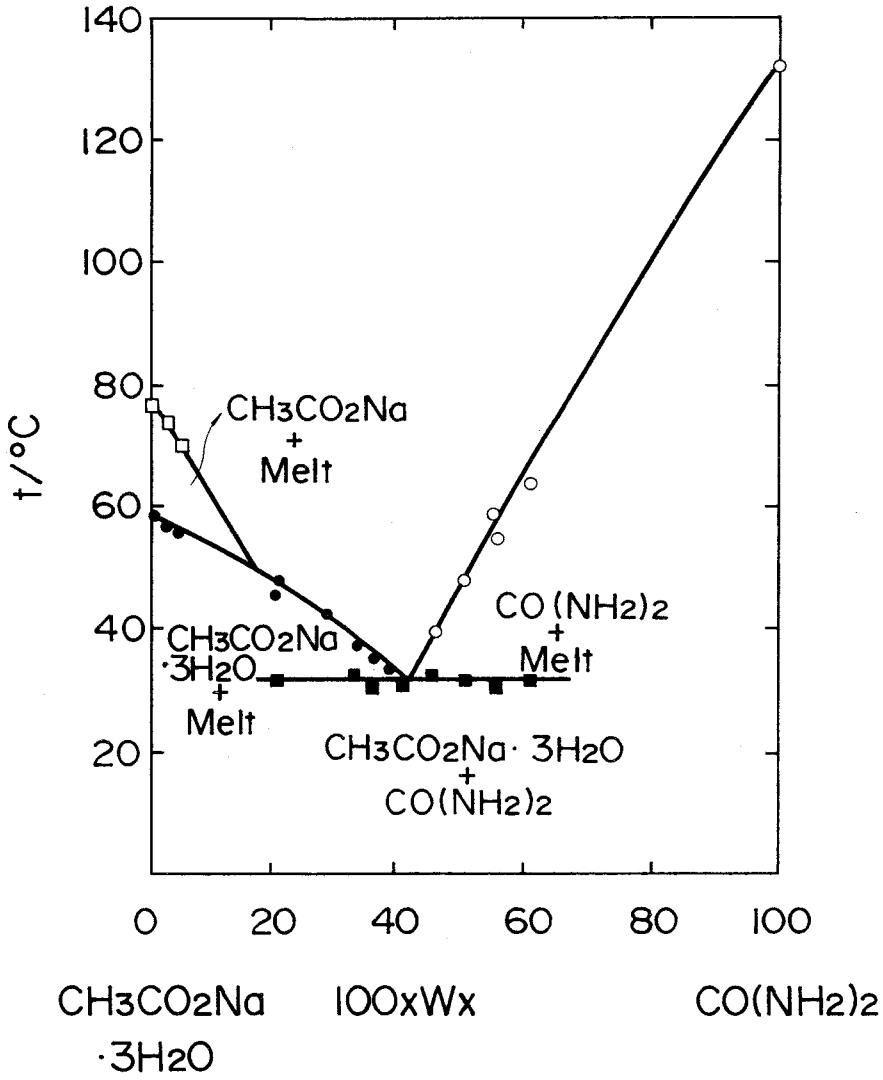

Fig. 57.. Pseudo-binary section in the ternary system CH_3CO_2Na-$CO(NH_2)_2$-H_2O at ambient pressure.
●: melting point of $CH_3CO_2Na \cdot 3H_2O$,
○: melting point of $CO(NH_2)_2$,
□: melting point of CH_3CO_2Na,
■: eutectic point.

apparent that as the mass fraction of $CO(NH_2)_2$, W_x, increases, the liquidus line on the $CH_3CO_2Na \cdot 3H_2O$ side shifts to lower temperature and that the liquidus line on the CH_3CO_2Na side shifts to higher concentration of CH_3CO_2Na.

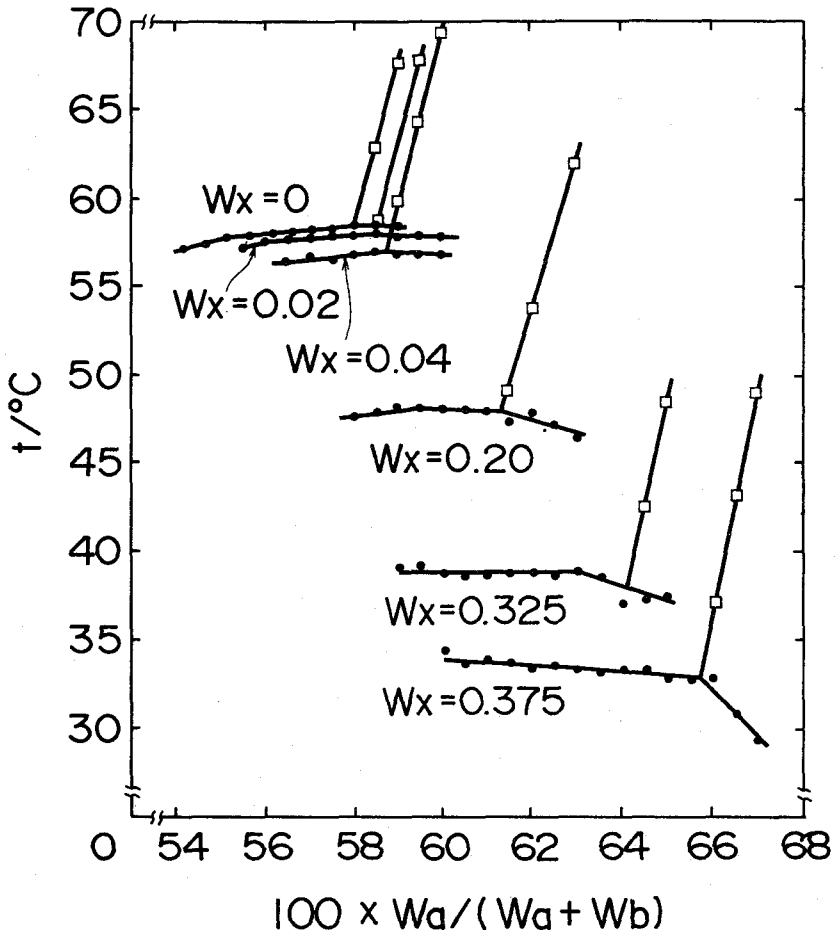

Fig. 58. Melting-point diagram of the ternary system, CH_3CO_2Na-$CO(NH_2)_2$-H_2O at ambient pressure.
●: melting point of $CH_3CO_2Na \cdot 3H_2O$,
□: melting point of CH_3CO_2Na.

A partial phase diagram of ternary system CH_3CO_2Na-$CO(NH_2)_2$-H_2O at ambient pressure, which is illustrated in Fig. 59, is constructed by using the results of Figs. 1, 57, and 58. From this figure, it can be understood that $CH_3CO_2Na \cdot 3H_2O$ comes to melt congruently when a sufficient amount of $CO(NH_2)_2$ or H_2O is added to it. Moreover, the liquidus line on the $CH_3CO_2Na \cdot 3H_2O$ side is lowered by addition of $CO(NH_2)_2$ or H_2O. Thus, the effect of addition of $CO(NH_2)_2$ to $CH_3CO_2Na \cdot 3H_2O$ is similar to that of addition of H_2O. The eutectic point of pseudo-binary system $CH_3CO_2Na \cdot 3H_2O$-$CO(NH_2)_2$ is

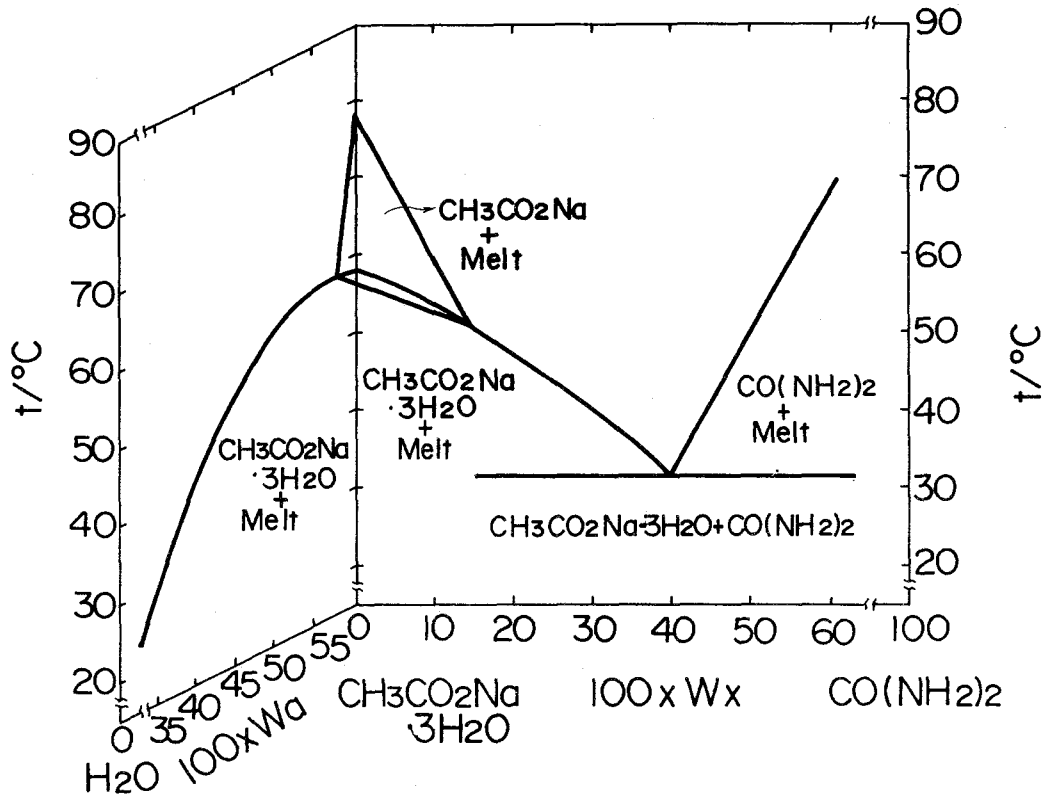

Fig. 59. **Partial phase diagram of the ternary system CH_3CO_2Na-$CO(NH_2)_2$-H_2O at ambient pressure.**

31.5°C, which is suitable for solar energy storage, whereas the eutectic point of system $CH_3CO_2Na \cdot 3H_2O$-H_2O is −18°C, which is too low. The reason why $CH_3CO_2Na \cdot 3H_2O$ is brought to the point of melting congruently by the addition of a sufficient quantity of $CO(NH_2)_2$ is that $CO(NH_2)_2$ acts not only as a solute in $CH_3CO_2Na \cdot 3H_2O$ melt but also as a solvent for anhydrous CH_3CO_2Na.

V. 3. 1. 2. Heat of Fusion of the Eutectic Mixture

The heat of fusion of the eutectic mixture of this pseudo-binary system is found to be 226 J/g by DSC. This value is larger than the heat of fusion of $CaCl_2 \cdot 6H_2O$ (mp: 29.5°C), which is shown in Table 1. The heat of fusion of $CaCl_2 \cdot 6H_2O$ is 180 J/g [10]. The heat of fusion of a binary eutectic mixture, ΔH_m^{eu}, is calculated from the equation [95].

$$\Delta H_m^{eu} = T_m^{eu} \times \left\{ W^A \left(\frac{\Delta H_m^A}{T_m^A} \right) + W^B \left(\frac{\Delta H_m^B}{T_m^B} \right) \right\}$$

where W^A and W^B are the mass fractions of components A and B, respectively, T_m^A, T_m^B, and T_m^{eu} are the melting points (in absolute temperature) of component A, component B, and eutectic mixture, respectively, and ΔH_m^A and ΔH_m^B are the heats of fusion per unit mass of components A and B, respectively. This equation is applicable to the eutectic mixture of pseudo-binary system $CH_3CO_2Na \cdot 3H_2O$-$CO(NH_2)_2$, by letting A and B correspond to $CH_3CO_2Na \cdot 3H_2O$ and $CO(NH_2)_2$, respectively. $CH_3CO_2Na \cdot 3H_2O$ melts incongruently at 58.4°C with a heat of fusion of 264 J/g, [10] and $CO(NH_2)_2$ melts at 133°C with a heat of fusion of 251 J/g [96]. Accordingly we take T_m^A = 332 K, T_m^B = 406 K, T_m^{eu} = 305 K, ΔH_m^A = 264 J/g, ΔH_m^B = 251 J/g, W^A = 0.60, and W^B = 0.40. Consequently, ΔH_m^{eu} is 221 J/g. This value is in good agreement with the experimental result, 226 J/g.

V. 3. 1. 3. Microstructure

Microphotographs of mixtures of $CH_3CO_2Na \cdot 3H_2O$ and $CO(NH_2)_2$ are given in Figs. 60-62. The study with a microscope clearly proves that the solid immediately separated out from a eutectic melt is entirely different in appearance from other solids. Large prisms of $CH_3CO_2Na \cdot 3H_2O$ in the eutectic matrix are shown in Fig. 60. White needles of

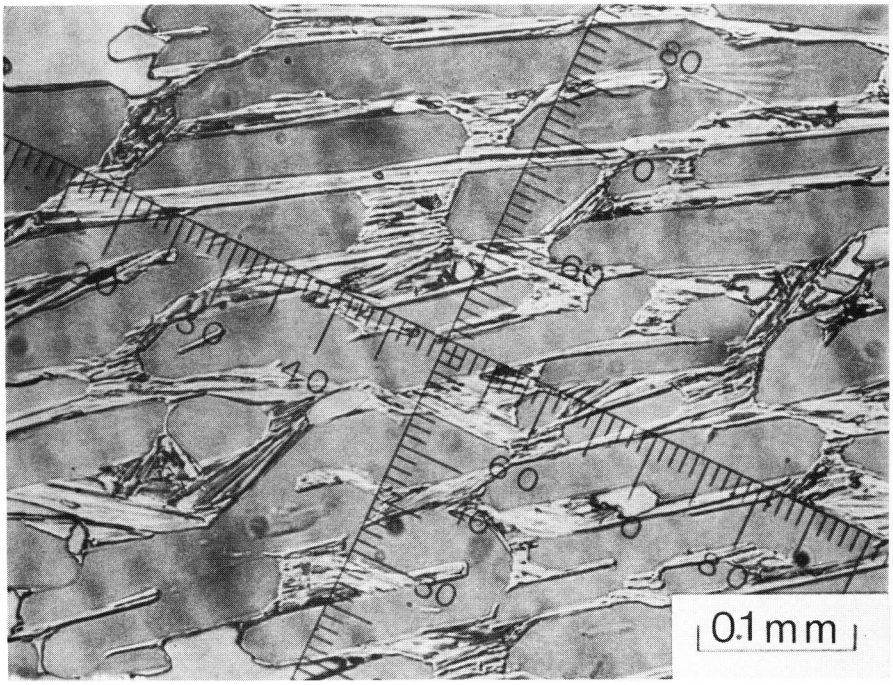

Fig. 60. Microstructure of mixture containing 0.2 mass fraction of $CO(NH_2)_2$.

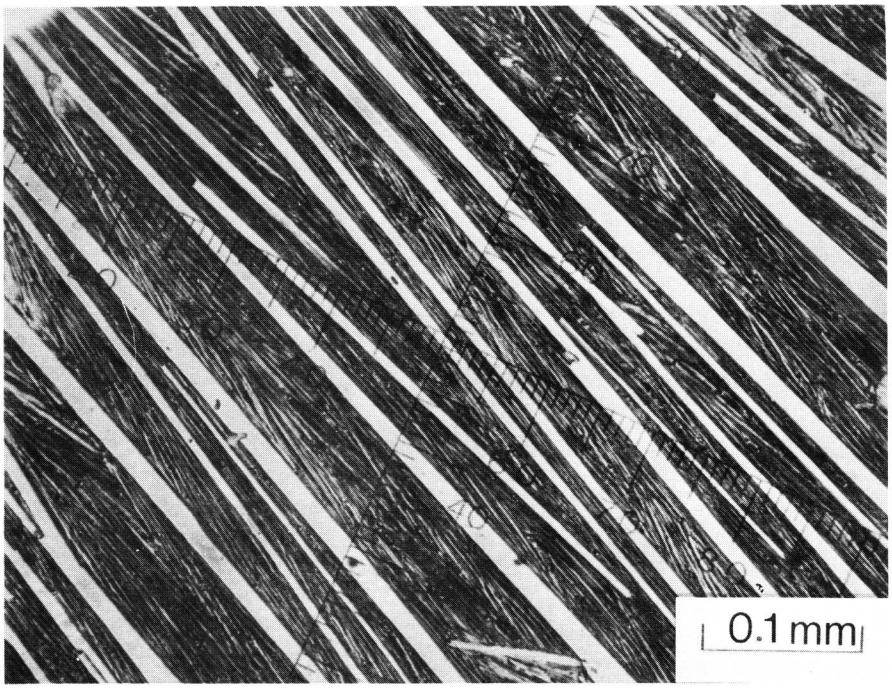

Fig. 61. Microstructure of mixture containing 0.6 mass fraction of $CO(NH_2)_2$.

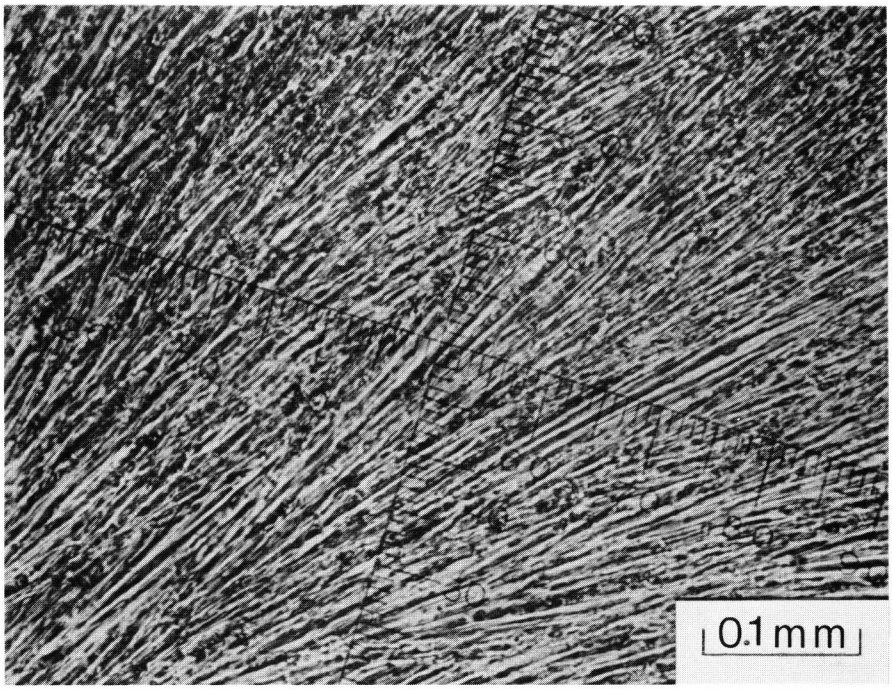

Fig. 62. Microstructure of eutectic mixture containing 0.4 mass fraction of $CO(NH_2)_2$.

$CO(NH_2)_2$ in the eutectic matrix are shown in Fig. 61. An extremely regular pattern for the solid eutectic matrix is shown in Fig. 62.

V. 3. 1. 4 Linear Velocity of Crystallization

Linear velocities of crystallization of various melts are plotted against the supercooling, $\Delta\theta(=\theta-\theta_m)$, in Fig. 63. The linear velocity of crystallization of $CH_3CO_2Na\cdot 3H_2O$ (W_x = 0) is in good agreement with the value determined by Dietz et al. [20]. It is clear that the linear velocity of crystallization of the melt containing 0.04 mass fraction of $CO(NH_2)_2$ at $\Delta\theta= -20°C$ falls to less than half of the linear velocity of crystallization of $CH_3CO_2Na\cdot 3H_2O$ at $\Delta\theta= -20°C$. The linear velocity of crystallization of this eutectic melt ($W_x= 0.40$)

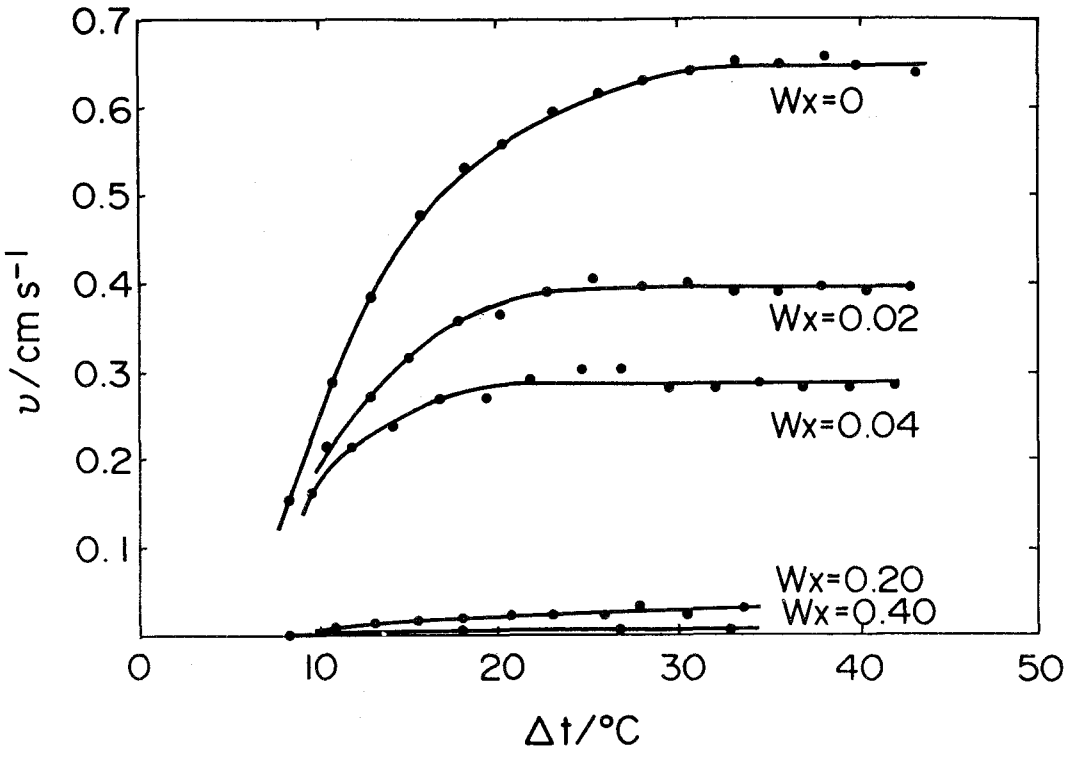

Fig. 63. Linear velocity of crystallization of various melts.

at $\Delta\theta = -20°C$, 0.002 cm/s, is about one three hundredth of the linear velocity of crystallization of $CH_3CO_2Na \cdot 3H_2O$ melt at $\Delta\theta = -20°C$.

V. 3. 1. 5 Crystallization Behavior

Crystallization temperature on slow cooling from a melt (t_c), glass transition temperature (T_G), and crystallization temperature on slow heating from a quenched vitrified solid (T_c) are plotted in the phase diagram of the pseudo-binary system $CH_3CO_2Na \cdot 3H_2O$-$CO(NH_2)_2$ as shown in Fig. 64. The number on the abscissa, $100XW_X$, is the weight percentage of $CO(NH_2)_2$ in the system.

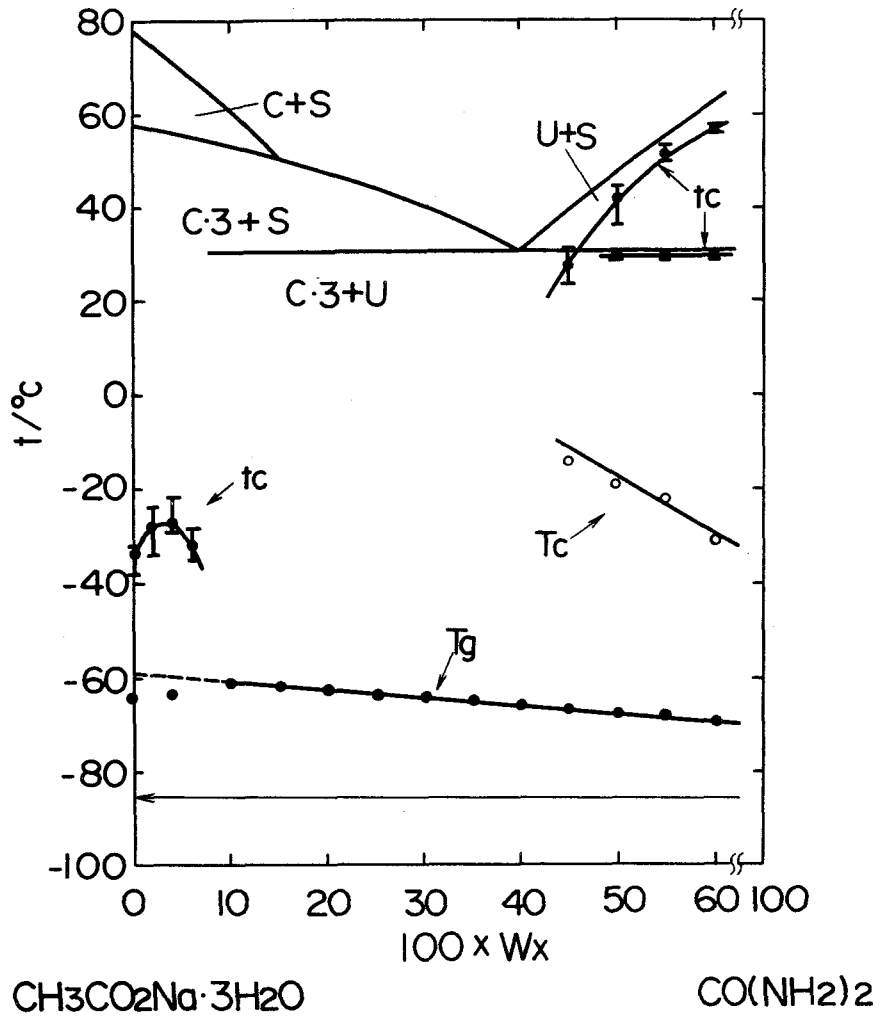

Fig. 64. **Crystallization temperature on slow cooling from a melt (t_c), glass transition temperature (T_G), and crystallization temperature on slow heating from a quenched vitrified solid (T_c), shown in the phase diagram of the pseudo-binary system $CH_3CO_2Na \cdot 3H_2O$-$CO(NH_2)_2$. Symbols: C: CH_3CO_2Na, C·3: $CH_3CO_2Na \cdot 3H_2O$, U: $CO(NH_2)_2$.**

On slow cooling, the melts of the composition near $CH_3CO_2Na \cdot 3H_2O$ crystallized at about −30°C. However, in the $CH_3CO_2Na \cdot 3H_2O$ rich side of the eutectic composition, except in the vicinity of $CH_3CO_2Na \cdot 3H_2O$, the melts hardly crystallized. In the $CO(NH_2)_2$ rich side of eutectic composition, the melt of $W_x = 0.45$ separated out only $CO(NH_2)_2$ crystals, and the melt of $W_x = 0.50$ separated out $CO(NH_2)_2$ crystals at about 5°C lower

temperature than the liquidus line and continuously separated out $CH_3CO_2Na \cdot 3H_2O$ at a few lower temperature than the eutectic point.

DSC curves for some quenched samples are illustrated in Fig. 65, where q is a heat flux. T_G and T_c are plotted against the CH_3CO_2Na concentration in Fig. 64. All the melts,

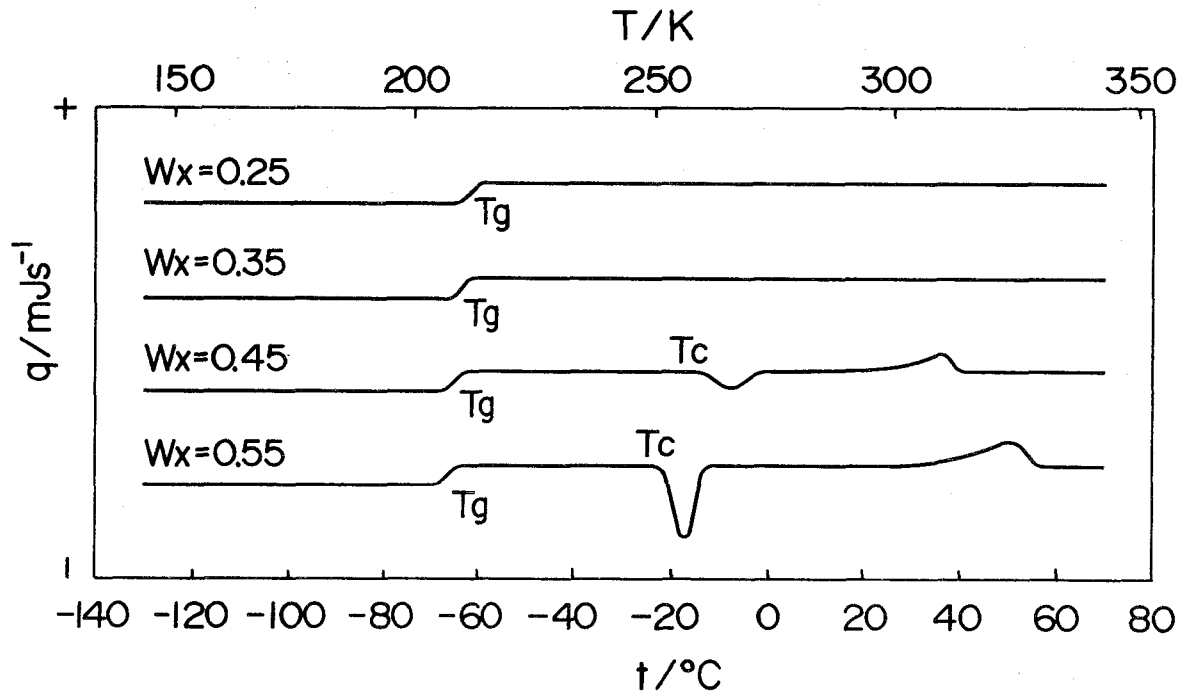

Fig. 65. DSC curves of some quenched vitrified solids of the pseudo-binary system $CH_3CO_2Na \cdot 3H_2O$-$CO(NH_2)_2$.

which were tested on the present experiment, vitrified by quenching. In Fig. 64, T_G varies linearly with the $CO(NH_2)_2$ concentration, and those of the samples containing $CO(NH_2)_2$ less than W_x = 0.10 lie below the T_G line. This deviation results from the decrease of CH_3CO_2Na concentration caused by separation of anhydrous CH_3CO_2Na crystals from the quenched sample. This results was confirmed by visual observation of these samples in a 3 mm diameter pyrex glass tubes put into liquid nitrogen. The extraporation of the

obtained T_G to pure $CH_3CO_2Na \cdot 3H_2O$ is $-59°C$ and in good agreement with the value obtained by the measurement of the binary system CH_3CO_2Na-H_2O. The extraporation to pure $CO(NH_2)_2$ gives $-74°C$ as the T_G of glassy $CO(NH_2)_2$.

The quenched samples in $CH_3CO_2Na \cdot 3H_2O$ rich side of eutectic composition, did not crystallize on heating after the glass transition. In $CO(NH_2)_2$ rich side of eutectic composition, the quenched samples crystallize on heating. The DSC curves show that the melting points of the samples with $W_x = 0.45$ and $W_x = 0.55$ are 35°C and 55°C respectively, which are in good agreement with the liquidus temperature of these composition. And the samples with $W_x = 0.45$ and 0.55 do not show the endothermic peak corresponding to the eutectic melting. Therefore, $CO(NH_2)_2$ is the only compound crystallized from the melts with $W_x \geqslant 0.45$. In $W_x \geqslant 0.45$, T_c lowers linearly with the increasing of the $CO(NH_2)_2$ concentration of the system.

V. 3. 1. 6 Heating and Cooling Cycles of the Eutectic Mixture with a Small Amount of the Nucleation Catalyst

In order to make sure that the mixture of system $CH_3CO_2Na \cdot 3H_2O$-$CO(NH_2)_2$ continuously repeats melting and freezing, 30 g of the eutectic mixture of pseudo-binary system $CH_3CO_2Na \cdot 3H_2O$-$CO(NH_2)_2$ in the presence of 0.3 g of $Na_4P_2O_7 \cdot 10H_2O$ as the nucleation catalyst for $CH_3CO_2Na \cdot 3H_2O$, was subjected to cycles of linearly programmed consequtive heating and coolings between 5 and 45°C in a manner similar to the one adopted previously. Melting points, θ_ms, and temperatures at which the supercooling is broken, θ_cs, determined by 1000 continuous heating and cooling cycles, are shown in Fig. 66. The supercooling, $\Delta\theta_c (= \theta_c - \theta_m)$, is calculated by using the results shown in Fig. 66 and plotted in Fig. 67. From these figures, it is apparent that the supercooling of this eutectic mixture, $\Delta\theta_c$, is almost $-6°C$ for all the cycles.

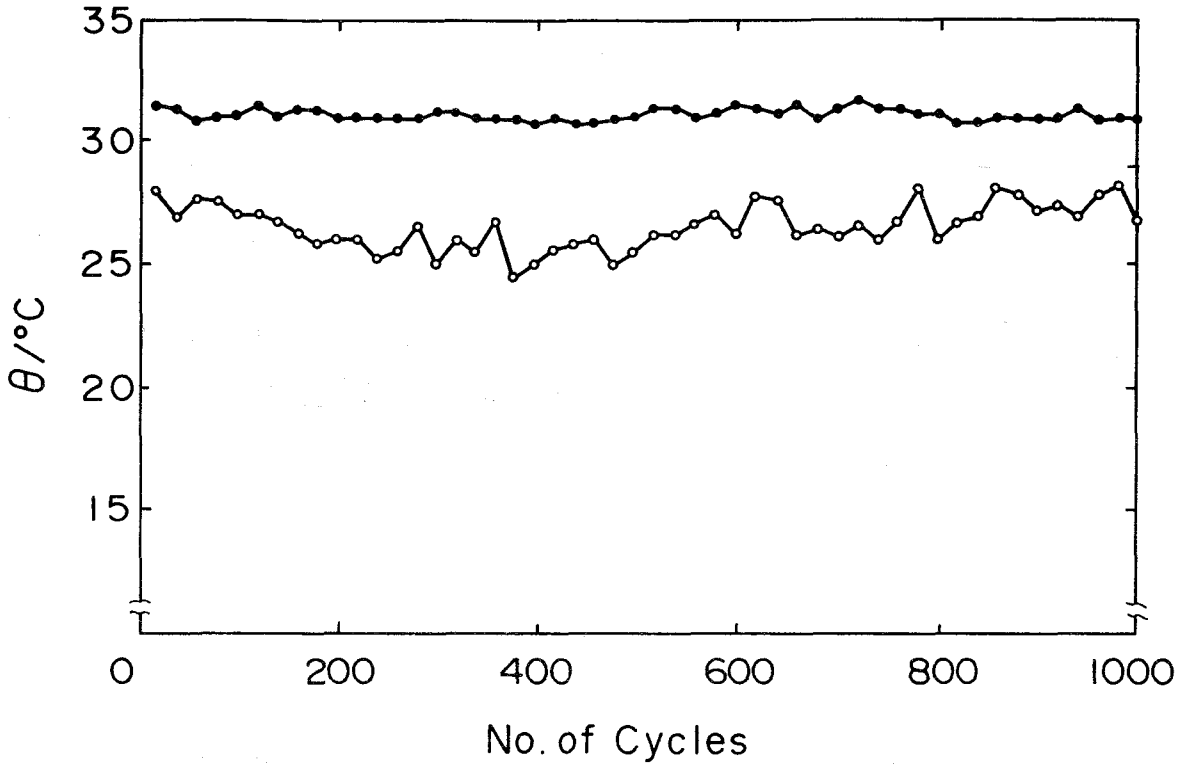

Fig. 66. **Changes in melting point, θ_m, and the temperature at which supercooling is broken, θ_c, with cycling for the eutectic mixture containing the nucleation catalyst.**
●: θ_m, ○: θ_c.

$CH_3CO_2Na \cdot 3H_2O$ starts to crystallize from the eutectic melt with the aid of $Na_4P_2O_7 \cdot 10H_2O$ crystals, and then $CO(NH_2)_2$ starts to crystallize soon. This eutectic mixture was observed not to separate into the components $CH_3CO_2Na \cdot 3H_2O$ and $CO(NH_2)_2$. After 1000 continuous heating and cooling cycles, the heat of fusion of this sample was measured by DSC. The value obtained was 222 J/g, which was in good agreement with the initial heat of fusion of this eutectic mixture, 226 J/g. Consequently, the mixtures of system $CH_3CO_2Na \cdot 3H_2O$-$CO(NH_2)_2$ are promising for solar energy storage.

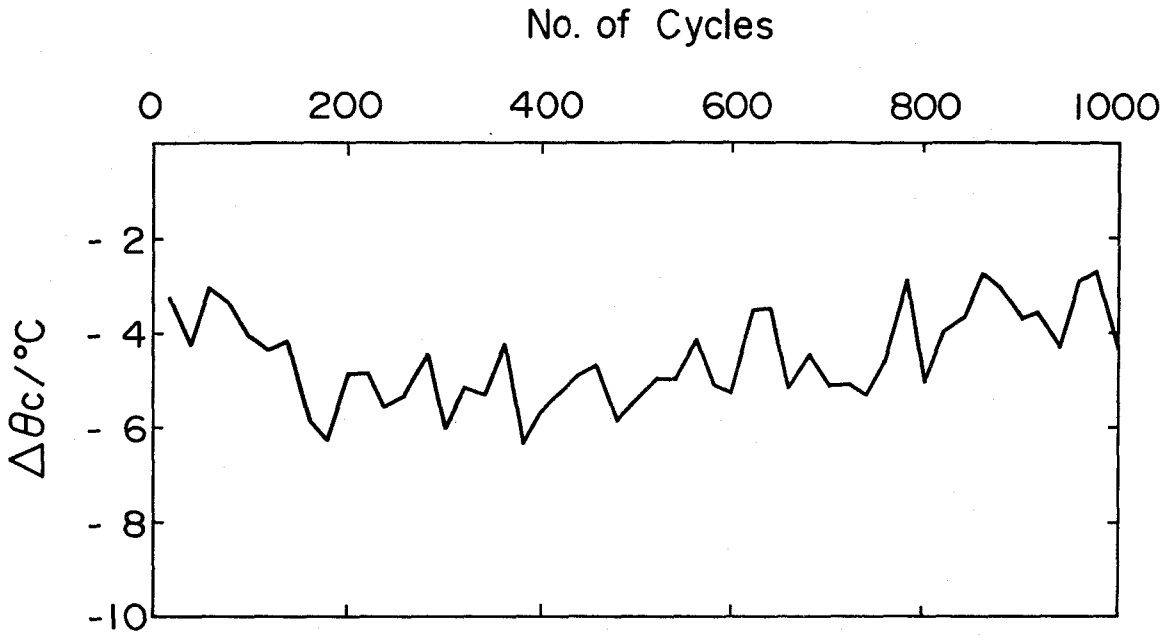

Fig. 67. Change in the supercooling, $\Delta\theta_c$, of the eutectic mixture containing the nucleation catalyst with cycling.

V. 3. 2 Pseudo-binary System $CH_3CO_2Na \cdot 3H_2O$-$HCONH_2$

V. 3. 2. 1 Phase Diagram

The DSC curves of some mixtures of the pseudo-binary system $CH_3CO_2Na \cdot 3H_2O$-$HCONH_2$ are illustrated in Fig. 58. In this figure, the number on the ordinate, q, indicates a heat flux. The heat absorption accompanying the dissolving of CH_3CO_2Na in its water of crystallization is much smaller than that accompanying the melting of $CH_3CO_2Na \cdot 3H_2O$ but it is illustrated in magnified scale. Considering the phase diagram of the system CH_3CO_2Na-H_2O shown in Fig. 1, we understand that the peak at 58.4°C of DSC curve of $CH_3CO_2Na \cdot 3H_2O$ corresponds to the melting of $CH_3CO_2Na \cdot 3H_2O$ and the change at 77.8°C corresponds to the entire dissolution of CH_3CO_2Na in its water of crystallization.

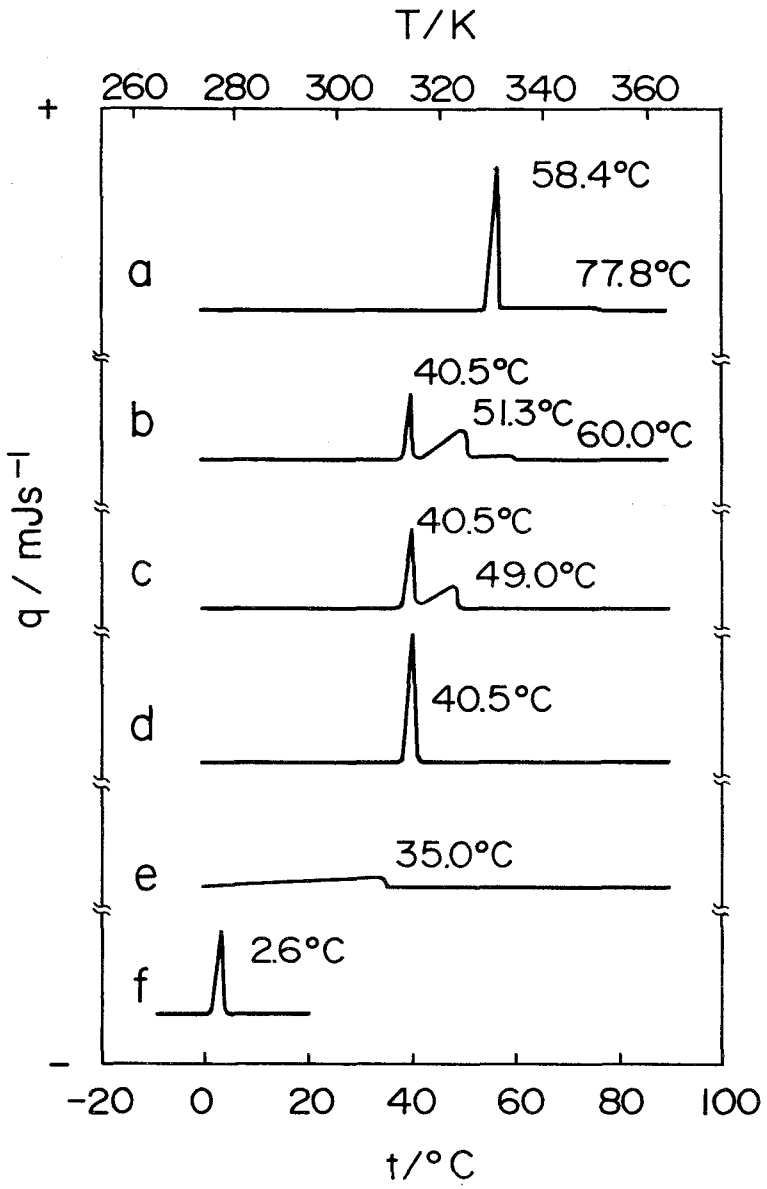

Fig. 68. **DSC curves of mixtures of the pseudo-binary system $CH_3CO_2Na \cdot 3H_2O$-$HCONH_2$.**
a: $CH_3CO_2Na \cdot 3H_2O$, b: 0.10 mass fraction of $HCONH_2$, c: 0.15 mass fraction of $HCONH_2$, d: 0.25 mass fraction of $HCONH_2$, e: 0.50 mass fraction of $HCONH_2$, f: $HCONH_2$.

The pseudo-binary section in a ternary system CH_3CO_2Na-$HCONH_2$-H_2O at ambient pressure, which is constructed from such DSC curves, is shown in Fig. 69. In this figure,

W_y shows mass fraction of $HCONH_2$, while Y_y, shows mole fraction of $HCONH_2$. From this figure, it can be understood that a one to one addition compound of the two components is formed. This addition compound, $CH_3CO_2Na \cdot HCONH_2 \cdot 3H_2O$, melts congruently at 40.5°C. The photograph of crystals of this addition compound is shown in Fig. 70. These crystals are colorless and transparent. The specific gravity of this crystal at room temperature is 1.404 g/cm^3.

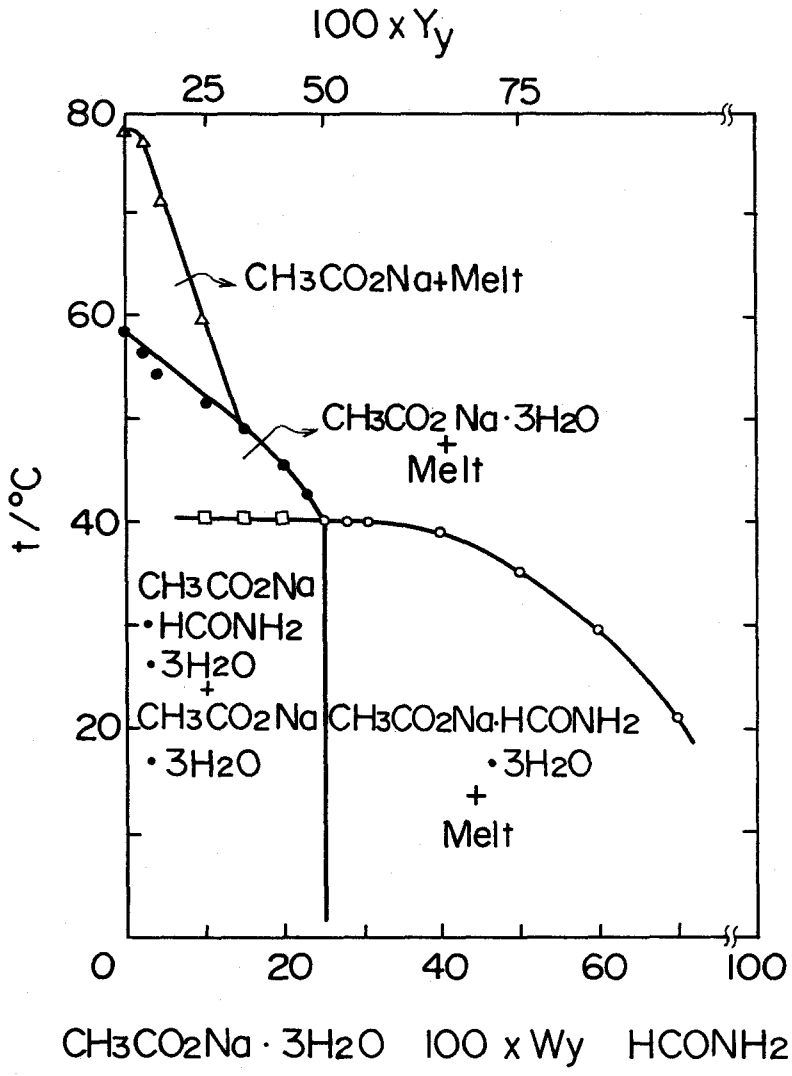

Fig. 69. **Pseudo-binary section in the ternary system CH_3CO_2Na-$HCONH_2$-H_2O at ambient pressure.**
●: melting point of $CH_3CO_2Na \cdot 3H_2O$,
○: melting point of $CH_3CO_2Na \cdot HCONH_2 \cdot 3H_2O$,
△: melting point of CH_3CO_2Na,
□: eutectic point.

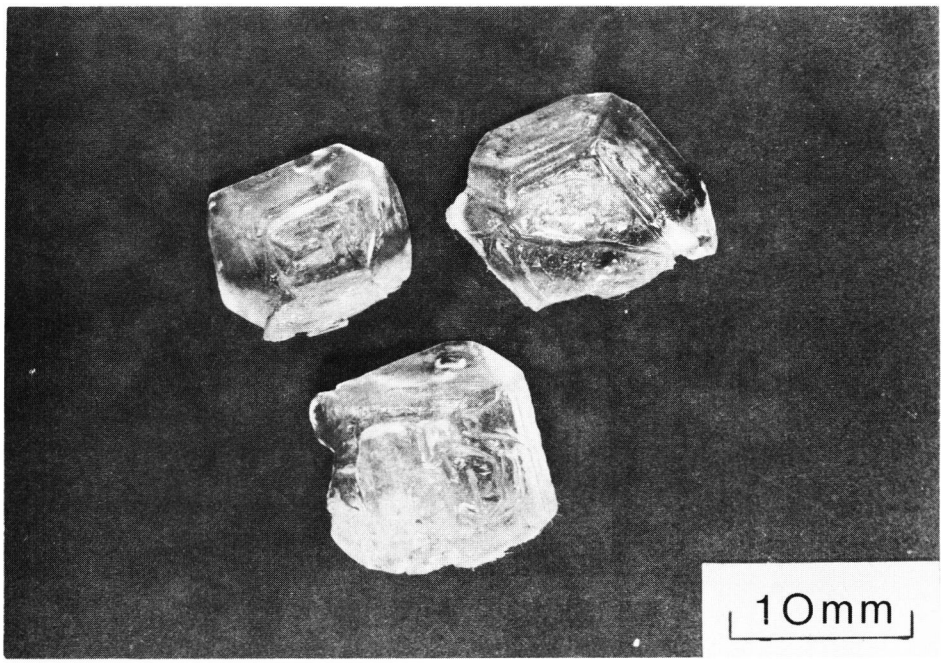

Fig. 70. Photograph of crystals of the addition compound, $CH_3CO_2Na \cdot HCONH_2 \cdot 3H_2O$.

The melting-point diagrams for the system CH_3CO_2Na-$HCONH_2$-H_2O at ambient pressure, where the mass fraction of $HCONH_2$ is kept constant in each system, are plotted in Fig. 71 by using DSC curves such as the curve (c) in Fig. 68. In this figure, the number on the abscissa, $100 \times W_a/(W_a+W_b)$, is weight precentage of CH_3CO_2Na in the system without $HCONH_2$ content. The melting-point diagram for the system CH_3CO_2Na-H_2O, which does not contain $HCONH_2$, is in good agreement with the reported data [18]. It is apparent that as mass fraction of $HCONH_2$, W_y, increases, the liquidus line on $CH_3CO_2Na \cdot 3H_2O$ side shifts to lower temperature and the liquidus line on CH_3CO_2Na side shifts to higher concentration of CH_3CO_2Na.

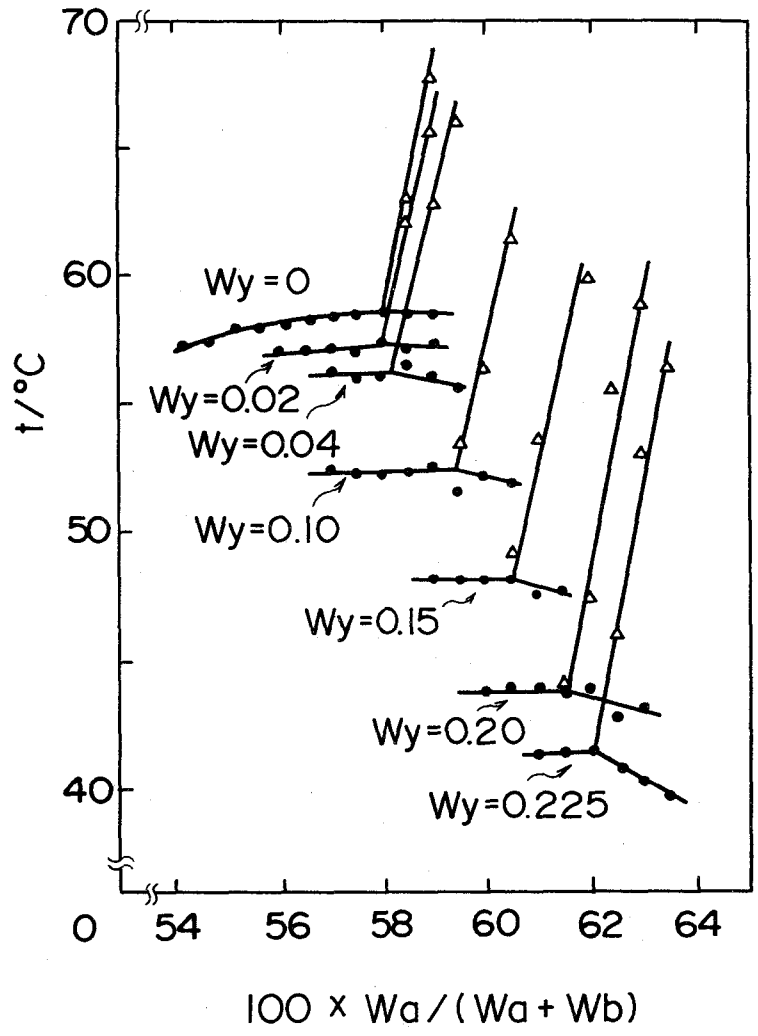

Fig. 71. **Melting-point diagram of the ternary system CH_3CO_2Na-$HCONH_2$-H_2O, at ambient pressure in which the mass fraction of $HCONH_2$ is kept constant in each system.**
●: melting point of $CH_3CO_2Na \cdot 3H_2O$,
△: melting point of CH_3CO_2Na.

The partial phase diagram of the ternary system CH_3CO_2Na-$HCONH_2$-H_2O at ambient pressure, which is shown in Fig. 72, is constructed by using the results of Figs. 1, 69, and 71.

The heat of fusion of the addition compound $CH_3CO_2Na \cdot HCONH_2 \cdot 3H_2O$ is found to

be 255 J/g by DSC. This value is much larger than the heat of fusion of $Ca(NO_3)_2 \cdot 4H_2O$ (mp: 43°C), 142 J/g [10].

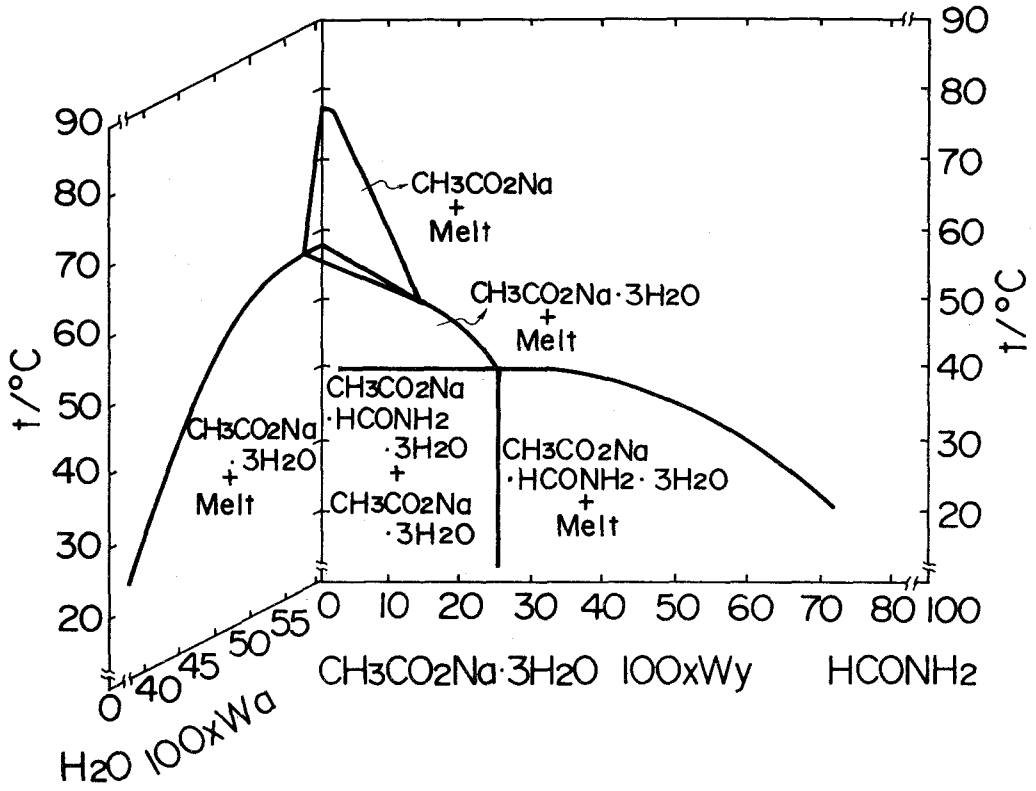

Fig. 72. Partial phase diagram of the ternary system CH_3CO_2Na-$HCONH_2$-H_2O at ambient pressure.

V. 3. 2. 2 Crystallization Behavior

Crystallization temperature on slow cooling from a melt (t_c), glass transition temperature (T_G), and crystallization temperature on slow heating from a quenched vitrified solid (T_c) are plotted in the phase diagram of the pseudo-binary system $CH_3CO_2Na \cdot 3H_2O$-$HCONH_2$, and shown in Fig. 73. The number on the abscissa, $100XW_y$ is the weight percentage of $HCONH_2$ in the system.

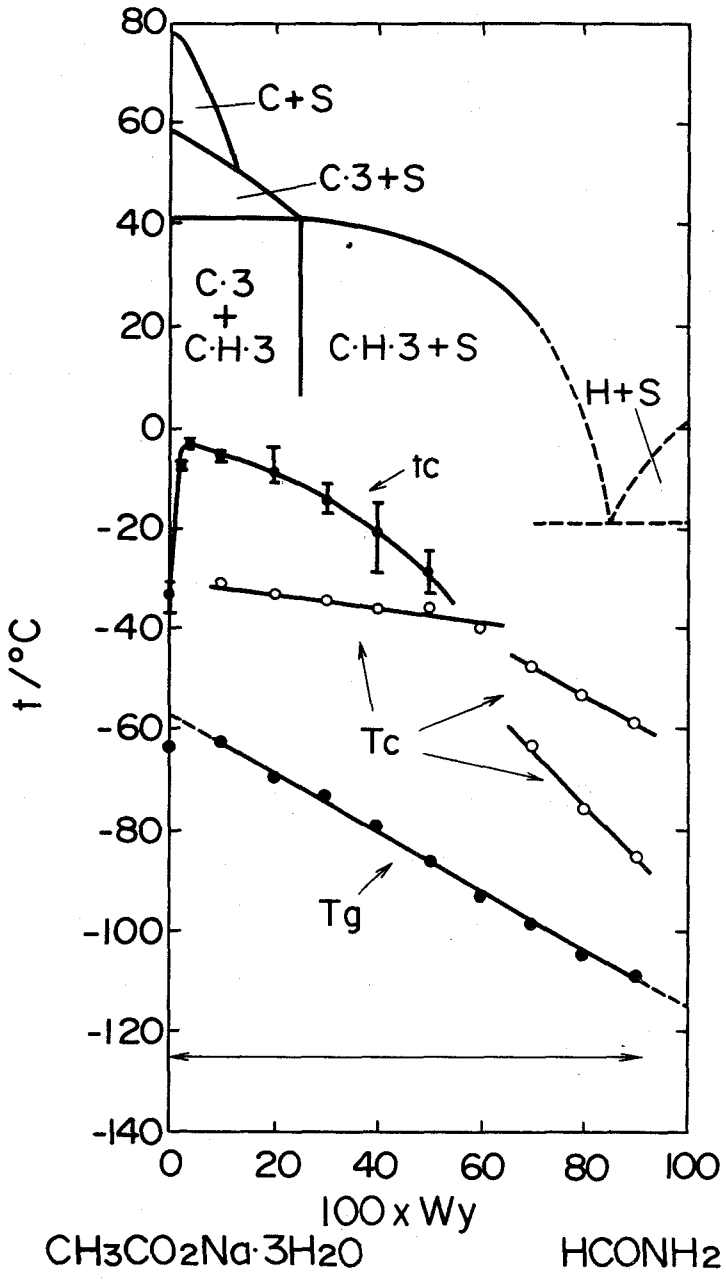

Fig. 73. Crystallization temperature on slow cooling from a melt (t_c), glass transition temperature (T_G), and crystallization temperature on slow heating from a quenched vitrified solid (T_c), shown in the phase diagram of the pseudo-binary system $CH_3CO_2Na \cdot 3H_2O$-$HCONH_2$. Symbols: C: CH_3CO_2Na, C·3: $CH_3CO_2Na \cdot 3H_2O$, C·H·3: $CH_3CO_2Na \cdot HCONH_2 \cdot 3H_2O$, H: $HCONH_2$.

On slow cooling, $CH_3CO_2Na \cdot 3H_2O$ melt crystallized at about $-30°C$. The melt with $W_y = 0.02$ crystallized at $-8°C$ and that with $W_y = 0.04$ crystallized at $-3°C$. It is interesting that an addition of a small amount of $HCONH_2$ promotes the crystallization of $CH_3CO_2Na \cdot 3H_2O$ from the melt. Taking the phase diagram into account, the crystallization of $CH_3CO_2Na \cdot 3H_2O$ is considered to be accompanied by a crystallization of the addition compound, $CH_3CO_2Na \cdot HCONH_2 \cdot 3H_2O$. The t_c of the melt having $W_y \geqslant 0.04$ was lowered with increasing of $HCONH_2$ concentration but the melts having $W_y \geqslant 0.60$ did not crystallize in all runs. The t_c of the melt having $0.50 \geqslant W_y \geqslant 0.04$ was about 60°C lower than the liquidus temperature of the system.

DSC curves for some quenched samples are illustrated in Fig. 74, where q is a heat flux. T_G and T_c are plotted against $HCONH_2$ concentration in Fig. 73. All the melts, except

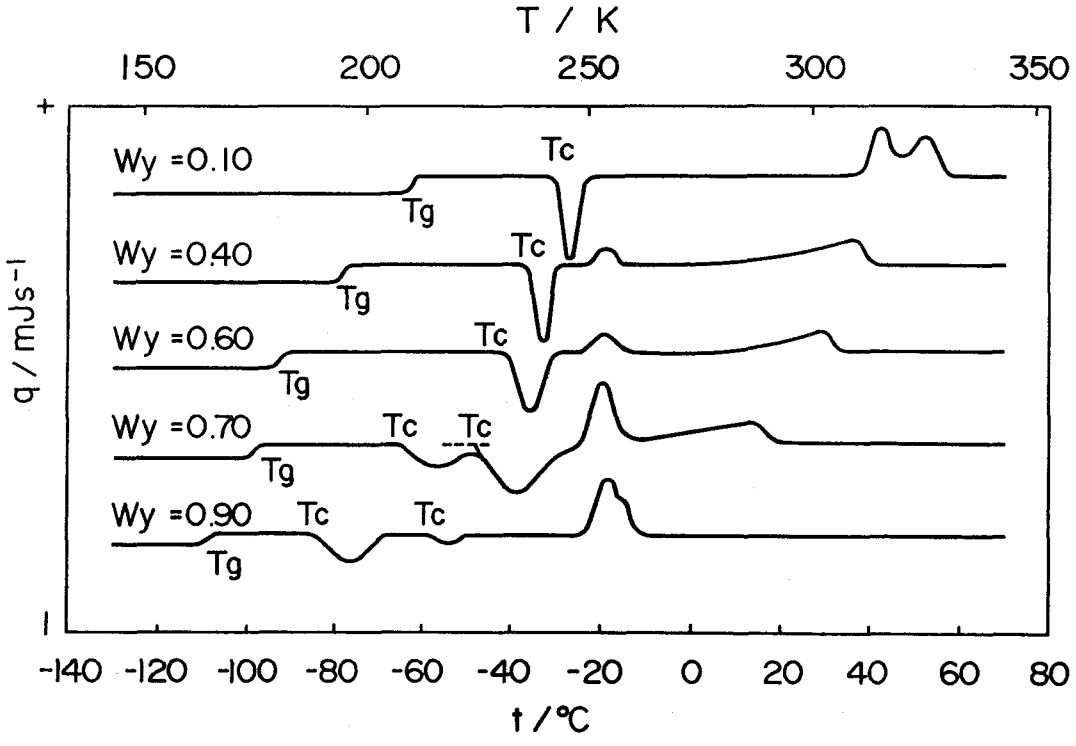

Fig. 74. DSC curves of some quenched vitrified solids of the pseudo-binary system $CH_3CO_2Na \cdot 3H_2O$-$HCONH_2$.

$HCONH_2$, were vitrified by quenching. This was confirmed by visual observation of these samples in a 3 mm diameter pyrex glass tube put into liquid nitrogen. In Fig. 73, T_G varies linearly with the $HCONH_2$ concentration, and the T_G of $CH_3CO_2Na \cdot 3H_2O$ lies below the T_G line. This deviation results from the decrease of CH_3CO_2Na concentration caused by separation of anhydrous CH_3CO_2Na crystals from the quenched samples, which was confirmed by visual observation using thin glass tube. The extraporation of the obtained T_G to pure $CH_3CO_2Na \cdot 3H_2O$ is $-57°C$ and in good agreement with the value obtained by the measurement of the binary system CH_3CO_2Na-H_2O. The extraporation to pure $HCONH_2$ gives $-115°C$ to the T_G of glassy $HCONH_2$.

The quenched $CH_3CO_2Na \cdot 3H_2O$ did not crystallize on heating after the glass transition, but the quenched sample with $W_y = 0.10$ crystallized at $-31°C$. The DSC curve with $W_y = 0.10$ shows that $CH_3CO_2Na \cdot 3H_2O$ and $CH_3CO_2Na \cdot HCONH_2 \cdot 3H_2O$ crystallize almost simultaneously, because there exist one exothermic peak corresponding to the crystallization of the sample, nevertheless there exist two endothermic peaks corresponding to the melting of eutectic mixture of the system $CH_3CO_2Na \cdot 3H_2O$-$CH_3CO_2Na \cdot HCONH_2 \cdot 3H_2O$ and to the melting of $CH_3CO_2Na \cdot 3H_2O$. However, taking the difficulty of crystallization of $CH_3CO_2Na \cdot 3H_2O$ into account, the crystallization of $CH_3CO_2Na \cdot 3H_2O$ is considered to be preceded by a crystallization of $CH_3CO_2Na \cdot HCONH_2 \cdot 3H_2O$. T_c is lowered linearly from $W_y = 0.10$ to $W_y = 0.60$. The DSC curve having $W_y = 0.70$ shows two exothermic peaks, in which one corresponds to the crystallization of $CH_3CO_2Na \cdot HCONH_2 \cdot 3H_2O$ and the other corresponds to the crystallization of $HCONH_2$. From the DSC curves in Fig. 74, it is not able to be determined which peak corresponds to the crystallization of $HCONH_2$.

V. 3. 2. 3 $CH_3CO_2Na \cdot HCONH_2 \cdot 3H_2O$ as a Latent Heat Storage Material

The new addition compound $CH_3CO_2Na \cdot HCONH_2 \cdot 3H_2O$ has some favorable characteristics for latent heat storage: *a.* high heat of fusion (255 J/g); *b.* optimum melting temperature for space heating; *c.* high specific gravity (1.404 g/cm^3). However, as mentioned above, $CH_3CO_2Na \cdot HCONH_2 \cdot 3H_2O$ melt tends to supercool. In order to use $CH_3CO_2Na \cdot HCONH_2 \cdot 3H_2O$ as a latent heat storage material, the nucleation catalyst should be added to it, but it has not been found yet so far. It is expected that the nucleation catalyst can be found taking the effect of the thermal hysteresis on heterogeneous nucleation into account.

CHAPTER VI SUMMARY AND CONCLUSION

This thesis describes the research and development of latent heat storage material consisting of $CH_3CO_2Na \cdot 3H_2O$ as a main component.

1) Crystallization behavior of $CH_3CO_2Na \cdot 3H_2O$ from the aqueous solution without the nucleation catalyst was clarified.
2) Supercooling of $CH_3CO_2Na \cdot 3H_2O$ was prevented by an addition of a small amount of the nucleation catalyst.
3) Decomposition of $CH_3CO_2Na \cdot 3H_2O$ melt was overcome by using the thickener.
4) Melting point of $CH_3CO_2Na \cdot 3H_2O$ was controlled by mixing with the organic compound, $CO(NH_2)_2$ or $HCONH_2$.

The results found in the present study are summarized below.

In Chapter II, the following results were obtained through the investigation of the crystallization behavior of the binary system CH_3CO_2Na-H_2O.

1) $CH_3CO_2Na \cdot 3H_2O$ hardly crystallizes in the solution without the nucleation catalyst. The crystallization temperature of $CH_3CO_2Na \cdot 3H_2O$ from the aqueous solution is from -50 to $-30°C$.
2) The addition of H_2O to $CH_3CO_2Na \cdot 3H_2O$ melt does not promote the crystal nucleation of $CH_3CO_2Na \cdot 3H_2O$.
3) Anhydrous CH_3CO_2Na is not directly related to the crystal nucleation of $CH_3CO_2Na \cdot 3H_2O$ from the solution.

In Chapter III, the results of the study on heterogeneous nucleation of $CH_3CO_2Na \cdot 3H_2O$ containing the nucleation catalyst were described as follows.

1) $Na_4P_2O_7 \cdot 10H_2O$ ($Na_4P_2O_7$), Na_2HPO_4, Na_2WO_4 or LiF acts as a crystal

nucleation catalyst of $CH_3CO_2Na \cdot 3H_2O$. In the case of adding $Na_4P_2O_7 \cdot 10H_2O$ to the CH_3CO_2Na aqueous solution, anhydrous $Na_4P_2O_7$ particles contribute to the heterogeneous nucleation of $CH_3CO_2Na \cdot 3H_2O$. In the case of adding Na_2HPO_4, $Na_2HPO_4 \cdot 2H_2O$ contributes to the nucleation of it.

2) Even if $Na_4P_2O_7 \cdot 10H_2O$, Na_2HPO_4, Na_2WO_4 or LiF is added to the CH_3CO_2Na aqueous solution, $CH_3CO_2Na \cdot 3H_2O$ hardly crystallizes from the solution, unless these nucleation catalysts are activated. The nucleation catalysts are activated by forcible crystallization of $CH_3CO_2Na \cdot 3H_2O$ from the solutions containing them.

3) The nucleation catalysts are deactivated at an elevated temperature above the melting point of $CH_3CO_2Na \cdot 3H_2O$. In the case of using $Na_4P_2O_7 \cdot 10H_2O$ as a nucleation catalyst, the deactivation temperature of it in the $CH_3CO_2Na \cdot 3H_2O$ melt is about 81°C. In the case of using Na_2HPO_4, Na_2WO_4 or LiF as a nucleation catalyst, they are about 81, 88 or 92°C respectively.

4) The deactivation temperature of the nucleation catalysts depends on the CH_3CO_2Na concentration of the solution and is lowered with decreasing CH_3CO_2Na concentration.

5) The deactivation temperature of the nucleation catalysts scarcely varies with preheating time.

6) The deactivation temperature of the nucleation catalysts depends on its activation process, such as aging temperature or aging time. The deactivation temperature of the nucleation catalysts is raised with lengthening the aging time for constant aging temperature (20°C). At the lower temperature than 20°C, the longer aging period is required to give a sufficient aging effect on the nucleation catalyst.

7) In the case of using any nucleation catalyst, the supercooling of bulk $CH_3CO_2Na \cdot 3H_2O$ melt is about −6°C and it is kept almost constant unless the melt containing it was preheated above its deactivation temperature.

8) The nucleation catalysts such as Na_2HPO_4, in the presence of the catalytic poison, $H_2NCH_2CO_2H$ or $C_4H_4O_6Ca \cdot 4H_2O$, are deactivated at much lower temperature than their usual deactivation temperatures.

From these results, the heterogeneous nucleation of $CH_3CO_2Na \cdot 3H_2O$ from the solution containing the nucleation catalyst was considered to proceed as follows.

i) As soon as $CH_3CO_2Na \cdot 3H_2O$ is forced to crystallize from a supercooled solution containing the nucleation catalyst, the incommensurate solid adsorbate is formed on the surface of the nucleation catalyst. The incommensurate solid adsorbate little contributes to the nucleation of $CH_3CO_2Na \cdot 3H_2O$.

ii) The incommensurate solid adsorbate transforms into commensurate solid adsorbate (crystalline adsorbate) with elapse of time. $CH_3CO_2Na \cdot 3H_2O$ crystallizes easily on the commensurate solid adsorbate. The commensurate solid adsorbate does not transform near the bulk melting point of $CH_3CO_2Na \cdot 3H_2O$ and thus the deactivation temperature of the fully aged nucleation catalyst is much higher.

iii) The commensurate solid adsorbate transforms into the liquid adsorbate at an elevated temperature. $CH_3CO_2Na \cdot 3H_2O$ hardly crystallizes on the liquid adsorbate. This transformation corresponds to the deactivation of the nucleation catalyst.

iv) The solid adsorbate will be formed again from the liquid adsorbate during cooling process because of the forced crystallization of $CH_3CO_2Na \cdot 3H_2O$ from the solution containing the nucleation catalyst.

In Chapter IV, the study on heat storage capacity of $CH_3CO_2Na \cdot 3H_2O$ during thermal cycling bore the following results.

1) The latent heat storage capacity of guaranteed grade $CH_3CO_2Na \cdot 3H_2O$ containing a nucleation catalyst is initially 254 J/g: after 30 cycles declines to 200 J/g; and after 400 cycles declines to 160 J/g.
2) The latent heat storage capacity of technical grade $CH_3CO_2Na \cdot 3H_2O$ containing a nucleation catalyst is initially 259 J/g; after 30 cycles declines to 235 J/g: after 400 cycles declines to 200 J/g.
3) The latent heat storage capacity of the thickened $CH_3CO_2Na \cdot 3H_2O$ is about 230 J/g, and this latent heat storage capacity scarcely decreases during thermal cycling. The thickener comprises polyvinyl alcohol, acetone and liquid paraffin.

In Chapter V, the following results were obtained through the study on controlling the melting point of $CH_3CO_2Na \cdot 3H_2O$.

A) Pseudo-binary system $CH_3CO_2Na \cdot 3H_2O$-$CO(NH_2)_2$

1) Pseudo-binary system $CH_3CO_2Na \cdot 3H_2O$-$CO(NH_2)_2$ forms a eutectic mixture without forming any new addition compound. The eutectic mixture of this system containing $CH_3CO_2Na \cdot 3H_2O$ and $CO(NH_2)_2$, in mass fraction ratio of 6:4, melts congruently at 31.5°C.
2) The heat of fusion of the eutectic mixture obtained by DSC, 226 J/g, is in good agreement with the calculated value, 221 J/g.
3) The linear velocity of crystallization of the melt containing 0.04 mass fraction of $CO(NH_2)_2$ at $\Delta\theta = -20$°C falls to less than a half of that of $CH_3CO_2Na \cdot 3H_2O$ melt at $\Delta\theta = -20$°C. The linear velocity of crystallization of the eutectic melt at $\Delta\theta = -20$°C, 0.002 cm/s, is about one three hundredth of that of $CH_3CO_2Na \cdot 3H_2O$ melt at $\Delta\theta = -20$°C.

4) On slow cooling, the melts having the composition near $CH_3CO_2Na \cdot 3H_2O$, crystallize at about $-30°C$. In the $CH_3CO_2Na \cdot 3H_2O$ rich side of the eutectic composition, except in the vicinity of $CH_3CO_2Na \cdot 3H_2O$, $CH_3CO_2Na \cdot 3H_2O$ hardly crystallizes from the melt.

5) From the eutectic mixture, $CH_3CO_2Na \cdot 3H_2O$ starts to crystallize with the aid of the nucleation catalyst, $Na_4P_2O_7 \cdot 10H_2O$, and the crystallization of $CO(NH_2)_2$ is followed. The eutectic mixture containing the nucleation catalyst, $Na_4P_2O_7 \cdot 10H_2O$, continuously repeats stable melting and freezing during thermal cycling between 5 and 45°C. This eutectic mixture did not decompose into the components.

B) Pseudo-binary system $CH_3CO_2Na \cdot 3H_2O$-$HCONH_2$

1) In the pseudo-binary system $CH_3CO_2Na \cdot 3H_2O$-$HCONH_2$, a one to one addition compound of the two components forms and this addition compound, $CH_3CO_2Na \cdot HCONH_2 \cdot 3H_2O$, melts congruently at 40.5°C. The crystal of the addition compound is colorless and transparent. The specific gravity of this crystal at room temperature is 1.404 g/cm^3.

2) The heat of fusion of the addition compound, $CH_3CO_2Na \cdot HCONH_2 \cdot 3H_2O$, is 255 J/g. In addition, the new addition compound has some favorable characteristics for latent heat storage but it can not be used as a latent heat storage material without the existence of the nucleation catalyst, because $CH_3CO_2Na \cdot HCONH_2 \cdot 3H_2O$ melt tends to supercool severely.

REFERENCES

1. T. Ozawa, Kogyo Zairyo, **26**, No. 9, 21 (1978).
2. M. Kamimoto, K. Sakuta, T. Ozawa and R. Sakamoto, Denshigijutsu Sogo Kenkyusho Chosa Hokoku, No. 196 (1978).
3. H. G. Lorsch, K. W. Kauffman and J. C. Denton, Energy Conversion, **15**, 1 (1975).
4. J. Kai, Kuki Chowa Eisei Kogaku, **52**, 885 (1978).
5. A. Abhat, Sol. Energy, **30**, 313 (1983).
6. K. Yamaguchi and M. Kurachi, Reito, **54**, 151 (1979).
7. J. Sohns, B. Seifert and E. Hahne, Int. J. Thermophys., **2**, 71 (1980).
8. M. Telkes, Ind. Eng. Chem., **44**, 1308 (1952).
9. M. Kamimoto, Kagaku To Kogyo, **33**, 598 (1980).
10. M. Telkes, "Solar Materials Science," ed. by L. E. Murr, Academic Press, New York (1980), Chapt. 11.
11. F. de Winter, Sol. Energy, **17**, 379 (1975).
12. M. J. Wetterwald, J. L. Salagnac, J. L. Chevalier, J. Guion and J. D. Sylvain, Cah. Cent. Sci. Tech. Batim. (in France), **245**, 1902 (1983).
13. K. Narita and J. Kai, Denki Gakkai Zasshi, **101**, 15 (1981).
14. B. Carlsson, H. Stymne and G. Wettermark, Sol. Energy, **23**, 343 (1979).
15. G. A. Lane, Sol. Energy, **27**, 73 (1981).
16. A. Seidell, "Solubility of Inorganic and Metal-Organic Compounds," ed. by Linke, Academic Press, Washington (1965), Vol. II, p. 854.
17. "Kagaku Dai Jiten," ed. by Kagaku Dai Jiten Henshu Iinkai, Kyoritsu Shuppan, Tokyo (1960), Vol. 3, p. 823.
18. W. F. Green, J. Phys. Chem., **12**, 655 (1908).
19. N. V. Sidgwick and J. A. Gentle, J. Chem. Soc., **121**, 1837 (1922).

20. P. L. Dietz, J. S. Brukner and C. A. Hollingsworth, J. Phys. Chem., **61**, 944 (1957).
21. A. Pebler, Thermochim. Acta, **13**, 109 (1975).
22. T. Ishibashi, "Shokuhin Tenkabutsu no Zenbo," Nanko Do, Kyoto (1979), p. 39.
23. K. Nagano, S. Yamane and K. Toyoshima, "Poval," Kobunshi Kanko Kai, Kyoto (1981), p. 109.
24. W. W. Conner, J. Am. Chem. Soc., **53**, 2806 (1931).
25. G. A. Lane, Int. J. Amb. Energy, **1**, 155 (1980).
26. R. Ulrich and F. Volker, Ger. Offen 2448739 (1976); Chem. Abstr., **86**, 31899e (1977).
27. W. T. Richards, J. Am. Chem. Soc., **54**, 479 (1932).
28. M. Volmer, Z. Electrochem., **35**, 555 (1929).
29. C. S. Herrick, ASHRAE Trans., **85**, 512 (1979).
30. H. L. R. Crooker, Fr. Patent 647572 (1928); Chem. Abstr., **23**, 2514 (1929).
31. T. P. Bell, U. S. Patent 1856166 (1932); Chem. Abstr., **26**, 2833 (1932).
32. T. P. Bell, U. S. Patent 1887618 (1932); Chem. Abstr., **27**, 1467 (1933).
33. J. A. C. Bowles and R. Lyman, U. S. Patent 2118586 (1938); Chem. Abstr., **32**, 55398 (1938).
34. H. Kimura, Nippon Kessho Seicho Gakkaishi, **7**, 215 (1980).
35. D. R. Biswas, Sol. Energy, **19**, 99 (1977).
36. M. Telkes, Sol. Energy Materials, **2**, 381 (1980).
37. S. Marks, Sol. Energy, **25**, 255 (1980).
38. C. S. Hrrick, Sol. Energy, **28**, 99 (1982).
39. J. D. Meakin, T. Stuchlik and F. A. Costello, ASME Winter Annual Meeting, New York (1976), Paper No. 76-WA/HT-35.
40. K. W. Böer, J. H. Higgins and J. K. O'Connor, IECIC '75 Record, 7 (1975).
41. N. Yoneda and S. Takanashi, Sol. Energy, **21**, 61 (1975).

42. A. V. Hook, "Crystallization, Theory and Practice," Reinhold Pub. Co., London (1961), p. 7.

43. H. Kimura, Ind. Eng. Chem. Fundam., **19**, 251 (1980).

44. R. Kiriyama and K. Yamada, Nippon Kagaku Zasshi, **71**, 558 (1950).

45. E. Williams and C. A. Angell, J. Phys. Chem., **81**, 232 (1977).

46. H. Kanno, I. Shirotani and S. Minomura, Bull. Chem. Soc. Jpn., **54**, 2607 (1981).

47. C. A. Angell and E. J. Sare, J. Chem. Phys., **52**, 1058 (1970).

48. M. Sugisaki, H. Suga and S. Seki, Bull. Chem. Soc. Jpn., **41**, 2591 (1968).

49. J. Nyvlt, J. Cryst. Growth, **314**, 377 (1968).

50. H. Hartley, B. M. Jones and G. A. Hutchinson, J. Chem. Soc., **93**, 825 (1908).

51. B. M. Jones, J. Chem. Soc., **93**, 1739 (1908).

52. D. Gernez, Compt. rend, **60**, 833 (1865).

53. L. de Boisbaudran, Compt. rend, **63**, 95 (1866).

54. Z. Stunic, V. Djurickovic and Z. Stunic, J. Appl. Chem. Biotechnol., **28**, 761 (1978).

55. J. W. Mullin, "CRYSTAL GROWTH," ed. by B. R. Pamplin, Pergamon Press, New York (1975), Chapt. 8.

56. J. Garside et al., Chem. Eng. Commun., **4**, 393 (1980).

57. K. A. Jackson, Ind. Eng. Chem., **57**, 29 (1965).

58. T. Kuroda, "Kessho wa Ikiteiru.", Saiensusha, Tokyo (1984), p. 61.

59. D. Turnbull and J. C. Fisher, J. Chem. Phys., **17**, 71 (1949).

60. M. Volmer, "Kinetik der Phasenbildung," Seinkopf, Dresden and Leipzig (1939).

61. D. R. Uhlmann and B. Chalmers, Ind. Eng. Chem., **57**, 18 (1965).

62. L. Royer, Bull. Soc. Franc. Mineral, **51**, 1 (1928).

63. B. Vonnegut, J. Applied Phys., **18**, 593 (1947).

64. P. V. Hobbs, "Ice Physics," Clarendon Press, Oxford (1974), p. 502.

65. H. A. Levy and G. C. Lisensky, Acta Crystallogr., Sect. B, **34**, 3502 (1978).

66. D. Turnbull and B. Vonnegut, Ind. Eng. Chem., **44**, 1292 (1952).

67. M. B. Ives and J. P. Hirth, J. Chem. Phys. **33**, 517 (1960).

68. A. Neuhaus, Z. Krist., **105**, 161 (1943).

69. P. Othmer, Z. Anorg. Allg. Chem., **91**, 235 (1915).

70. D. Turnbull, J. Chem. Phys., **18**, 198 (1950).

71. D. Turnbull, J. Appl. Phys., **20**, 817 (1949).

72. M. E. Fine, "Introduction to Phase Transformations in Consensed System," The Macmillan Co., New York (1964), Chapt. 2.

73. C. N. Hinshelwood and H. Hartley, Phil. Mag., **43**, 78 (1922).

74. W. T. Richards, E. C. Kirkpatrick and C. E. Hutz, J. Am. Chem. Soc., **58**, 2243 (1936).

75. L. E. Evans, Trans. Faraday Soc., **63**, 1 (1967).

76. G. R. Edwards, L. F. Evans and A. F. Zipper, Trans. Faraday Soc., **66**, 220 (1970).

77. G. R. Edwards and L. F. Evans, J. Atmos. Sci., **28**, 1443 (1971).

78. K. T. Wei and D. L. Ward, Acta Crystallogr., Sect. B, **33**, 522 (1977).

79. T. S. Cameron, K. M. Mannan and Md. O. Rahman, Acta Crystallogr., Sect. B, **32**, 87 (1976).

80. H. Kimura, Nippon Kessho Seicho Gakkaishi, **9**, No. 3, 73 (1982).

81. H. Shiba, Kotai Butsuri, **7**, 504 (1981).

82. S. Sugano and N. Hamada "Hyomen no Bishiteki Kozo" in "Butsurigaku no Saizensen," ed. by Y. Otsuki, Kyoritsu Shuppan, Tokyo (1984), Vol. 6, p. 55.

83. D. R. Nelson and B. I. Halperin, Phys. Rev. B, **19**, 2457 (1979).

84. M. Jaubelt, A. Glachant, M. Bienfait and G. Boato, Phys. Rev. Lett., **46**, 1679 (1981).

85. R. Funk, Ber., **33**, 3696 (1900).

86. J. H. Payne, J. Am. Chem. Soc., **59**, 947 (1937).

87. K. Y. Leung and C. Calvo, Can, J. Chem., **50**, 2520 (1972).

88. M. Catti, G. Ferraris and M. Franchini-Angela, Acta Crystallogr., Sect. B, **33**, 3449 (1977).

89. R. P. Mitra and H. K. L. Verma, Indian J. Chem., **7**, 598 (1969).

90. F. S. Galasso, "Structure and Properties of Inorganic Solid," Pergamon Press, Oxford (1970), p. 63.

91. P. Bak, "Modern Theory of Crystal Growth," in "Crystals," ed. by A. A. Chernov and H. Muller-Krumbhaar, Springer-Verlag, New York (1983), Vol. 9, p. 22.

92. K. Kishita, Nippon Butsuri Gakkai Shi, **37**, 156 (1982).

93. M. Telkes, U. S. Patent 3986969 (1976); Chem. Abstr., **86**, 93089b (1977).

94. S. Marks, Solar Energy, **30**, 45 (1983).

95. M. Kamimoto, T. Tanaka, T. Tani, and T. Horigome, Solar Energy, **24**, 581 (1980).

96. T. Ozawa, M. Kamimoto, R. Sakamoto. Y. Takahashi and K. Kanari, Densoken Iho, **43**, 289 (1979).

LIST OF PUBLICATIONS

1. Studies on Salt Hydrate for Latent Heat Storage. I.
   Crystal Nucleation of Sodium Acetate Trihydrate Catalyzed by Tetrasodium Pyrophosphate Decahydrate
   T. Wada and R. Yamamoto
   Bull. Chem. Soc. Jpn., **55**, 3603–3606 (1982).

2. Studies on Salt Hydrate for Latent Heat Storage. II.
   Eutectic Mixture of Pseudo-binary System $CH_3CO_2Na \cdot 3H_2O$-$CO(NH_2)_2$
   T. Wada, F. Kimura and R. Yamamoto
   Bull. Chem. Soc. Jpn., **56**, 1223–1226 (1983).

3. Studies on Salt Hydrate for Latent Heat Storage. III.
   Pseudo-binary System $CH_3CO_2Na \cdot 3H_2O$-$HCONH_2$
   T. Wada, F. Kimura and R. Yamamoto
   Bull. Chem. Soc. Jpn., **56**, 1575–1576 (1983).

4. Studies on Salt Hydrates for Latent Heat Storage. IV.
   Crystallization in the Binary System CH_3CO_2Na-H_2O
   T. Wada, F. Kimura and Y. Matsuo
   Bull. Chem. Soc. Jpn., **56**, 3827–3829 (1983).

5. Studies on Salt Hydrates for Latent Heat Storage. V.
   Preheating Effect on Crystallization of Sodium Acetate Trihydrate from Aqueous Solution with a Small Amount of Sodium Pyrophosphate Decahydrate

T. Wada, K. Matsunaga and Y. Matsuo

Bull. Chem. Soc. Jpn., **57**, 557–560 (1984).

6. Studies on Salt Hydrates for Latent Heat Storage. VI.

Preheating Effect on Crystallization of Sodium Acetate Trihydrate from Aqueous Solution with a Small Amount of Disodium Hydrogenphosphate

T. Wada and Y. Matsuo

Bull. Chem. Soc. Jpn., **57**, 561–563 (1984).

7. Equilibria in the Aqueous Ternary System Containing Na^+, $CH_3CO_2^-$, and $P_2O_7^{4-}$ between 38 and 85°C

T. Wada, F. Yokotani, and Y. Matsuo

Bull. Chem. Soc. Jpn., **57**, 1671–1672 (1984).

8. Equilibria in the Aqueous Ternary System Containing Na^+, $CH_3CO_2^-$, and HPO_4^{2-} between 38 and 75°C

T. Wada, F. Yokotani, and Y. Matsuo

Bull. Chem. Soc. Jpn., **57**, 2021–2022 (1984).

9. Heat Storage Capacity of Sodium Acetate Trihydrate During Thermal Cycling

T. Wada, R. Yamamoto, and Y. Matsuo

Solar Energy, **33**, 373–375 (1984).

10. Studies on Salt Hydrates for Latent Heat Storage. VII.

The Relation between Activation Process of the Crystal Nucleation Catalysts for Sodium Acetate Trihydrate and their Deactivation Temperatures

T. Wada and H. Yoneno

Bull. Chem. Soc. Jpn., **58**, 919–925 (1985).

11. Heterogeneous Nucleation of $CH_3CO_2Na \cdot 3H_2O$ from Aqueous Slutions Containing a Nucleation Catalyst

T. Wada and H. Yoneno

J. Cryst. Growth, submitted for publication.

12. Latent Heat Storage Material

T. Wada, K. Matsunaga, F. Kimura, R. Yamamoto, T. Kusuda, and Y. Ise

National Technical Report, **29**, 58–68 (1983).

ACKNOWLEDGMENT

I would like to express my sincere gratitude to professor Mitsue Koizumi for his hearty encouragement to prepare this thesis.

I am also deeply grateful to Dr. Shinichi Kikkawa for his many kind advices. I am deeply indebted to Dr. Hiroshi Takubo for his interesting and helpful discussions.

I wish to express my thanks to Dr. Ryoichi Kiriyama for his many helpful discussions throughout this work.

I am greatly indebted to Dr. Tsuneharu Nitta, Dr. Eiichi Hirota, Mr. Yukihiko Ise, and Dr. Masanari Mikoda for their continuous interests and supports.

I am also grateful to Dr. Yoshihiro Matsuo, Dr. Ryoichi Yamamoto, Mr. Hiroshi Yoneno, and Mr. Toshihiro Mihara for their valuable suggestions and discussions.

I express my thanks to Mr. Tomoyuki Hosokawa and Kazuo Yamashita for their many helpful suggestions and discussions relating to the application.

The special appreciation is extended to Mr. Koji Matsunaga and Mrs. Fumiko Yokotani for their helps and co-works.

I am grateful to Dr. Hiromichi Mitsuda for his assistance in smaple analysis.

Finally, many thanks are given to my family for their understanding and perpetual support.